UNIVERSITA' DEGLI STUDI DI NAPOLI "FEDERICO II"

TESI DI DOTTORATO IN "INGEGNERIA DEI MATERIALI E DELLE STRUTTURE" - XX CICLO

INFLUENCE OF CARBON NANOTUBES ON THE PROPERTIES OF FILMS OF POLYPROPILENE PREPARED BY FILM BLOWING

Relatore:

Prof. Domenico ACIERNO

Dottorando:

ing. Francesca IANNACE

Ad Alessandra

INDEX

Abstract

The influence of carbon nanotubes on mechanical and bi-elongational properties of films of polypropylene prepared with film blowing technique were studied. The carbon nanotubes (CNTs) adopted as fillers were contained in a polypropylene pre-compounded with 20 wt% of carbon nanotubes (masterbatches). To investigate on the effect of moelecular and/or carbon nanotube orientation on the mechanical properties of PP, the tensile test were performed eiher on suitable composite sample plates, obtained by pressing the granulated melt-mixed composites, either on film samples. Furhermore, blown film samples were tested either in the blow-up direction (BD) either the take-up one (TD). Different response to the tensile tests were displayed by the blown films samples in the two directions of testing as a consequence of the biaxial orientation of molecules (and/or the carbon nanotubes) during the film blowing. Excellent improvement of the mechanical properties (Young's modulus and strength) for certain weight fractions of CNT of the blown composite films compared to the neat PP were revealed. Furthermore, the bubble formation and stability in the film blowing process of PP nanocomposites were correlated to their underlying rheology, structure, and crystallization behavior.

Introduction

The majority of polymer films are manufactured by film blowing (blown film extrusion). In this process, an extruder is used to melt the polymer and pump it into a tubular die (Figure 1). Air is blown into the center of the extruded tube and causes it to expand in the radial direction, while a couple of a certain number of nip rolls collect the film, as well as sealing the top of the bubble to maintain the air pressure inside. Extension of the melt in both the radial and down-stream direction stops at the freeze line (frost line) due to the cooling air which is blown outside del bubble and determine the crystallization of the melt. This process is used extensively with polyolephines, like polyethylene and polypropylene.

In particular, PP is an inexpensive, ductile, low strength material with reasonable outdoor performance. The material surface is soft wax-like and scratches easily.

In many ways, PP is similar to HDPE, but it is stiffer and melts at 165-170 °C and can be manufactured by all the methods used for thermoplastics.

Mechanical and rheological properties of polypropylene are generally modified by melt mixing with particulate (talc, mica, clay) [1-4] and fibrous (glass, jute, aramid, and carbon

fibers [5-9] as well as by melt blending with other polymers [10-13]. Reinforcement at nanoscale to improve mechanical and other properties including changes in polymer elongational behaviour is being attempted [14-20]. Carbon nanotubes (CNTs), due to their high tensile strength and modulus [21-23], are excellent candidates for nano-reinforcement of variety of polymer matrices. There has been intense recent research concerning the fabbrication, characterization and application of polymer/carbon nanotube composites, driven by the evidence of the unique mechanical, elettrical, thermal and other materials-related properties of carbon nanotubes. Examples of mechanical property improvements using nano-reinforcement are available in literature and include polypropylene/carbon nanofibers [18], pitch/SWNTs [24], PMMA/SWNTs [25] and PBO/SWNT fibers [26]. Evidence of enhancement regarding mechanical properties have suggested that carbon nanotubes may hold promises as possible reinforcing phase in new kind of composite materials. Such development still presents great pratical challenges, expecially when attempting to devise new techniques to produce materials containing aligned carbon nanotubes. Recent progress have shown the possibilities of making films of aligned nanotubes

by using magnetic field [27-29] and making fibers of aligned nanotubes by using an electrophoretic process [30, 31] or by directly spinning an acqueous suspension [32].

Alignment consists in a preferred orientation of a tube (in their longitudinal axes) within a three-dimensional sample which can be of interest if mechanical enhancement is desired in a preferential direction. Alignment can be accompanied by disentaglement or stretching of curved tubes.

Usually, OM [33], SEM and TEM were used to visualize these effects in phin films or fibers. Effort was made to assess the nanotubes alignment via TEM in specimens of drawn monofilament fibers [37] and extruded thin films [36]. Sennet et al. [37] showed enhanced MWNT alignment in the flow direction after melt spinning with increasing draw speed. Cooper et al. [36] used TEM to get orientation distribution of 4 wt.% MWNT in PMMA, however, the TEM micrographs presented in [36] do not seem to be very suitable for this purpose.

More often indirect methods are used to get information about nanotubes orientation and alignment. Raman spectroscopy [34, 38, 39] and X-ray diffraction [40] have been used to obtain information about orientation and degree of

alignment in specimens either in mechanically stretched or oriented during fiber spinning.

In the past few years, many researchers have focused their studies on the mechanical properties of polymer/nanotubes composites structures. It has been recognised that high mechanical properties could be achieved when nanotubes are alligned parallel to the load direction in the composite structures. However, the study on the mass production and especially of the their alignment in the polymeric matrix towards the pre-determined direction is still under research.

A key issue in producing superior CNT composites is also the possibility to control deagglomeration and dispersion of CNTs in polymer matrices which are directly correlated to the hoped properties (conductivity, mechanical, etc). In most cases homogeneous dispersion of nanotubes is hindered by both the syntesis induced “entangled” and aggregated” structures of nanotubes as well as the tubes tendency to form agglomerate, due to the intermolecular van der Waals intercactions between them. Single-walled carbon nanotubes (SWNTs) are usually produced as bundles, whereas multi-walled carbon nanotubes (MWNTs) are formed as entangled

curved agglomerate [41]. The agglomeration problem present a major challenge irrespective of the method of composite preparation. In context with industrial application of polymer/nanotubes systems, melt mixing is the preferred method of composite preparation.

Applying shear is described to be very efficient in order to minimize nanotube aggregate formation [38, 42-44] and, thus, to enhance nanotube dispersion. In this context, Haggenmueller et al. [38] showed an enhanced SWNT dispersion after melt dispersion after melt processing of polymethimethacrilate-SWNT samples which were prepared by solution mixing.

On the other hand, characterization or quantification of the state of nanotubes dispersion is a difficult task. Direct microscopic observation of the nanotubes dispersion in composites is difficult to apply due to the extreme differences in radial and axial dimension of the nanotubes. Optical microscopy (OM) only assesses very big agglomerates of nanotubes and is incapable to analyse the dispersion at submicron scale [33-37]. Surface based methods, scanning electron microscopy (SEM) and atomic force microscopy

(AFM) only show a cross section of the three dimensional arrangement of the nearly one-dimensional nanotubes. This makes it difficult to observe an entire CNT or to distinguish between different CNTs [36,37,45,46]. Trasmission electron microscopy (TEM) on thin sections, as shown by Sennet et al. [37] for different melt mixed composites of polycarbonate (PC) with MWNTs and SWNTs, has the advantage of showing all segments of nanotubes located within the thickness of the section; but even here it is difficult to conclude from the micrograph of a three-dimensional arrangement and the state of dispersion. In the case of curved and interconnected nanotubes structure this problem is much more pronounced. Thus, discussion of the state of nanotubes dispersion based on microspcopic method is rare in literature and in most case not very convincing.

One of the indirect methods which are suitable to compare the state of nanotubes dispersion at a given concentration (e.g. depending on processing conditions or addition of modifiers) are elettrical conductivity of measurements. This was shown by Ferguson et al. [47], by comparing the electrical conductivity of PC-MWNT composites obtained by mixing a diluited masterbatch with

different amounts of reprocessed compounds. Reprocesing in a Buss Kneader led tobetter dispersion of the nanotubes resulting in increased conductivity. Another very sensitive method is oscillatory melt rheology, as shown by Mitchell et al. [48]. They compared composites of polystyrene (PS) with unfunctionalized and functionalized SWNTs and found much higher storage modulus and complex viscosity values at very low frequencies by using functionalized nanotubes. The increase in modulus and complex viscosity was assigned to the better dispersion of functionalized nanotubes. Visual observation of dispersions of nanotubes composites in a polymer solvent also can help to distinguish between agglomerated and well dispersed tubes. This was shown by Barraza et al. [35] comparing dispersions in toluene of microemulsion polymerization of PS-SWNT.

Two are the most common ways of introducing nanotubes in polymer matrix. In the first case the nanotubes are directly incorporated inside the polymer matrix, and in the other case, commercially available masterbatches of polymer/nanotubes composite [41] are used as starting material which is diluited by pure polymer in a subsequent melt mixing process [45].

In this study the approach has been to produce PP-MWNT composites with varying concentration of nanotubes by melt mixing technology, starting from a masterbatch. At 20 wt.% MWNT (masterbatch) structure consists of highly entangled and “percolated” nanotubes in the PP matrix which are well wetted by the polymer matrix. The addition of PP into the network like structure should expand the MWNT structure gradually by incorporating the PP chains between the individual tubes maintaining the “tube percolation”. Eventually with very high amount of PP added (and therefore, low amount of MWNTs) the percolated structure of the tubes will no longer exists and the MWNTs will be uniformly distributed, as fine dispersion, without touching each other.

Currently, nearly nothing is reported in the literature about the production of CNT reinforced polymeric films prepared with the blow film extrusion. Here the influence of carbon nanotubes on mechanical and biaxial elongational properties of films of polypropilene prepared with film blowing technique were studied. The tensile test were performed eiher on suitable composite sample plates, obtained by melt-pressing the composite granulates either on film samples in order to analyze the effect of moelecular and

carbon nanotube orientation on the mechanical properties of PP. Furthermore, tensile tests were conducted on the films either in the take-up direction (TD) either in the blow-up direction (BD). The results have shown a clear enhancement of the mechanical properties for certain weight fraction of CNT of the blown composite films compared to the neat PP and different tensile behaviours in the two direction of testing as a consequence of the biaxial orientation of the molecule occurred during the blowing process.

Furthermore, the bubble formation and stability in the film blowing process of PP nanocomposites are correlated to their underlying rheology, structure, and crystallization behavior.

PART I

MATERIALS AND PROCESSING

CHAPTER 1:Carbon nanotubes

1.1 State of art

In the mid ‘80s, Smalley and co-workers at Rice University developed the chemistry of fullerenes [56] which are geometric cage-like structure of carbon atoms that are composed of exagonal and pentagonal faces. The first closed, convex structure formed was C60 molecule. Named in the behealth of the architect R. Buckminster Fuller known for designing geodesic domes, buckminsterfullerene is a closed cage of 60 carbon atoms where each side of a pentagon is the adiacent side of a hexagon similar to a soccer ball, for that the C60 molecule is often referred to as a bucky ball [56]. A few years later, their discovery led to the syntesis of carbon nanotubes. Nanotubes are long slender fullerenes where the walls of the tubes are hexagonal carbon (graphite structure) and often capped at each end.

These cage-like forms of carbon have been demonstrated to exibit exceptional material properties as a consequence of their symmetric structure. Many researchers have reported

mechanical properties of the nanotubes that are superior to those of any other existing material. Theoretical and experimental results have shown extremely high elastic modulus, greater than 1 TPa (the elastic modulus of diamond is 1.2 TPa) and strengths 10-100 times higher than the strongest steel at a fraction of the weight.

To unlock the potentiality of carbon nanotubes for application in polymer nanocomposites, it is foundamental to fully understand the mechanical properties as well as the interactions at the nanotube/matrix interface. With respect to their fiber-reinforced composites counterparts [57], for the case of carbon nanotubes the scale of reinforcement phase diameter has changed from micrometers (e.g. glass and carbon fibers) to nanometers.

In addition to the exceptional mechanical properties, the carbon nanotube also posses superior thermal and elecric properties: thermally stable up to 2800°C in vacuum, thermal conductivity about twice as high as diamond, electric-current-currying capacity 1000 times higher than copper wires [58]. These exceptional properties of carbon nanotubes have been investigated for devices such as field-emission displays [59]

scanning probe microscopy tips [60] and micro-electronic devices [61,62].

1.2 Atomic structure and morphology of carbon nanotubes

Carbon nanotubes can be visualized as a sheet of graphite that has been rolled into a tube. Unlike diamond, where a 3-D diamond cubic crystal structure is formed with each carbon atom having four nearest neighbors arranged in tetrahedron, graphite is formed as a 2-D sheet of carbon atoms arranged in a hexgonal array. In this case, each carbon atom have three nearest neighbors. ‘Rolling’ sheets of graphite into cylinders form carbon nanotubes. The properties of nanotubes depend on atomic arrangement (how sheets of graphite are ‘rolled’), the diameter and length of the tubes, and the morphology, or nano structure. Nanotubes can exist as single-walled (SWCNTs) or multi-walled structures (MWCNTs) where the multi-walled nanotubes are simply composed of concentric sigle walled nanotubes.

1.2.1 Nanotube structure

The atomic structure of nanotubes is described in terms of tube chirality, or helicity, which is defined by the chiral vector, *Ch*, and the chiral angle, *q*. In Figure 1 it is reported the schematic diagram showing the cutting of graphite sheet along the dotted lines and rolling the tube so that the tip of the chiral vector touches its tail. The chiral vector, often known as the roll-up vector, can be described by the following equation:

$$\vec{C}_h = n\vec{a}_1 + m\vec{a}_2$$

where the integers (n, m) are the number of steps along the zig-zag carbon bonds of the hexagonal lattice and $\vec{a}_1$ and $\vec{a}_2$ are unit vectors shown in Figure 1. The chiral angle determines the amount of “twist” in the tube.

Two limiting case exist when the chiral angle is at 0° and 30°. These limiting cases are referred to as zig-zag (0°) and armchair (30°) based on the geometry of the carbon bonds around the circumference of the nanotube. The difference in armchair and zig-zag structures is shown in Figure 2. In terms of roll-up vector, the zig-zag nanotube is (n,0) and the armchair nanotube is (n,n). The roll-up vector of the nanotube

also defines the nanotube diameter since the inter-atomic spacing of the carbo atoms is known.

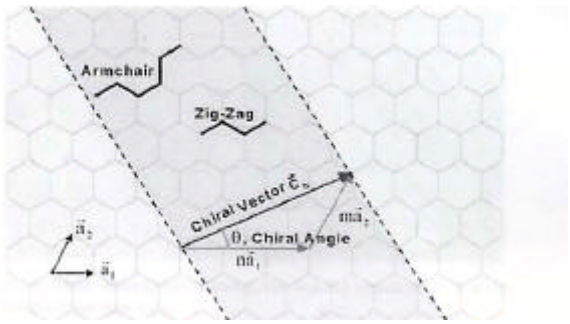

Figure 1: Schematic diagramshowing a hexagonal sheet of graphite "rolled" to form a carbon nanotube

The chirality of the carbon nanotubes has deep implication on the material properties. In particular, the chirality is known to have a strong impact on the electronic properties of carbon nanotubes. Graphite is considered to be a semi-metal, but it has been shown that nanotubes can be either metallic or metallic or semiconducting, depending on tube chirality [64].

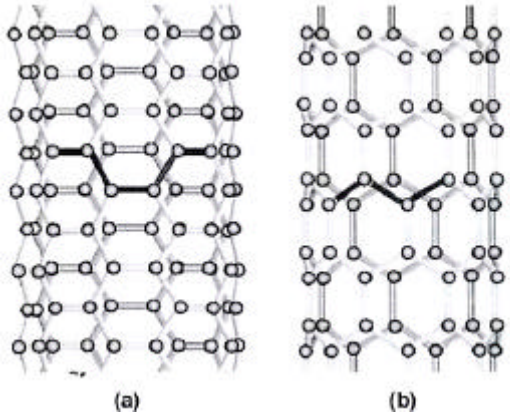

Figure 2: Illustrations of the atomic structures of (a) an armchair and (b) a zig-zag nanotube.

Studies on the influence of chirality on the mechanical properties have also been reported. The analytical work of Yakobson et al. [63,64] examined the instability of carbon nanotubes beyond linear response. Their simulations showed that the carbon nanotubes are remarkably resilient, sustaining extreme strain with no signs of brittleness or plasticity. Although the chirality has a relatively small influence on the elastic stiffness, they concluded that the Stone-Wales transformation plays a key role in the nanotubes plastic deformation under tension. The Stone-Wales transformation (Figure 3) is a reversible diatomic interchange where the resulting structure is two pentagons and two heptagons in pairs and occurs when an armchair nanotubes is stressed in axial direction. Nardelli et al. [66] theorized that the Stone-Wales

transformation results in ductile fracture for armchair nanotubes.

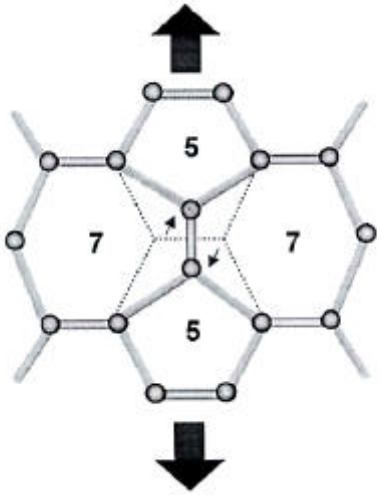

Figure 3: Stone-Wales transformation occurring in an armchair nanotube under axial tension.

1.2.2 Nanotube morphology

As mentioned before, fullerenes are closed. Convex cages that are composed of pentagons and hexagons. The Stone-Wales transformation introduces a new defect in the nanotubes structure, the heptagon. Heptagons allow for concave areas within nanotubes which can result in many possible equilibrium shapes. Indeed, most nanotubes are not straight cylinders with hemispherical caps. In addition to different tube

morphologies resulting from defects, carbon nanotubes can be single-walled or multi-walled structure. A transmission electron microscope (TEM) image showing the nanostructure of a multi-walled carbon nanotubes where several layers of graphitic carbon and a hollow core is reported In Figure 4.

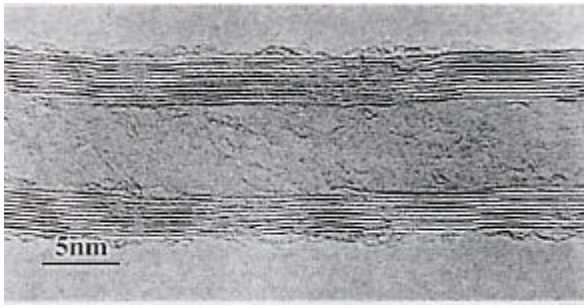

Figure 4: TEM micrograph of a the layered structure of a multiwalled carbon nanotube.

Multi-walled carbon nanotubes are essentially concentric single walled tubes, where each individual tube can have different chirality. These concentric nanotubes are held together by secondary, van der Waals bonding. Single-walled nanotubes are most desired for fundamental investigations of the structure/property relashionships in carbon nanotubes, since the intra-tube interactions further complicate the properties of carbon nanotubes.

1.3 Processing of carbon nanotubes for composite materials

Since the discovery of carbon nanotubes nearly a decade ago, there have been a variety of of techniques developed for producing them. Iijima [55] first observed multiwalled nanotubes and Iijima et al. [67] and Bethune et al. [68] independently reported reported the syntesis of SWNTs a few years later. Primary syntesis methods for single and multi-walled carbon nanotubes include arc discharge [55,69], laser ablation [70], gas-phase catalytic growth from carbon monoxide [71] and chemical vapour deposition (CVD) from hydrocarbons [72] methods. For application of carbon nanotubes in composites, large quantities are required, but the scale-up limitations of arc discharge and laser ablation techniques would make the cost of nanotubes based composites prohibitive. During the syntesis of nanotubes, impurities in the form of catalyst particles, amorphous carbons and non-tubolar fullerenes are also produced. Thus, subsequent purification steps are required to separate the tubes. The gas-phase processes tend to produce nanotubes with fewer impurities and are more amenable to large scale processing, but the gas-phase techniques, such as CVD, for nanotubes growth offer the best

potential for the scaling-up of nanotubes production for the processing of composites. In Figure 5 the schematic of the arc discharge technique is shown. This technique generally involves the use of two high purity graphite rods as the anode and cathode. The rods are brought together under a helium atmosphere while a voltage is applied until a stable arc is achieved. The exact process variables depend on the size of graphite rods. As the anode is consumed, a constant gap between the anode and the cathode is maintained by adjusting the position of the anode. The materials then deposits on the cathode to form a build-up consisting of an outside shell of used material and a softer fibrous core containing nanotubes and other carbon particles. To achieve single-walled nanotubes, the electrodes are doped with a small amount of metallic catalyst particles [67-69,75,76].

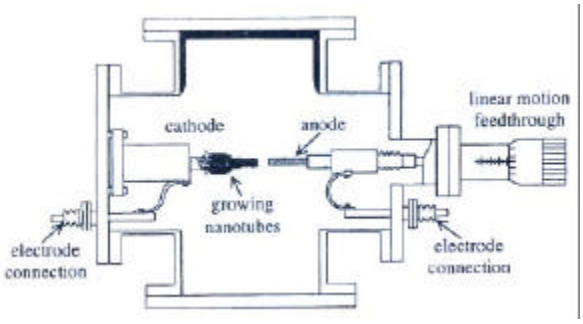

Figure 5: Schematic illustration of the arc discharge technique [76]

Laser ablation was first adopted for the initial syntesis of fullerenes. Over the years, this technique has been improved to allow the production of single-walled nanotubes [70,77,78]. In this technique, a laser is used to vaporize a graphite target held in controlled atmosphere oven at a temperatures near 1200°C. The general set-up for laser ablation is depicted in Figure 6. To produce single-walled nanotubes, the graphite target is doped with cobalt and nickel catalyst [70]. The condensed material is then collected on a water cooled target.

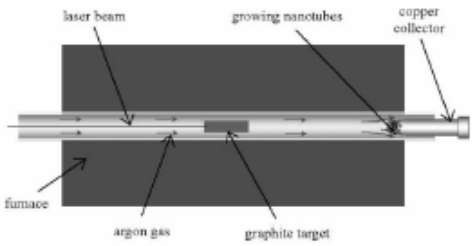

Figure 6: Schematic of laser ablation process [58]

Both the arc-discharge and the laser-ablation techniques are limited in the volume of samples that they produce in relation to the size of the carbon source (the anode in arc-discharge and the target in laser ablation). In addition, subsequent purification steps are necessary to separate the tubes from undesiderable by-products. These limitations have pushed the

development of gas-phase technique, such as chemical vapour deposition (CVD), where the nanotubes are formed by the deposition of a carbon-containing gas. The gas-phase technique are amenable to mass processes since the carbon source are continually replaced by flowing gas. In addition, the final purity of the as-produced nanotubes can be quite high thanks to subsequent purification steps.

Nikolaev et al. [71] describe the gas-phase growth of single-walled carbon nanotubes with carbon monoxide as carbon source. They reported the highest yields of single-walled nanotubes occurred at the highest accessible temperature and pressure (1200°C, 10 atm).

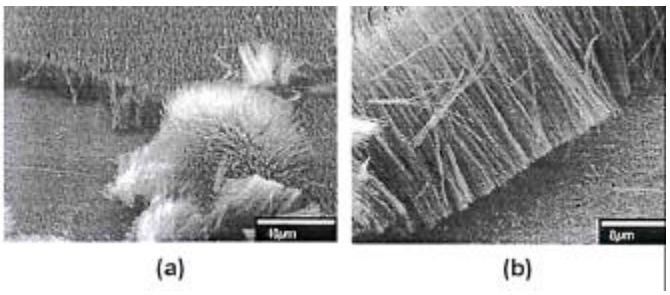

Figure 7: Micrographs showing the straightness on MWNTs grown via PECVD [73]

Smalley and his co-workers at Rice University have refined the process to produce large quantities of single-walled carbon nanotubes with remarkable purity. The so-called HiPco nanotubes (high pressure conversion of carbon monoxide) have received considerable attention since the technology has been commercialized by Carbon Nanotechnologies Inc (Huston, TX) for large scale production of high-purity single-walled carbon nanotubes.

Other gas-phase techniques uses hydrocarbon gases as carbon source for production of both single and multi-walled carbon nanotubes via CVD [79-82].Nikolaev et al. [71] pointed out that hydrocarbons pyrolize readilyon surface heated above 600-700°C. As a consequence, nanotubes grown from hydrocarbons can have substantial amorphous carbon deposits on the surface of the tubes and will require further purification steps. Although the dissociation of hydrocarbons at low temperature affects the purity of the as-processed nanotubes, the lower processing temperature enables the growth of carbon nanotubes on a wide variety of substrates, including glass.

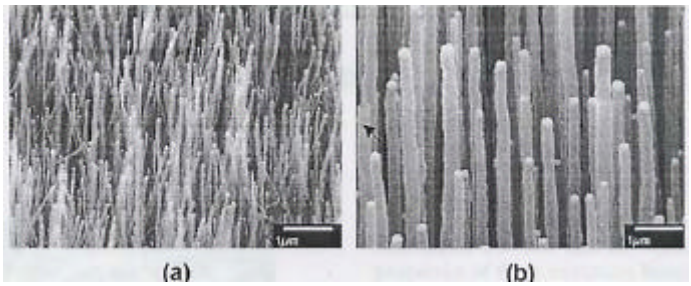

Figure 8: Micrographs showing control over nanotube diameter: (a) 40-50 nm and (b) 200-300 nm aligned carbon nanotubes [73]

One unique aspect of CVD techniques is its ability to synthesize aligned arrays of carbon nanotubes with controlled diameter and length. The synthesis of well aligned and straight nanotubes on a variety of substrate has been accomplished by the use of plasma-enhanced chemical vapour deposition (PECVD) where the plasma is excited by a DC source [72-74] or a microwave source [83-87]. In Figure 7a and b it is shown the ability to grow straight carbon nanotubes over a large area with excellent uniformity in diameter, length straightness and site density. By adjusting the thickness of the catalyst layer it is possible to control the diameter of the tubes, as shown in Figure 8a and b.

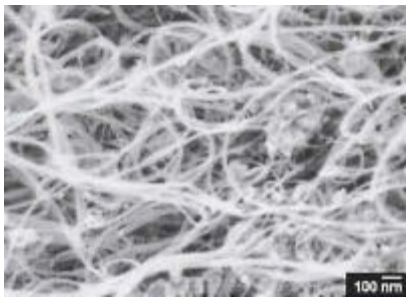

Figure 9: Micrographs showing (a) nanotubes aligned normal to the surface of glass fiber and (b) the influence of MPECVD on the structure of nanotubes [83]

In addition to highly aligned arrays of carbon nanotubes, large quantities of carbon nanotubes can be produced by conventional CVD processes. Unlike PECVD, which requires the use of specialized plasma equipment, tangled carbon nanotubes are grown in a tube furnace. In Figure 9 a SEM micrograph of the furnace-grown carbon nanotubes showing the same random, curled structure associated with thermal CVD shown in Figure 10 is reported. The outer diameters of these tubes range from 10-50 nm. These tangled (spaghetti like) nanotubes can be produced in large quantities and with a lower cost than PECVD tubes, but there is less control over length, diameter and structure.

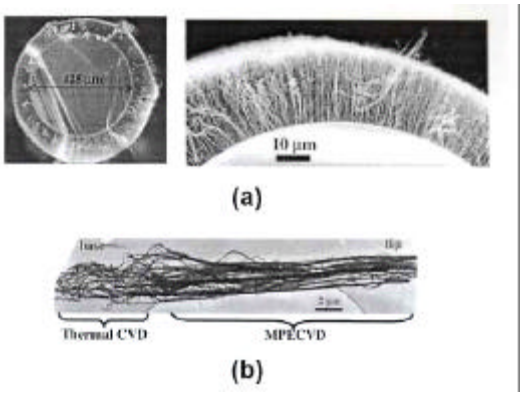

Figure 10: Micrograph showing tangled, spaghetti like carbon nanotubes grown through conventional CVD technique

1.4 Characterization of carbon nanotubes

In order to better understand the mechanical properties of carbon nanotubes, a number of researchers have attempted to characterize them directly. Trecy et al. [88] first investigated the elastic modulus of isolated multi-walled nanotubes by measuring the amplitude of their intrinsic thermal vibration in the transmission electron microscope. The average value obtained over 11 samples was 1.8 TPa. Direct measurements of the stiffness and the strength of individual, structurally isolated single-walled nanotubes was made with atomic-force microscope (AFM). Wong and co-workers [89] were the first to perform this type of measurement on individual, structurally isolated single-walled nanotubes using atomic force microscopy. The nanotubes was pinned at one end to

molybdenum disulfide surface and load was applied to the tube with AFM tip. The bending force was measured as a function of the displacement along the unpinned length and a value of 1.26 TPa was found for the elastic modulus, while the average bending strength measured was 14.2± 8GPa. Single-walled nanotubes tend to assemble in “ropes” of nanotubes. Salvetat et al. [89] measured the properties of these nanotubes bundles with AFM. As the diameter of the tube bundles increases , the axial and shear moduli decreases significantly. This suggest slipping of the nanotubes within the bundle. Walters et his co-workers [92] further investigated the elastic strain of nanotubes bandles with AFM. On the basis of their experimental strain measurements and with an assumed elastic modulus of 1.25 TPa, they calculated a yield strength of 45±7 GPa for the nanotubes ropes. Indeed, their calculation would be much lower if the elastic modulus of the bundle is decreased as a consequence of slipping within bundle.

Yu et al. [92,93] have investigated the tensile loading of multi-walled nanotubes and single-walled nanotubes ropes. In their work, the nanotubes were attached between two opposing AFM tips and loaded under tension. Their experimental set-up is shown in Figure11. For multi-walled carbon nanotubes [92]

the failure of the outermost tube occurred followed by pullout of the inner nanotubes. A micrograph of this “sword and sheath” telescoping failure mechanism of multi-walled carbon nanotubes in tension is shown in Figure 11. The experimentally calculated tensile strengths of the outermost from 11 to 63 GPa and the elastic modulus ranged from 270 to 950 GPa. In their subsequent work of single-walled nanotubes ropes [93] they assumed that only the outermost tubes assembled in rope carried the load during the experiment and they calculated tensile strengths of 13 to 52 GPa and average elastic moduli of 320 to 1470 GPa. Xie and his co-workers [94] also tested ropes of multi-walled nanotubes in tension and the obtained tensile strengths and modulus were 3.6 and 450 GPa, respectively. The lower values for strengths and stiffness were considered to be a consequence of defects in the CVD-grown nanotubes.

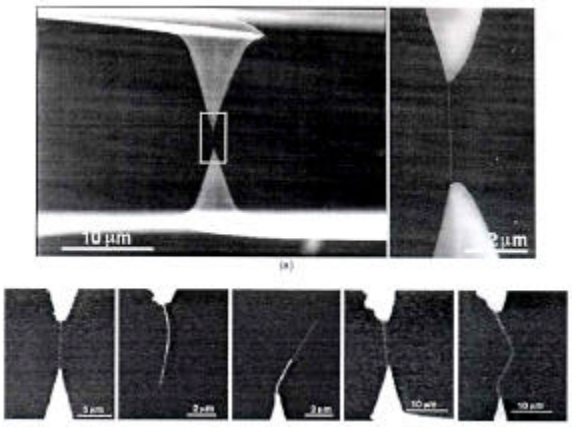

Figure 11: Micrographs showing (a) the apparatus for tensile loading of MWNTs and (b) the telescoping "sword and sheath" fracture behavior of MWNT [92]

1.5 Mechanics of carbon nanotubes

As discussed earlier, nanotubes deformation has been widely examined sperimentally. Recent studies have shown that carbon nanotubes possess remarkable mechanical properties, such as exceptionally high elastic modulus [89,90], large elastic strain and fracture strain sustaining capability [95,96]. Similar conclusions have also been reached through some theoretical studies [97-100] although still very few correlations between theoretical predictions and experimental studies have been made. In this section we examine the mechanics of both single walled and multi-walled nanotubes.

1.5.1 Single-walled nanotubes

Theoretical studies concerning the mechanics of SWNT have been persued extensively. Overney et al [98] investigated the low-frequency vibrational modes and structural rigidity of long nanotubes consisting of 100, 200 and 400 atoms. The calculations were based on empirical Keating Hamiltonian with parameters determined from first principles. A comparison of the bending stiffness of single-walled nanotubes and an iridium beam was presented. The bending stiffness of the iridium beam was deduced from the Bernoulli-Euler theory of beam bending. Overney et al. concluded that the beam bending stiffness of a nanotubes exceeds the highest value found in any other current available materials.

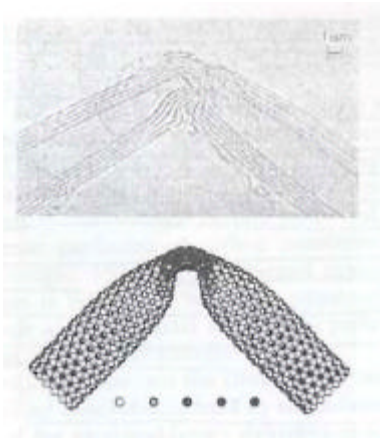

Figure 12: TEM micrograph and computer simulation of nanotube buckling [101]

Besides their experimental observations, Iijima and his co-workers [101] examined behaviour of nanotubes under compression using molecular dynamics simulations. They simulated the deformation properties of single and multi-walled nanotubes bent to large angles. Their experimental results showed that the nanotubes are remarkably flexible. The bending is completely reversible up to angles in excess of 110°, despite the formation of complex kink shapes. In Figure 12 their numerical and experimental results are showed, demonstrating the exceptional resilience of carbon nanotubes at large strain.

Ru [102] noticed that actual bending stiffness of single-walled nanotubes is much lower than that given by the elastic elastic-continuum shell model if the commonly defined representative thickness is used. Ru proposed the use of an effective nanotubes bending stiffness as a material parameter not related to the representative thickness. With the aid of this concept, the elastic shell equations can be readily modified and then applied to single-walled nanotubes. The computational results based on this concept showed a good

agreement with the results from molecular dynamics simulations.

Vaccarini and his co-workers [103] investigated the influence of nanotubes structure and chirality on the elastic properties in tension, bending and torsion. They found that the chirality played a small influence on the nanotube tensile modulus. However, the chiral tubes exhibit asymmetric torsional behaviour with respect to left and right twist, whereas the armchair and zig-zag tubes do not exhibit this asymmetric torsional behaviour.

A relative comprehensive investigation of the elastic properties of single-walled nanotubes was reported by Lu [98]. In this study, Lu adopted an empirical lattice-dynamics model [104], which has been successfully adopted in calculating the phonon spectrum and elastic properties of graphite. In this model, atomic interactions in a single carbon layer are approximated by a sum of pair-wise harmonic potentials between atoms. The local structure of a nanotubes layer is constructed from conformal mapping of a graphite sheet on to a cylindrical surface. Lu et al. [105] attempted to answer such basic questions as: (a) how do elastic properties of nanotubes depend on the structural details, such as size and chirality?

And (b) how do elastic properties of nanotubes compare with those of graphite and diamond Lu concluded that the elastic properties of nanotubes are insensitive to size and chirality. The predicted Young's modulus (~1 TPa), shear modulus (~0.45 TPa) and bulk modulus (~0.74 TPa) are comparable to those of diamond. Hernandez et al. [105] performed similar calculations and found slightly higher values (~ 1.24 TPa) for the Young's modulus of the tubes. But unlike Lu, they found that the elastic moduli are sensitive to both diameter and structure.

Besides their unique elastic properties, the inelastic behaviour of nanotubes has also received considerable attention. Yakobson et al.[64,100] examined the instability behaviour of carbon nanotubes beyond linear response by using a realistic many-body Tersoff-Brenner potential and molecular dynamics simulations. Their simulations showed that carbon nanotubes, when subjected to large deformations, reversibly switch into different morphological patterns. Each shape change corresponds to an abrupt release of energy and a singularity in the stress/strain curve. These transformation are well explained by a continuum shell model. With appropriately chosen parameters, their model provided a very accurate

"rodmap" of nanotubes behaviour beyond the linear elastic regime. They also made molecular dynamics simulations to single and double-walled nanotubes of different chirality and temperature [99]. Their work showed that nanotubes have an extremely large breaking strain (30-40%) and the breaking strain decreases with temperature. Yakobson [65] also applied dislocation theory to carbon nanotubes for describing their main routes of mechanical relaxation under tension. They concluded that the yield strength of a nanotubes depends on its symmetry and it was believed that there exit an intra-molecular plastic flow. Under high stress, this plastic flow corresponds to a motion of dislocations along helical paths within the nanotubes wall and causes a stepwise necking, a well defined new symmetry, as the domains of different chiral symmetry are formed. As a result, both the mechanical and electronic properties of carbon nanotubes are changed.

The single-walled nanotubes produced by laser ablation and arc-discharge techniques have a greater tendency to form ropes or aligned bundles [69,77], thus theoretical studies have been made to investigate the mechanical properties of these bundles. Ru [106] presented a modified elastic-honeycomb model to study elastic buckling of nanotubes ropes under high pressure.

Ru gave a simple formula for the critical pressure as a function of nanotubes Young's modulus and wall thickness-to-radius ratio. It was concluded that single-walled ropes are susceptible to elastic buckling under high pressure and elastic buckling is responsible for the pressure-induced abnormalities of vibration modes and electrical resistivity of single-walled nanotubes.

1.5.2 Multi-walled carbon nanotubes

Multi-walled nanotubes are composed of a number of concentric sigle-walled nanotubes held together by relatively weak van der Waals forces. The multi-layered structure of these nanotubes further complicates the modelling of their properties.

Rouff and Lorents [109] derived the tensile and bending stiffness constants of ideal multi-walled nanotubes in terms of the known elastic properties of graphite. It was suggested that unlike the strongly anisotropic thermal expansion in conventional carbon fibers and graphite, the thermal expansion of carbon nanotubes is essentially isotropic. However, the thermal conductivity of nanotubes is believed to be highly

anisotropic and its magnitude along the axial direction is perhaps higher than that of any other material.

Lu [110] also calculated the elastic properties of many multi-walled nanotubes formed by single-layer tubes with empirical-lattice dynamics model. It was found that elastic properties are insensitive to different combinations of parameters, such as chirality, tube radius and number of layers, and the elastic properties are the same for all nanotubes with a radius larger than 1 nm. Interlayer van der Waals interaction has a negligible contribution to both the tensile and shear stiffness.

Govindjee and Sackman [110] were the first to examine the use of continuum mechanics to estimate the properties of multi-walled nanotubes. They studied the validity of the continuum approach by using Bernoulli-Euler bending to infer the Young's modulus. They used a simple elastic sheet model and showed that at the nanotube scale the assumptions of continuum mechanics must be carefully respected in order to obtain reasonable results. They showed the explicit dependence of "material properties" on system size when a continuum cross-section assumption was used.

Ru [111] used the elastic-shell model to study the effect of van der Waals forces on the axial buckling of a double-walled carbon nanotube. The investigation showed that the van der Waals forces do not increase the critical axial buckling strain of a double-walled nanotube. Ru [112,113] thereafter alo proposed a multiple column model that considers the interlayer radial displacement coupled through the van der Waals fores. This model was used to investigate the effect of interlayer displacements on column buckling. They concluded that the effect of interlayer displacements could not be neglected unless the van der Waals forces are extremely strong.

Kolmogorov and Crespi [114] studied the interlayer interaction in two-walled nanotubes. A registry-dependent two-body graphite potential was developed. They demonstrated that the tightly constrained geometry of a multi-walled nanotubes could produce an extremely smooth solid-solid interface wherein the corrugation against sliding does not grow with system size. Furthermore, the energetic barrier to interlayer sliding in defect-free nanotubes containing thousand of atoms can be comparable to that of a single unit cell of crystalline graphite.

1.6 Nanotube-based composites

The reported exceptional properties of nanotubes have pushed the researchers to investigate sperimentally the mechanics of nanotubes-based composite films. Uniform dispersion within the polymer matrix and improved nanotubes/matrix wetting and adhesion are critical issues in the processing of these nanocomposites. In the work of Salvetat et al. [90], slipping of nanotubes when they are assembled in ropes significantly affects the elastic properties. In addition to slipping of tubes that are not bonded to the matrix of a composite, the aggregates of the nanotubes ropes effectively reduce the aspect ratio (length/diameter) of the reinforcement. It is however, difficult to obtain a uniform distribution in the polymer matrix. Shaffer and Windle [115] processed carbon nanotubes/polyvynil-alchol composite films for mechanical characterization. The tensile elastic modulus and damping properties of the composite films were assessed with dynamic mechanical thermal analysis (DMTA) as a function of nanotubes loading and temperature. Using the theory developed for short-fiber composites, a nanotubes elastic modulus of 150 MPa was obtained from experimental data. This value is well below the values reported for isolated

nanotubes. This discrepancy may be either a consequence of imperfections in the graphite layers of catalytically grown nanotubes either related to a fundamental difficulty in stress transfer.

Qian et al. [116] characterized carbon-nanotubes/polystyrene composites. With only the addition of 1% by weight (about 0.5% by volume) they achieved between 36-42% increase in the elastic stiffness and 25% increase in the tensile strength. In Figure13 it is reported a TEM micrograph of their nanotubes film showing the mechanism of fracture. In analogy with conventional fiber composites, it can be seen nanotubes pull-out, nanotube fracture, as well as crack bridging by the nanotubes. They also used short-fiber composite theory to demonstrate that 10% by weight of carbon fibers (about 5% by volume) in the research of Tibbetts and McHugh [117] would be required to achieve the same increase in elastic modulus with 1 wt.% of carbon nanotubes.

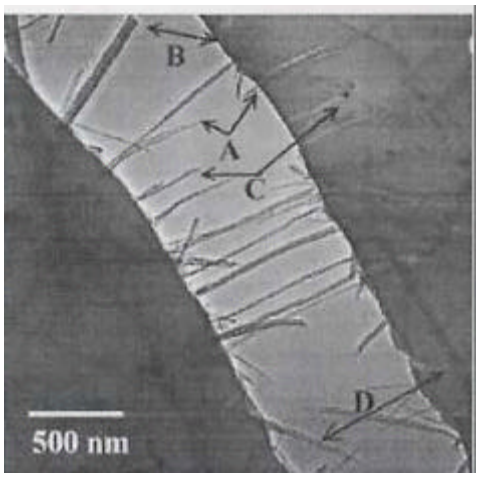

Figure 13: Fracture mechanisms in nanotube-based composites [116]

Figure 13 shows significant pull-out of the nanotubes from the matrix. Beside the reinforcement in stiffness and strength of the composite, to take full advantage of the exceptional stiffness, strength and resilience of carbon nanotubes strong interfacial bonding is critical. Jia and his co-workers [118] showed that the nanotubes can be initialized by a fre-radical initiator, AIBN (2,2'-azobisisobutyronitrile), to open their π bonds. In their study of carbon-nanotube/poly(metyl-methacrylate) (PMMA) composites, the possibility exists to form C-C bond between the nanotube and matrix. Gong et al. [119] investigated surfactant-assisted processing of nanotubes composites with a nonionic surfactant. Improved dispersion and interfacial bonding of the nanotubes in a epoxy matrix

resulted in a 30% increase in elastic modulus with addition of 1 wt% nanotubes

Lordi and Yao [120] studied the molecular mechanics of bonding in nanotubes-based composites. In their work, they used force-field based molecular-mechanics calculations to determine the binding energy sliding frictional stresses between pristine carbon nanotubes and different polymer matrices. The binding energies and frictional forces were found to play only a minor role in determining the strength of the interface. The key factor in forming a strong bond at the interface is having a helical conformation of the polymer around the nanotubes. They concluded that the strength of the interface may result from molecular-level entanglement of the two phases of forced long-range ordering of the polymer.

Because the interaction at the nanotubes/matrix interface is critical to understanding the mechanical behaviour of nanotube-based composites, a number of researchers have investigated the efficiency of interfacial stress transfer. Wagner and his co-workers [121] examined stress-induced fragmentation of multi-walled carbon nanotubes in polymer films. Their nanotubes-containing films had a thickness of approximately 200 μm. The observed fragmentation

phenomenon was attributed to either stress resulting from curing of the polymer or tensile stress generated by polymer deformation and transmitted to the nanotube. From estimated values of nanotubes axial normal stress and elastic modulus, Wagner et al. concluded that the interfacial shear stress is on the order of 500 MPa and higher. This value, if reliable, is an order of magnitude higher than the stress transfer ability of current advanced composites and, therefore, such interfaces are more able than other the matrix or the nanotubes themselves to sustain shear.

Even with improved dispersion and adhesion, micro-mechanical characterization of these composites is difficult because the distribution of the nanotubes is random. Thus, attempts have been made to align nanotubes in order to better understand the reinforcement mechanisms. Jin and his co-workers [122] showed that aligned nanotubes composites could be obtained by stretching the composite. X-ray diffraction was used to determine the orientation and the degree of alignment.

Haggenmueller et al [123] showed that melt spinning of singl-walled nanotubes in fibers can also be used to create a well-aligned nanotubes composite.

In addition to alignment of carbon nanotubes, researchers have attempted to spin carbon fibers from carbon nanotubes [124-126]. Andrews and his co-workers [125] dispersed 5 wt.% single-walled nanotubes in isotropic petroleum pitch. Compared to the isotropic petroleum fibers without nanotubes, the tensile strength was improved by ~90%, the elastic modulus by ~150% and the electrical conductivity by~340%.

Because the pitch matrix is isotropic, the elastic modulus is 10-20 times less than that of mesophase pitch fibers used in composite materials.

Further developments in this area may potentially involve the formation of new form of carbon fiber with esceptionally flexibility as well as stiffness and strength. Figure 14 shows the exceptional flexibility of the as-spun nanotube composite fiber broduced by Vigolo et al. [126].

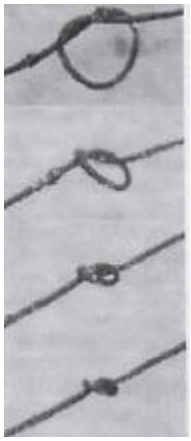

Figure 14: Micrograph showing the exceptional flexibility of carbon nanotube-based fiber [126]

CHAPTER 2: Film blowing

2.1 The process

The blown film extrusion (film blowing) is an important industrial process thin biaxially oriented polymeric film. This process basically consists in extruding a tube of molten thermoplastic polymer at constant mass flowrate and a biaxial orientation is produced by internal pressurization, by continuously inflating it to several times the initial diameter, and axial drawing to form a thin tubular product that can be used directly, or slit to form a flat film. Air jets surrounding the bubble provide cool air.

More in details, polymer melt is thus extruded through an annular slit die, usually vertically, to form a thin walled tube. Air is introduced via a hole in the centre of the die to blow up the tube like a balloon. Mounted on top of the die, a high-speed air ring blows onto the hot film to cool it. The tube of film then continues upwards, continually cooling, until it passes through nip rolls where the tube is flattened to create what is known as a ' lay-flat' tube of film. This lay-flat or collapsed tube is then taken back down the extrusion ' tower'

via more rollers. On higher output lines, the air inside the bubble is also exchanged. This is known as IBS (Internal Bubble Cooling).

The lay-flat film is then either kept as such or the edges of the lay-flat are slit off to produce two flat film sheets and wound up onto reels. If kept as lay-flat, the tube of film is made into bags by sealing across the width of film and cutting or perforating to make each bag. This is done either in line with the blown film process or at a later stage.

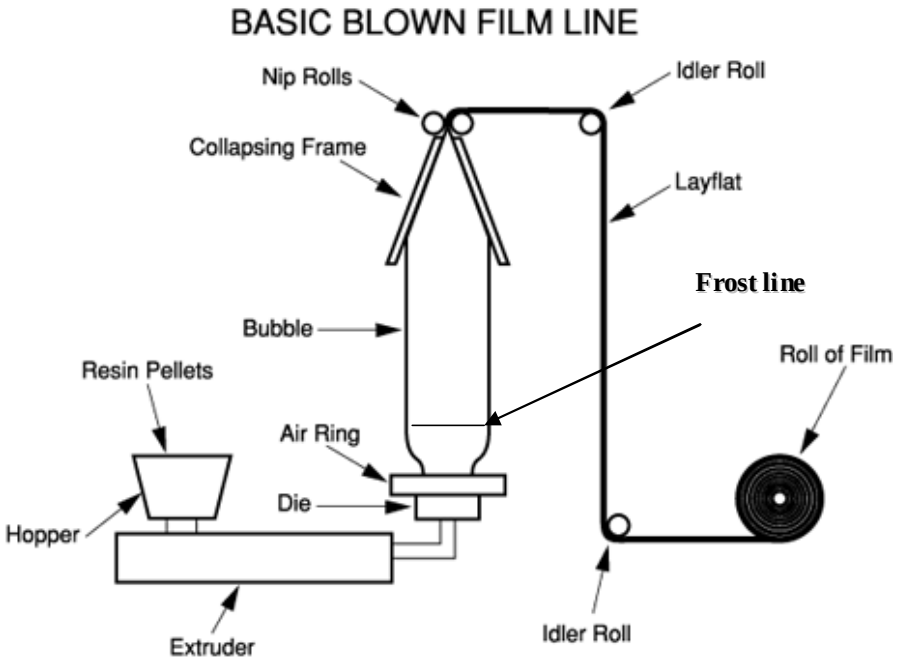

Figure 15: Schematic of film blowing process

The drawdown between the melt wall thickness and the cooled film thickness occurs in both radial and longitudinal directions and is easily controlled by changing the volume of air inside the bubble and by altering the haul off speed. This gives blown film a better balance of properties than traditional cast or extruded film which is drawn down along the extrusion direction only. Extension of the melt in both the radial ("transverse") and down-stream ("machine") direction stops at the "freeze line" (frost line) due to the cooling air which is blown outside del bubble and determine the crystallization of the melt. This therminology arises from the loss of transparency due to the crystallization of the polymer and not the presence of any condensed moisture on the film. Furthermore, it is not a true "line" but a narrow zone over which solidification occurs. In fact, the solidification occurs first at the cooled surface, at the melt-solid interface, and then moves away from this surface through the thickness of the film as it moves upwords, as shown in Figure 15. The height of the freeze line can be controlled through the air flowrate such that negligible deformation occurs beyond the freeze line in most process [127,128].

The main advantages in using this process are follows:

- Produce tubing (both flat and gussetted) in a single operation
- Regulation of film width and thichness by control of the volume of air in the bubble, the output of the extruder and the speed of the haul-off
- Eliminate end effects such as edge bead trim and non uniform temperature that can result from flat die film extrusion
- capability of biaxial orientation (allowing uniformity of mechanical properties)
- Very high productivity
- Permits the combination of a number of different materials and properties

Blown film can be used either in tube form (e.g. for plastic bags and sacks) or the tube can be slit to form a sheet.

Typical applications include Industry packaging (e.g. shrink film, stretch film, bag film or container liners), Consumer packaging (e.g. packaging film for frozen products, shrink film for transport packaging, food wrap film, packaging bags, or form, fill and seal packaging film), Laminating film (e.g. laminating of aluminium or paper used for packaging for

example milk or coffee), Barrier film (e.g. film made of raw materials such as polyamides and EVOH acting as an aroma or oxygen barrier used for packaging food, e. g. cold meats and cheese), films for the packaging of medical products, Agricultural film (e.g. greenhouse film, crop forcing film, silage film, silage stretch film

This process is used extensively with polyolephines, like polyethylene and polypropylene. In some cases, these materials do not gel together, so a multi-layer film would delaminate. To overcome this, small layers of special adhesive resins are used in between. These are known as “tie layers”.

The final film dimensions are determined by a number of process variables such as the “blow up ratio” (BUR), which is a ratio of the bubble radius a the freeze line to the radius of the die, and the machine direction draw down ratio (DDR), which is the ratio of velocity at the nip rollers to the velocity of the polymer melt exiting the die. Typically, the expansion ratio between die and blown tube of film would be 1.5 to 4 times the die diameter. The solidified film is flattened into a double-layered sheet by the nip rollers forming an almost airtight seal at the top of the bubble. After the bubble has been

flattened by the nip rollers the flat film is reeled up under constant tension either as tubular film or after slitting into sheet film. The width of the flattened tube is called the "layflat width" and this is equal to π times the final bubble radius.

Rheological properties play a fundamental role in film blowing. They govern the shape and the stability of bubble and the onset of sharkskin (surface roughness). Because of the complexity of the flows involved, it generally impossible to establish simple quantitative correlations between these phenomena and easy-measured rheological properties. However, an understanding of how variations in the rheological behaviour of melts can affect the process and the properties of blown films is essential to achieve optimum results from this process.

The objective of the film blowing process is to produce a thin film having a uniform gauge and good optical and mechanical properties. Since the film is quite thin, it is especially important to avoid the presence in the extrudate of unmelted material, gels or foreign matter, as these will be readily visible in the final product. I order to achieve good

mechanical properties it is often advantageous, particularly in the case of packaging films, to have molecoular orientation in the film that is as much as possible “balanced” in the machine and transverse directions.

Ultimate film properties are controlled by molecular orientation and stress induced crystallisation [129].

A stable bubble in the film blowing process is a requirement for the continuous operation of the process and the production of an acceptable film [130]. In general there are three forms of instabilities or combinations of these reported in literature. These are as follows:

1. Axisymmetric periodic variations of the bubble diameter, known as bubble instability (BI).
2. Helical motions of the bubble, described as helical instability (HI).
3. Variations in the position of the frost line height (FLHI).

BI and HI have been reported by a number of researchers [131–135], however, FLHI was only recently reported by Ghaneh-Fard et al. [131,135], after previous authors were

using the term “meta stable” [128] which was misleading for time-dependent oscillations in FLH. Results on bubble stability have generally been qualitative until recently when Sweeney et al. [136] utilised a video analysis system as an effective non-contact, real time device for quantifying instabilities during film blowing. Sweeney and his co-workers al. [136] first proposed the diameter range (*D*r) concept for measuring the degree of helical instability.

The average diameter, *D*, and the degree of helical instability (DHI) are then derived from the following equations:

$$\overline{D} = \overline{P}_1 - \overline{P}_r \qquad (2.1.1)$$

$$D\max = P\mathrm{l},\max \,.\, P\mathrm{r},\min, \qquad (2.1.2)$$

$$D\min = P\mathrm{l},\min \,.\, P\mathrm{r},\max, \qquad (2.1.3)$$

$$D\mathrm{r} = D\max \,.\, D\min, \qquad (2.1.4)$$

$$DHI = \frac{Dr}{\overline{D}} \times 100 \qquad (2.1.5)$$

where $\overline{D}$ is the average diameter of the bubble and $\overline{P}$ the average distance of the bubble from a reference line, as shown in Figure 16, where a typical bubble for a stable PP is shown. The subscript r denotes the distance of the right bubble edge

and l the distance of the left bubble edge from the reference line. The bubble was defined as stable if the DHI was less than 20%, partially helically stable if the DHI was between 20 and 40% and helically unstable if the DHI was greater than 40%.

The analysis of bubble stability in film blowing has largely focused on PEs (HDPE, LLDPE and LDPE), mainly due to their superior melt strength in comparison to other polymers such as PP. Only recently have results been reported on the bubble stability of PP [135]. Ghaneh-Fard et al. [135] studied the bubble stability of PP and found PP to have a much smaller stable operating window in comparison to PEs.

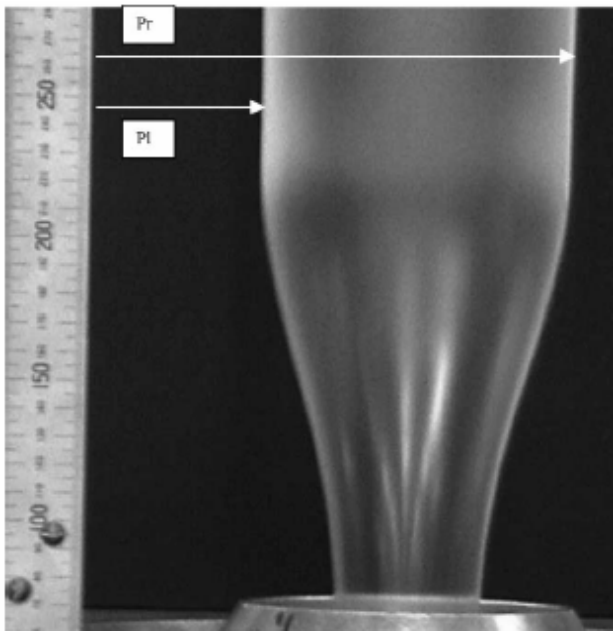

Figure 16: Typical bubble shape observed for a stable PP bubble

2.2. Governing equations of film blowing

Pearson and Petrie [137,138] first developed in detail the kinematic and dynamic equations describing fluid flow in film blowing. This was based on the thin shell theory where the thickness of the bubble was small in comparison to the bubble diameter. The kinematic and dynamic analysis of the bubble is

discussed below and has provided the theoretical framework for most subsequent studies.

For the continuous steady state operation of an incompressible fluid, the law of conservation of mass at any point along the bubble yields the following relationship for volumetric throughput:

$$Q = 2paHvs = \text{constant}, \qquad (2.2.1)$$

where *vs* is the meridional velocity, *Q* the total volumetric flow rate through the die, *a* the local bubble radius and *H* the local film thickness. Since the problem is axisymmetric, *vt* (velocity in the transverse direction) is zero and *vn* (velocity in the normal direction) is not exactly zero since the film is changing thickness, but is negligible, similar to fibre spinning and lubricating flows.

The derivative of Eq. (2.2.1) with respect to, *s*, the distance along the film yields a relation between the deformation rates in film blowing:

$$\frac{dv_s}{ds} = -\frac{1}{H} v_s \frac{dH}{ds} - \frac{1}{a} v_s \frac{da}{ds} \qquad (2.2.2)$$

The left-hand side represents the rate of stretching along the film, while the two terms on the right-hand

side are, respectively, the negatives of the stretch rate in the thickness (*n*) and tangential directions (*t*).

The rate of stretching in each direction is a function of measurable quantities.

The equilibrium force balance in the normal direction yields

$$\frac{\Delta P}{H} = \frac{s_s}{r_s} + \frac{s_t}{r_t} \qquad (2.2.3a)$$

where *ss* and *st* are the extensional stresses in the meridional, *s*, and transverse, *t*, direction, respectively;

DP the internal pressure measured relative to the external (atmospheric) pressure; and *?s*, *?t* the principal

radii of curvature in the two directions. It can be shown by simple differential geometry that:

$$r_s = \frac{[1+(da/dz)^2]^{3/2}}{d^2a/dz^2} \qquad (2.2.3b)$$

$$r_t = a\left[1+\left(\frac{da}{dz}\right)^2\right]^{1/2} \qquad (2.2.3c)$$

A force balance in the direction of the axis of symmetry, z, yields

$$F_z = -\Delta P p a^2 + 2paHs_s \cos ?, \qquad (2.2.4)$$

where F is the applied tension at $z = X_F$, and

$$\cos q = \left[1+\left(\frac{da}{dz}\right)^2\right]^{-1/2} \qquad (2.2.5)$$

In the analysis of Pearson and Petrie [137,138] inertia, gravity, surface tension and air drag effects are neglected. These are generally realistic assumptions due to the thin film bubble membrane and the viscous forces dominating the process for polymer melts. The governing equations can be

easily extended to include these effects by incorporating appropriate physical data.

These equations combined with a rheological constitutive equation, relating the stresses to the strains or strain rates in the bubble, result in a series of equations which are solved to yield predictions for various film blowing process characteristics (film temperature, bubble radius and velocity profiles).

PART II

EXPERIMENTAL

CHAPTER 3:

Experimental parameters and devices

3.1 Polypropilene material, carbon nanotubes and composite preparation

The base material was PP Moplen (HP502H) supplied by Basell. The carbon nanotubes (MWNT's) adopted as fillers were contained in granulates polypropilene pre-compounded with 20% by weight of carbon nanotubes (masterbatch) supplied by Hyperion Catalysis International, Inc. According to the supplier, the MWNTs were produced by chemical vapour deposition (CVD) and have diameter of approximately 10nm while the length is at least 10 nm after the production with CVD such that the aspect ratio is about 1000. The masterbatches were melt-mixed through a HAAKE double screw contro-rotating extruder with pure PP at 200-220°C in order to obtain diluted PP/CNT composites with respectively 1, 3, 5 and 10% of weight composition of CNTs. Mixing was performed at a rotational speed of 30 rpm and a throughput of 0,5 kg/h using the premixted granulates. At the exit of the

extruder the material was then granulated and in part adopted to build the suitable test samples and in part forworded to the blown extrusion.

3.2 Differential Scan Calorimeter (DSC)

The DSC were performed with the a TA Instruments device. The samples of about 12 mg were heated from –20° to 250°C at ramp rate of 10°C/min and held for 10 min in order to eliminate any thermal history of the material. Subsequently, the samples cooled to –20°C with the same scan rate. In order to observe the melting peak temperature after the crystallization, the samples were then heated to 250°C.

3.3 Thermogravimetic Analysis (TGA)

The thermogravimetric analysis (TGA) was conducted on a Du Pont Instruments device in the range of temperature 30÷600°C with a ramp rate of 10°C/min.

3.4 Rheological characterization

The rheological analysis was conducted with ARES Rheometric Instruments, model LN2, at 220°C in nitrogen

atmosphere and run with 25 mm parallel-plate geometry and 1 mm sample gap. The dynamic viscoelstic properties were determined using low strain values (1 %) with frequency range from 0.1 to 100 rad/s, which were within the linear viscoelastica region for these materials.

For the preparation of the suitable samples, the materials were dried for 12 h at 60°C and molten for 12 min under vacuum at a temperature of 220°C, in a Collin P300P press, pressed for 20 min and then quenched to ambient temperature.

3.5 Mechanical and dynamic mechanical tests

Tensile tests were conducted either on plate samples either on blowed film samples.

Blown film samples were prepared by cutting the films with a razor blade with a rectangular samples of approximate planar dimensions of 25x4 mm^2. On blown films samples tensile tests were conducted either in the BD either in the TD to analyze the influence of the biaxial orientation in the PP/CNT films on the bielongational properties. All the tensile experiments were carried out at ambient temperature at a strain rate of 50 mm/min. At least five samples were tested for each type of material.

The plate sample were obtained by heating the granulates at 220°C in a COLLIN press, model P300P , holding for 3 min and then pressed at 10 bar for 1 min before being cooled between two cooled metal blocks. Afterwords, suitable samples for tensile testing were cut according to the standard ASTM D 638-03, type IV. At least five samples were tested for each type of material.

Dynamic mechanical analysis was carried out with a Triton Technology device, model TRITEC 2000 DMA. Temperature scan were conducted at at 1 and 10H in the range –30÷110°C , with dynamic displacement of 0.05%.

Frequency/temperature scan tests were also performed in the range 0.01÷35 Hz and 20÷80°C, with 1 N static load, 0.05% dynamic strain and a heating rate of 5°C/min. 1mm of initial sample lengths was used for this type of testing.

In both type of DMA experimnts, suitable testing samples were obtained from the pressed composites plates by cutting rectangular section cylynders of 20x7x0.7 mm dimension.

3.6 Morphological analysis

A Leica 420 scanning electron microscope (SEM) was used to characterize the composites. Samples taken directly from the masterbatch the composite granulates were obtained by cutting with a razor blade to cause fracture. SEM images were captured on the surface of the fractured region.

The surface of composite films, instead, were more efficiently analyze through a Leica AZ16 APO optical microscopy (OM).

3.7 Film preparation

As described upwords, the let downs of the masterbatches were obtained by melt-mixing with pure PP at different weight composition.

The extruded strands were then pelletized and re-extruded in a COLLIN single screw extruder which is coupled with the machine COLLIN TEACH LINE BL50T to prepare blown films of PP/CNT at different concentration.

The most important specifications concerning the melt-mixing and the blown film extrution are listed in Table 1.

The melt temperature was kept at 220°C and the throughput at 2 kg/h (45 rpm). The air pressure in the bubble was controlled in a way that the blow-up ratio, defined as $BUR=R/r_0$ were R is the radius of the blown-up bubble, r_0 that of the anular die, was adjusted to the value of 2.

The take-up ratio, defined as $TUR=v_T/v_0$ where v_T is the speed of the take-up device, v_0 the velocity of the melt exiting the die, was mantained constant to 40.

The frost line of the melt was set to a height of 7 cm above the die outlet by a corresponding adjustment of the cooling system.

Table 1: Processing parameters and abbreviations for extrusion and blown extrusion

Sample	wt % CNT	Extrusion			Blown extrusion			
		T profile [°C]	Rot speed [rpm]	D_{die} [mm]	T profile [°C]	Rot speed [rpm]	$Dint_{die}$ [mm]	$Dest_{die}$ [mm]
PP	0	210-210-220-220-220-220-220-220-220	30	1	210-220-220-220	45	28	30
PP1	1	210-210-220-220-220-220-220-220-220	30	1	210-220-220-220	45	28	30
PP3	3	210-210-220-220-220-220-220-220-220	30	1	210-220-220-220	45	28	30
PP5	5	210-210-220-220-220-220-220-220-220	30	1	210-220-220-220	45	28	30
PP10	10	210-210-220-220-220-220-220-220-220	30	1	210-220-220-220	45	28	30

The homogeneity of the thickness of the film were quantitatively measured by cutting a 1m long film for all materials and measuring the thickness on at least five positions every 20cm. The bubble stability was instead assessed visually.

In Table 2 the measured thickness and diameter with relative standard deviation along with the assessments of the bubble stability are reported for PP and composite films.

Table 2: average thickness and diameter of PP and PP/CNT composite films

Sample	d [mm]	s [mm]	Stability
PP	147	0.4	good
PP1%	142	0.5	good
PP3%	148	0.3	good
PP5%	139	0.4	good
PP10%	133	0.6	good

CHAPTER 4:Results and discussion

4.1 Chemical-physical analysis (DSC, TGA)

The effects of CNTs on the crystallization of PP are analyzed by non-isothermal DSC experiments. In Figure 17 a comparison of the dynamic thermograms obtained on pure PP and CNTs/PP composites is reported. Also, the crystallization peak (Tc), the apparent melting temperature of crystallized samples (Tm) and the glass transition temperature (Tg) as well as crystallization enthalpy (ΔH) as a function of weight CNT content are reported in Figures 18-21.

It can be noticed that when cooled at 10°/min, the pure polypropylene crystallized at 110°C, while the crystallization in 1 wt.% CNTs/PP composites occurred at 125°C. The addition of CNT content higher than 3 wt% still affect the Tc that increases almost linearly with CNT wt content.

A relevant effect is visible on the melting temperature (from ~150° to 155°C) for the addition of carbon nanotubes in the PP matrix and the glass transition temperature increases almost linearly with wt.% of CNT of almost 10°C from ~ -22°C of the pure PP to -12°C for the PP/masterbatch.

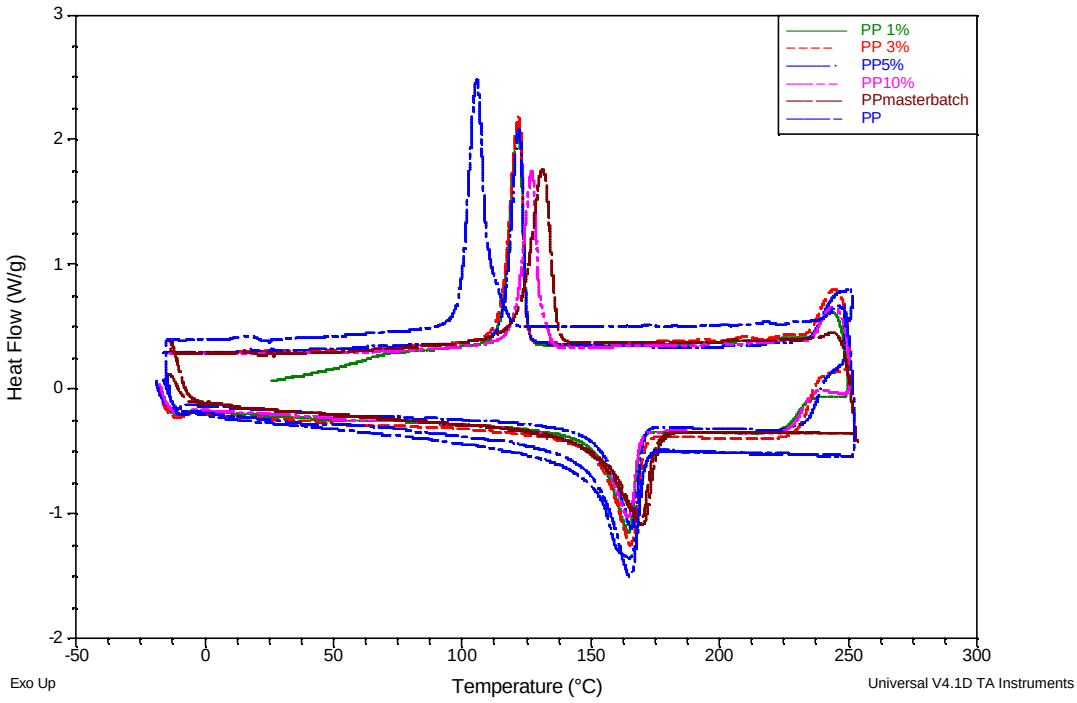

Figure 17: DSC thermograms of pure PP and PP/CNT composites

Figure 16 shows that both the melting and crystallization peaks in PP/CNT composites are narrower then the pure PP and the full width at half maximum of crystallization peaks for PP is greater than that of PP/CNTs. Narrower crystallization and melting peak suggest a narrower crystallite size distribution in the CNT/PP composite as compared to pure PP.

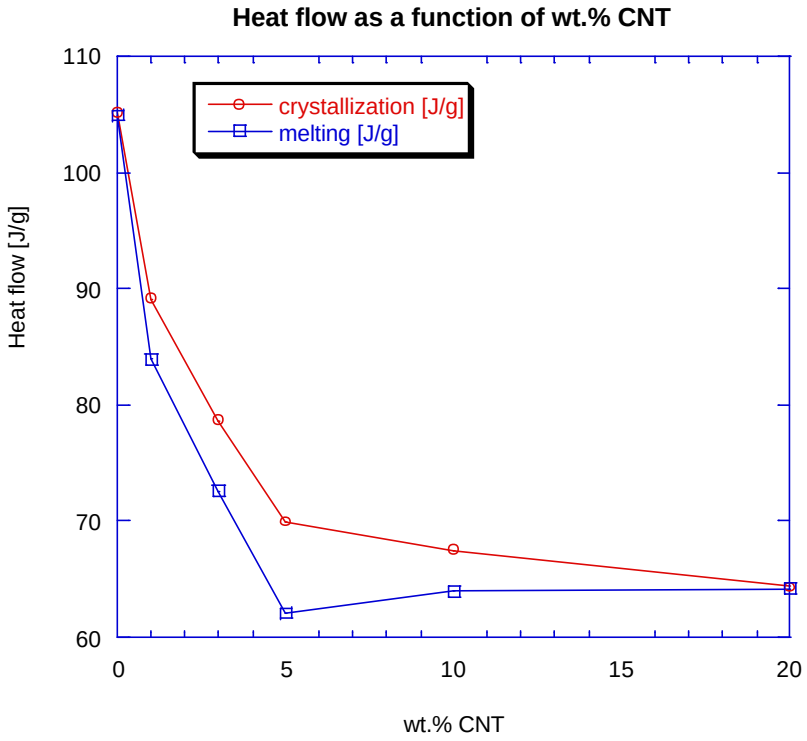

Figure 18: Melting and crystallization heat flow as a function of wt.% CNT

Higher thermal conductivity of the carbon nanotubes with respect to that of the polymer, at least in part may justify the sharper crystallization and melting peaks, as heat distribution will be more uniform inside the samples containing the carbon nanotubes.

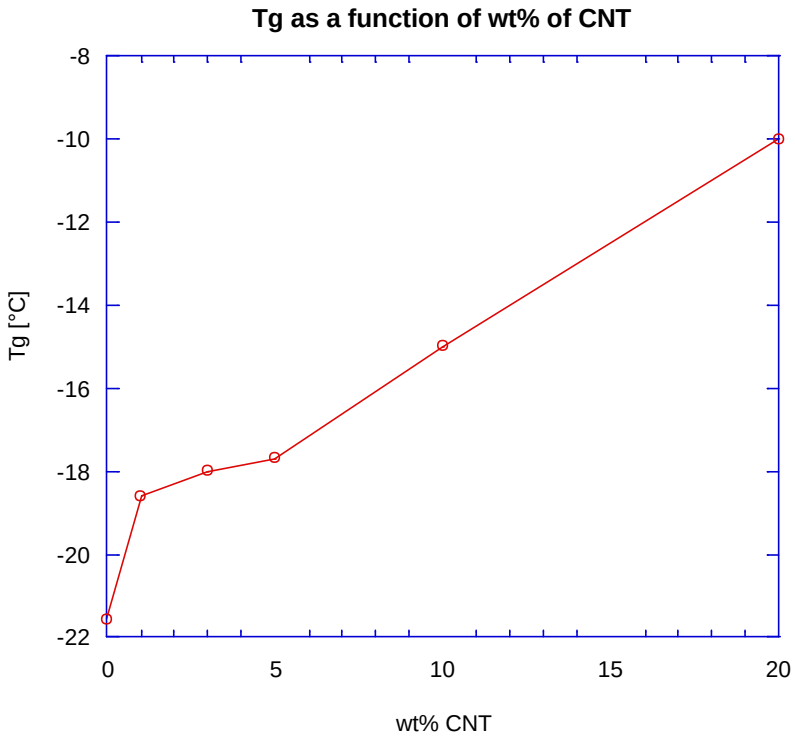

Figure 19: T_g variation against wt.% CNT

The observed dynamic crystallization behaviour shows the positive effects of nanotubes on crystallization kinetics of PP. In particular, Figure 19 confirm that the addition of CNTs in the polymer matrix produces an increase in the crystallization temperature. The relative shift of the Tc is the evident at the lowest reinforcement content with a slow but continuous further increase with CNTs content. These results confirm that the addition of a low concentration of nanotubes enhances the nucleation process on PP crystallization. Crystals within the polymer will increase selected mechanical

properties but it is more important to have orientation in combination with crystallization.

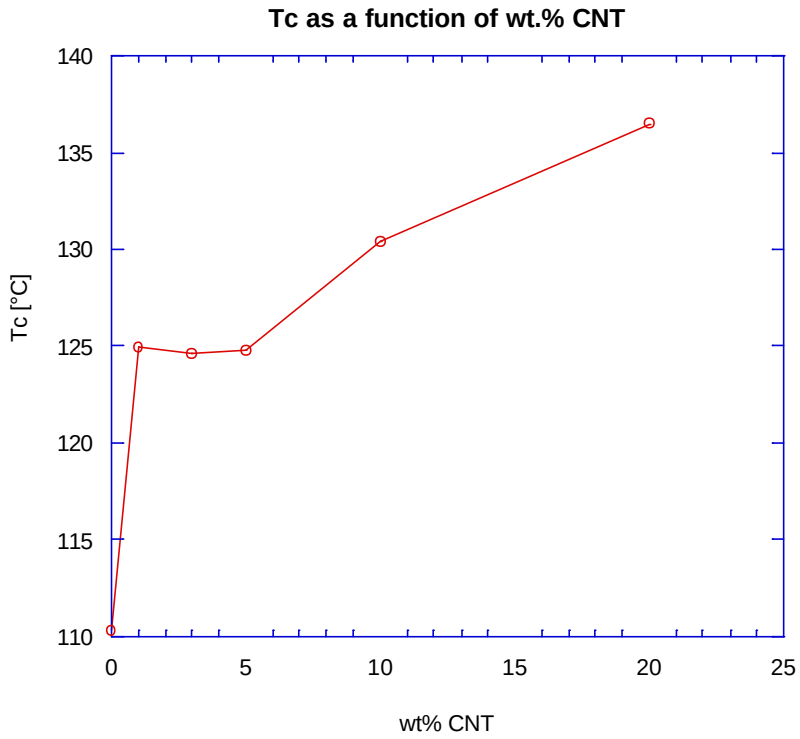

Figure 20: Tc variation against wt.% CNT

The decrease of ΔH with increasing the nanotubes content can be directly attributed to the proportional reduction of PP concentration in the composites. Furthermore, no significant changes in the melting point of PP phase are detected in the composites.

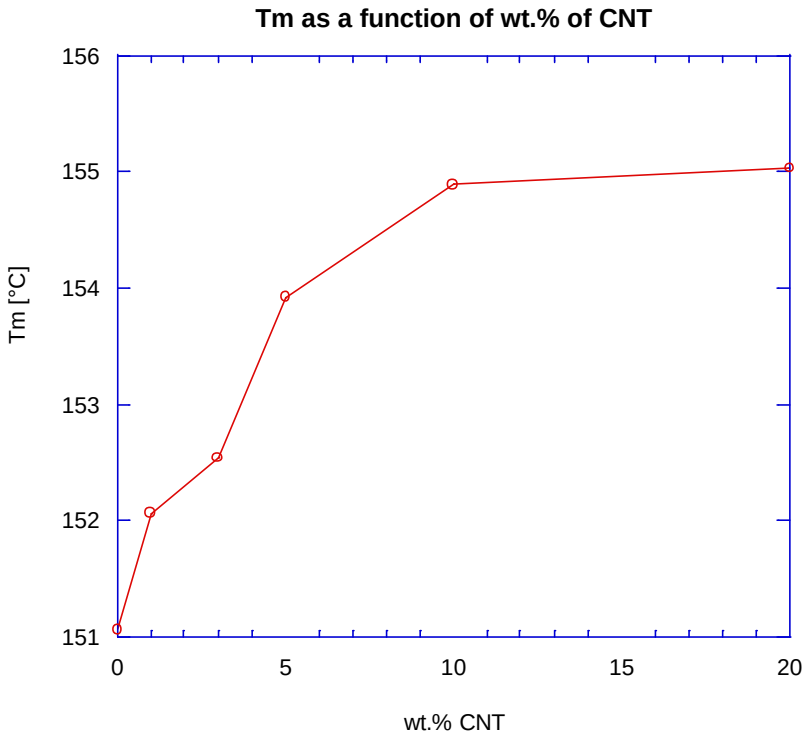

Figure 21: T_m variation against wt.% CNT

The effect of CNT on the thermogravimetric behavior of PP were analyzed through TGA experiments. The comparison of weight loss % for the PP/CNTs composites as a function of temperature is reported in Figure 22. These results show that PP degradates with a single narrow degradation stage at around 355°C. This stage corresponds to he thermal degradation of PP initiated primarily by thermal scissions of C-C chain bonds accompained by a transfer of hydrogen at the site of scission [...]. The results of the PP/MWNT samples also show single

degradation stage, but the temperatures at sign change are about 50°C higher than that of PP, ranging from ~355°C for PP up to ~415°C for PP10%. This increase in the degradation temperature is an indication of an improvement in the thermal stability of PP. Three are the main reasons to justify this behaviour in the thermal stability: (1) the uniformly dispersed carbon nanotubes presumably provided thermo-oxidative stability in the vicinity of the tube surface; (2) the enhanced thermal conductivity of the composite can facilitate heat transport and thus increase its thermal stability [...]; (3) like fullerene (C_{60}), carbon nanotubes possibly can lead to the formation and stabilization of the CNT_bonded macroradicals [...].

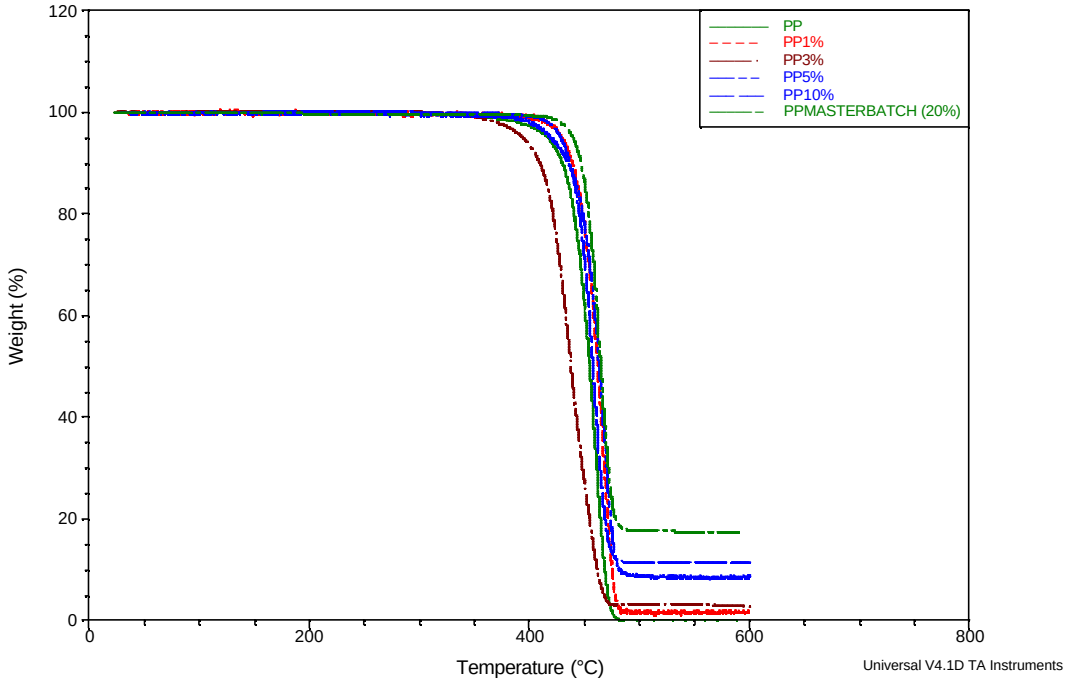

Figure 22: TGA weight loss % versus temperature for PP and PP/CNT composites

The residual weight percent in the TGA study of PP/CNTs composites reported in Figure 24 above 500°C should represents the weight of the CNTs. Discrepancies from the theoretical line may be ascribed to the possible presence of impurities in the carbon nanotubes. In the case of our materials, discrete agreement with the linear prevision of the residual % (R=0.97095) indicates acceptable level of purity of the adopted carbon nanotubes.

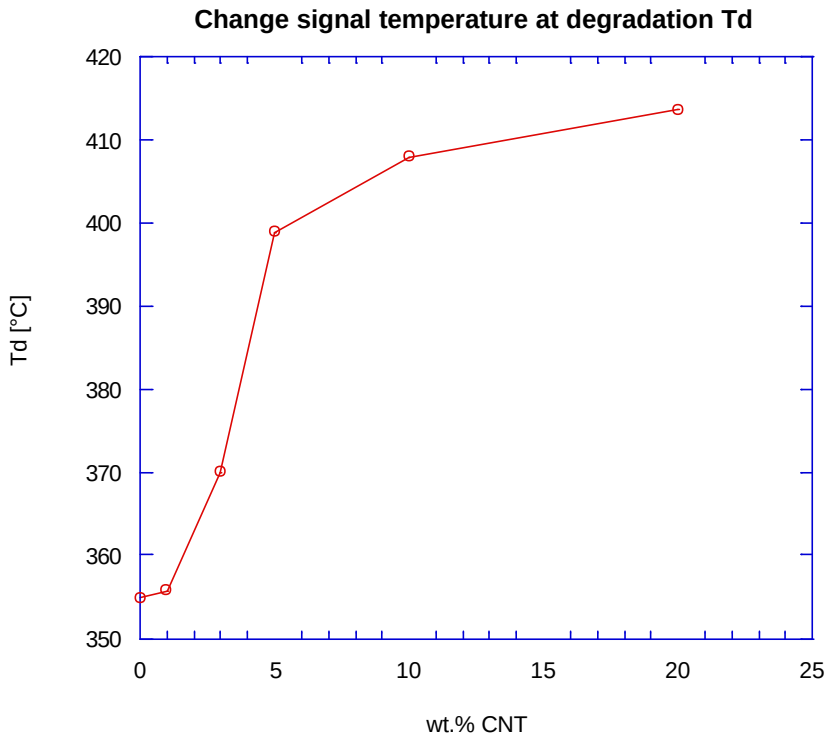

Figure 23: Variation of degradation temperature T_d against wt.% CNT

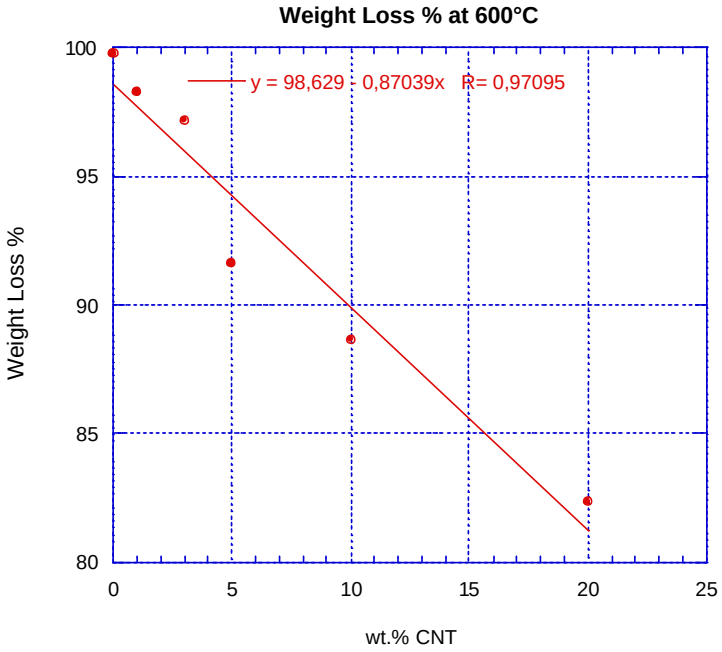

Figure 24: Weight loss % at 600°C against wt.% CNT

4.2 Mechanical and dynamic-mechanical characterization

Carbon nanotubes can be assumed as ultimate carbon fibers. The mechanical properties of nanotubes (strength, stiffness) is expected to approach that of ideal carbon fiber, which has the perfect orientation of defect-free grapheme layers along the fiber axis. Theoretical predictions on single-walled nanotubes (SWNTs) suggest that the Young's modulus should be close to that of the inplane elastic modulus of graphite (1060 GPa) and the value of tensile strength would be ~200 GPa. For multi-walled nanotubes (MWNTs), the strength will be limited by the ease with which individual graphene cylinders slide with respect to each other. Experimental measurements on individual MWNTs suggest values for Young's modulus around 1000 GPa, which corresponds to one of the stiffest materials known.

Thanks to their high aspect ratio, high modulus and strength, nanotubes are promising fillers in polymer composites. If load can be effectively transferred then the modulus of the composite should be similar to that of randomly oriented short fiber composite containing fibers of extremely high modulus and strength. In addition, the high

surface area of nanotubes creates a large interfacial region which can have properties different from the bulk matrix. There is, infact, a bound polymer layer of low mobility, in nanoparticulate polymer composites.

Load transfer depends on the interfacial shear stress between the fiber and the matrix. A high interfacial shear stress will transfer the applied load to the fiber over a short distance and a low interfacial shear stress will require a long distance. Three are the main mechanisms of load transfer from a matrix to a filler. The first is micromechanical interlocking: this could be difficult in nanotubes composites due to their atomically smooth surface. The second is chemical bonding between the nanotubes and matrix. The third mechanism is a weak van der Waals bonding between the fiber and the matrix. In order to assess the success of nanotubes as fillers, a key issue is represented by the load transfer. This latter presents results which highlight the peculiarities of nanotubes system when used as mechanical reinforcement in polymer composite.

In the present study, the tensile properties of PP/CNT composites were investigated through quasi-static tensile tests. In particular, tensile tests were performed eiher on suitable composite sample plates either on film samples, in

order to analyze the effect of moelecular and/or carbon nanotube orientation on the mechanical properties of PP.

The results of the tensile tests in terms of Young's modulus, yield stress and strain of the plates and films with the respective standard deviations, corresponding to an average of at least five samples tested for each type of films and plates, are reported respectively in Tables 3. In the next paragraphs the mechanical properties resulted from these tests are discussed for the two respective cases of composite films and plates.

Table 3: Mechanical properties of composite films and plates

Sample plates	**wt % CNT**	**Young's Modulus, E [MPa]**	**Tensile strength at yield, sy [MPa]**	**Percent elongation at break, e_b [mm]**	**Energy per unit volume, W [J/mm ^{3}]**
PP	0	490.5± 0.21	30.3± 0.62	4.60± 0.60	80.400
PP1	1	937.4± 0.45	33.2± 0.72	0.22± 0.43	6.3100
PP3	3	1006.7± 0.56	34.0± 0.59	0.20± 0.96	5.5500
PP5	5	1247.7± 0.73	36.8± 0.48	0.180± 0.59	6.0600
PP10	10	1113.8± 0.30	26.3± 0.20	0.030± 0.49	0.5670
Sample films					
PPTD	0	83.1 ± 0.28	1.74 ± 0.41	1.97 ± 0.13	2.86
PP1TD	1	73.5 ± 0.16	1.56± 0.12	1.29 ± 0.31	1.76
PP3TD	3	87.3 ± 0.14	1.80 ± 0.19	0.21 ± 0.39	0.32
PP5TD	5	239.5 ± 0.39	3.87 ± 0.26	0.12 ± 0.42	0.38
PP10TD	10	95.6 ± 0.10	1.49 ± 0.10	0.10 ± 0.28	0.14
PPBD	0	55.2 ± 0.23	1.29 ± 0.21	0.09 ± 0.37	0.09
PP1BD	1	42.2 ± 0.32	0.87 ± 0.35	0.32 ± 0.23	0.40
PP3BD	3	123.1 ± 0.16	4.73 ± 0.26	0.06 ± 0.17	0.23
PP5BD	5	114.0 ± 0.18	3.46 ± 0.22	0.04 ± 0.26	0.11
PP10BD	10	93.0 ± 0.20	1.59 ± 0.18	0.06 ± 0.22	0.08

4.2.1 Mechanical properties of plates

In Figure 25 the average stress-strain curves of at least five samples for each type of prepared composite plates is showed. In Figures 26-28 the increment relative to PP of Young's modulus E and yield stress s_y as well as the energy per unit volume W of the composite plates are reported as a function of the weight fraction percent of CNT. The value of the Young's modulus is very useful because it is an intrinsic material property, it is directly related to the crystallinity and bond orientation of the molecules and/or the filler and if those structural properties are increased, so must do the modulus. The strengths shown by each material are extrinsic properties that depend only on the weakest part of the material during the elongational stress. As can be observed, the addition of CNT determines a relevant increment of the rigidity and a slight increment of the ultimate properties (yield strength) along with a detriment of the ductility of the material.

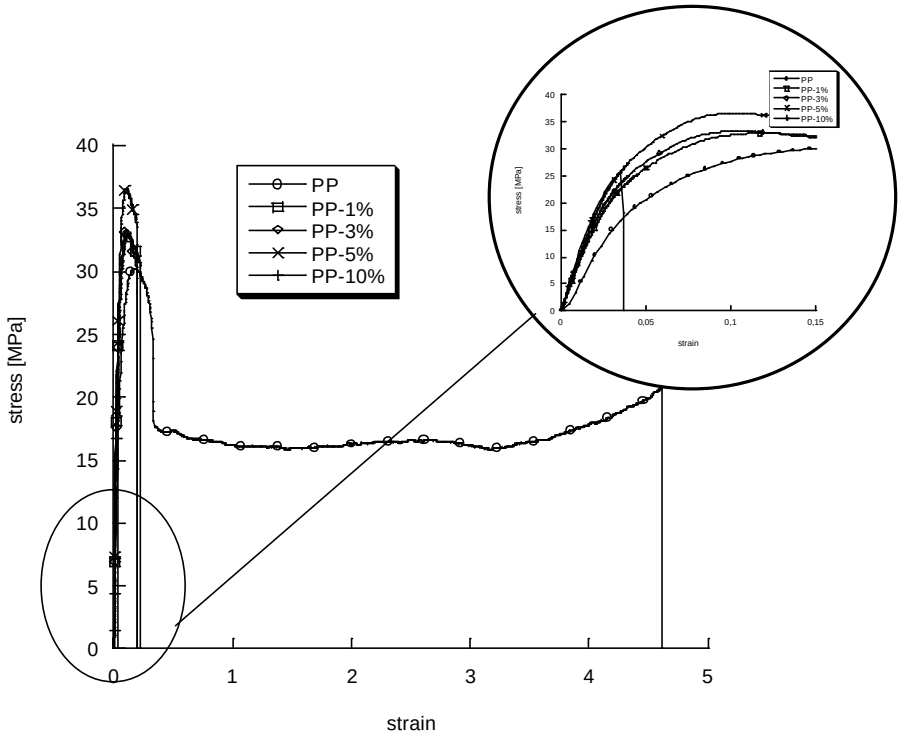

Figure 25: Typical averaged stress-strain curves of PP and PP/CNT composites.

In particular, the mechanical tests performed on the plates showed that even by adding 1 % of CNT a strong increment of

the Young Modulus of almost 90% occours with respect of the pure PP. Higher concentration of CNT further increase the stiffness of the composite reaching an remarkable increment for 5 and 10wt% of CNT (113 and 127%). On the other hand, the addition of CNT also determine a detriment of the ductility of polymer which can be deduced by observation of Figure 26 in which the increment relative of the area under the stress-strain curve is reported aginst the wt% of CNT. This area represents the energy per unit volume dissipated by the sample during the deformation and is indicative of the work to failure and thus the fracture toughness of the material.

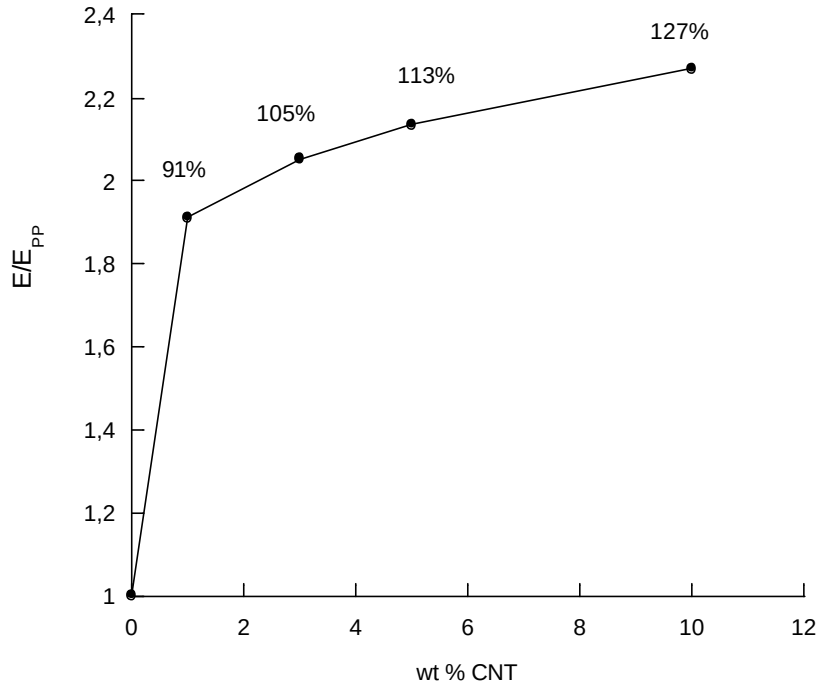

Figure 26: Increment relative to PP of Young's modulus E against wt.% CNT for PP/CNT composite plates

It can be noticed that the addition of CNT in the polymer matrix determines a detriment of the toughness of the material for any value of CNT content indicating that the material has became much more rigid but, on the other hand, more fragile.

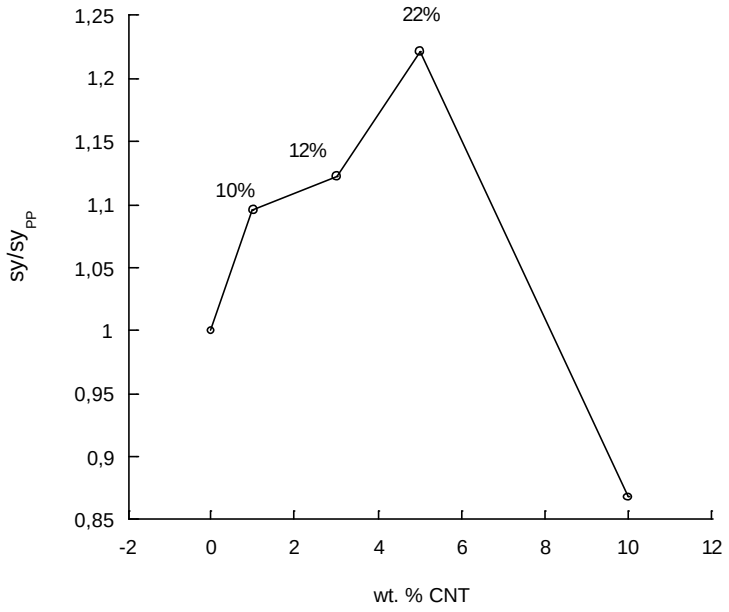

Figure 27: Increment relative to PP of strength at yield against wt.% CNT for PP/CNT composite plates

The remarkble improvement of the Young's modulus occurred at even 1 wt% may be related to the possible presence of a network structure (percolation) of the CNT. Percolation means that at least one pathway of connected nanotubes exists in the sample which (in case of conductive fillers allows to flow of charge through the sample).

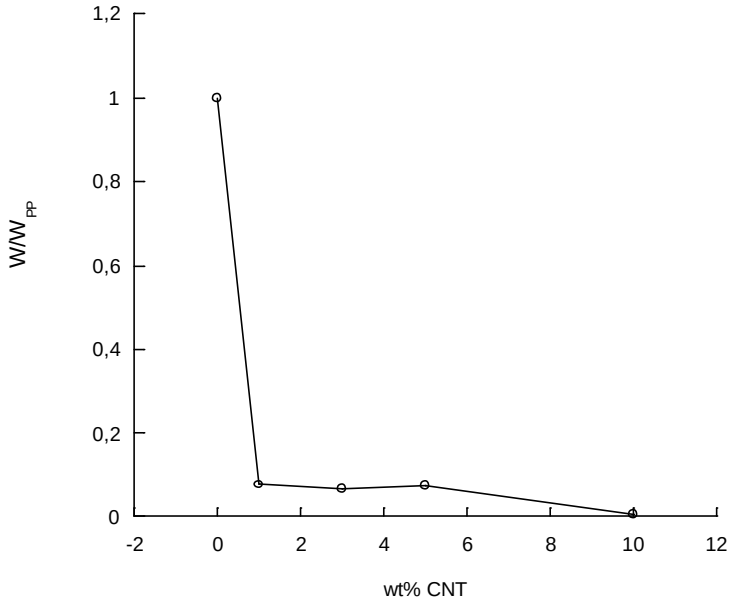

Figure 28: Increment relative to PP of energy per unit volume against wt.% CNT for PP/CNT composite plates

Furthermore, when the concentration of CNT reaches too high levels, there might happen an agglomeration which exerts a significant weakening effect to the reinforced composites. This effect is likely to be due to the high shear stress occurring during the melt mixing as a consequence of the very high viscosity of the composite which might provoke the formation of low molecular weight molecules inside the composites and a subsequentially weakening effect on the mechanical properties.

.

Feng et al. [146] studied the constitutive relation and failure behaviors of carbon nanotube-reinforced composites using methods of micromechanics and nanomechanics. They first examined the factors that influence the overall mechanical properties of carbon nanotube composites, including the weak bonding between carbon nanotubes and matrix, the curviness and agglomeration of carbon nanotubes and second established a hybrid continuum/micromechanics/atomistic method to investigate the defect nucleation and fracture behaviours of CNTs in polymers.

Three are the main effects on the stiffening mechanisms of carbon nanotubes: the waviness effect, the agglomeration effect and the interface effect.

With regarding to the waviness effect, because CNTs have very low bending stiffness due to the small tube diameter (~ 1 nm), most CNTs in composites exist in a curved state. Feng et al. [146] presented a theoretical model to examine the waviness effect of curved CNTs on the elastic properties of CNT-reinforced composites. They observed that the modulus of carbon nanotubes composites decreases rapidly as waviness increases.

As also discussed in the introductive section, a key issue in producing superior CNT composites is the possibility to control deagglomeration and dispersion of CNT in polymer matrices which are directly correlated to the hoped properties (conductivity, mechanical, etc). In most of the cases homogeneous dispersion of nanotubes in hindered by both the syntesis induced “entangled” and aggregated” structures of nanotubes as well as the tubes tendency to form agglomerate in the polymer matrix, due to the intermolecular van der Waals interactions between them, their low bending stiffness and high aspect ratio. Feng et al., in the same work, developed a model to study the influence of agglomeration of CNTs on the effective elastic moduli of CNT-reinforced composites. The spatial distribution of CNTs in the matrix was assumed to non-uniform such that some local regions have a higher concentration of CNTs than the average volume fraction in the material. Those regions with concentrated CNTs were assumed to have spherical shapes, and considered as “inclusions” with different elastic properties from the surronding material. Thus, the CNT-reinforced composites were considered as a system consisting of inclusions of sphere shape embedded in a hybrid matrix. Both the matrix and inclusions contained CNTs. They estimated the effective elastic stiffness of the composite

containing either straight or curved CNTs by using this micromechanical model. They found that the agglomeration of CNTs exert a significant weakening effect to CNT-reinforced composites.

Interfaces also play a significant role in mechanical and physical properties of nanostructured materials. For CNT-reinforced composites, the high surface area of CNTs creates a large interfacial region, which has properties different from the bulk matrix. For a weak interface, the effective elastic moduli are insensitive to the interface thickness. These results can be easily understood because the axial elastic modulus of CNTs in much higher than that of the polymer matrix and the interface phase, and so the stiffening effect of CNTs is predominated by the elastic constants, geometric parameters, spatial distribution and microstrucures of CNTs in composites.

4.2.2 Mechanical properties of blown films

In Figures 29, 30 the typical stress-strain curves of the prepared composite films for the two directions are shown. These values correspond to an average of at least five samples which are tested for the films in the two directions (LD and

TD) of the applied stress. In Figures 31-34 the Young's modulus E, yield stress s_y and elongation at break $\varepsilon_{b,}$ as well as the energy per unit volume W of the blown films are reported as a function of the weight fraction percent of CNT for the two directions. These results are also resumed in Table 2 where also the weight compositions and the relative abbreviations of the prepared material are reported. Furthermore, in Figures 33-36 the increment relative to PP of the same properties are reported for the two directions of testing as a function on the wt% of CNT.

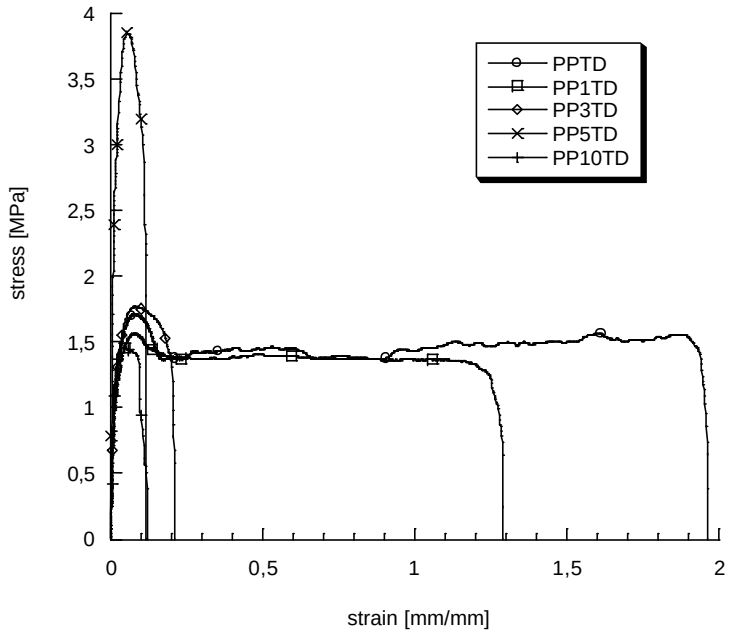

Figure 29: Typical averaged stress-strain curves of PP and PP/CNT composites film in the Take-up direction (TD)

The first issue which worth noticing in these results is that, during the tensile tests, the composite films showed different responses in the two directions (TD and BD). To understand this behaviour one should consider what is the stress field acting on the film during the blowing extrusion.

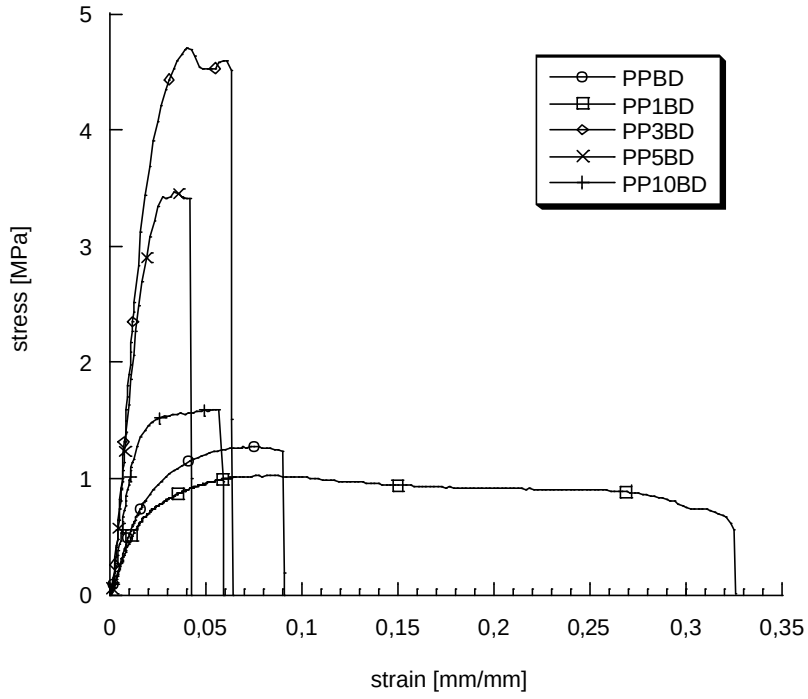

Figure 30: Typical averaged stress-strain curves of PP and PP/CNT composites film in the Blow-up direction (BD)

When the polymer exit the tubular die it is mainly subjected to a couple of external forces: Fb, associated to the internal air pressure which causes it to expand in the radial direction and Ft associated to the take-up of the film for the collection. This extension of the melt in both the radial and down-stream direction stops at the freeze line (frost line) at which the polymer is already crystallized and is no more subjected to deformation. If the combination of these two forces gives as

results a predominant orientation of the macromolecules at 45° with respect the two directions then the mechanical properties of the film will be similar in both TD and BD, otherwise discrepancies in the mechanical properties will be displayed. Furthermore, we have to consider that, for the composite films, during the blowing process the molecular biorientation is also influenced by the presence of the CNT which might represent physical constraints to the free movement of the molecules. In consideration of the type of stress filed which occurs during this process, the spatial distribution of the CNT in the matrix is expected to be non-uniform, and their orientation strongly dependent on their concentration in the matrix.

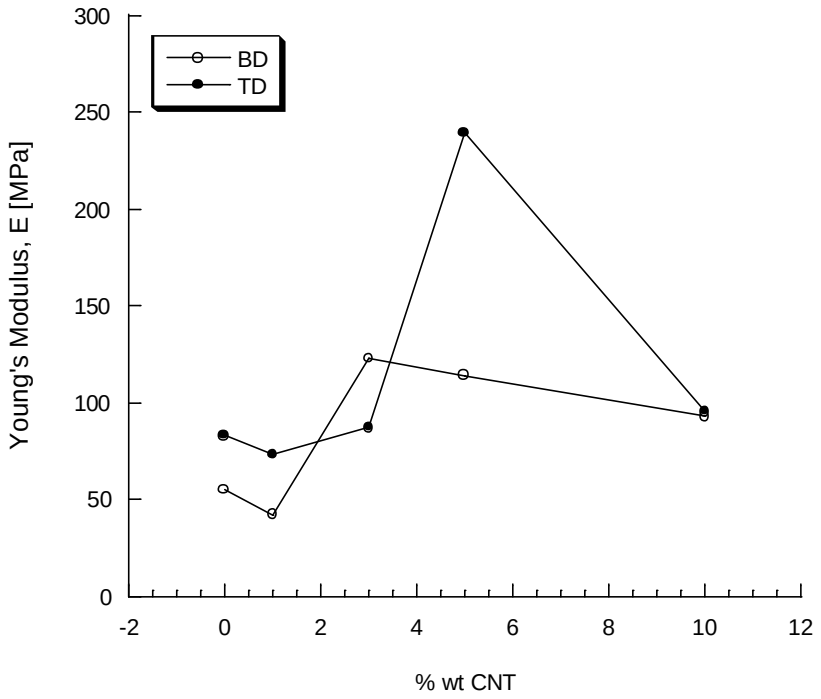

Figure 31: Comparison of Young's modulus versus wt.% CNT in the two direction TD and BD

If we take a look to graph reported in Figure 31, we can observe that for the pure PP the modulus in the take-up direction (TD) is slightly higher then in the blow-up direction (BD) while the elongation at break in the TD is order of magnitude higher the BD. This situation indicates that during the blown film extrusion the molecules were subjected to a predominant orientation in the TD than in the BD which has rendering the film much more ductile in the TD then in BD. In

the BD the addition of 1 wt% of CNT determines a slight decrement of both the Young Modulus E and the strength at yield s_y (Figure 31,32) while a strong increment of the rigidity (123%) along with also an excellent increase of the strength (267%) with respect to pure PP is displayed for 3 wt% of CNT. For higher concentration (5 wt%) the increment keeps to decrease (106% and 168%) to drop down for 10 wt% reaching a value almost as high as that of the pure PP. In the TD a slight decrement of both E and the sy is displayed also in this case for 1 wt% of CNT. For 3 wt% these properties are similar to that of the pure PP, while for 5 wt% of CNT a great increment (122% and 188%) is displayed for the composite films. As the CNT content reaches 10 wt% their benefit ends and the mechanical properties reach the values almost as high as that of the PP.

With regarding to the ductility of the films, in the BD this property increases of 233% for 1 wt% of CNT (Figure 31), while for higher concentration it is almost similar to that of the pure PP. A different situation is revealed in the TD, at which the addition of CNT determines a reduction of the ductility for any level of the nanofiller content, even for 1 wt%.

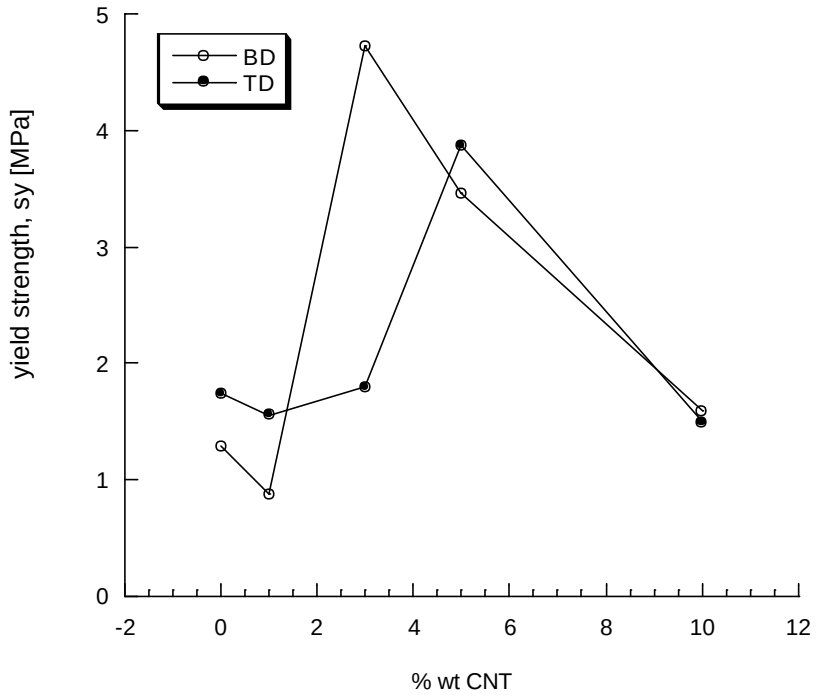

Figure 32: Comparison of strength at yield versus wt.% CNT in the two direction TD and BD

Finally, in the graph reported in Figure 38 the relative increment of the integral area under the stress-strain curve, W/W_{pp}, for each value of CNT content is reported for the two directions of testing. In accordance with the other results, in the TD direction the addition of CNT determines a detriment of the toughness of the material for any value of CNT content indicating that the material in this direction has became much more rigid but, on the other hand, more fragile.

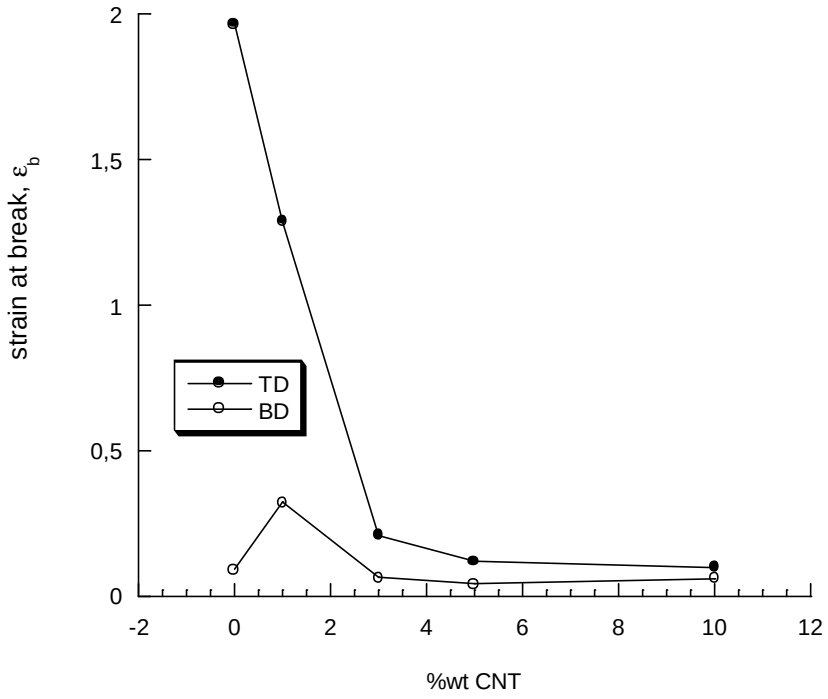

Figure 33: Comparison of strain at break versus wt.% CNT in the two direction TD and BD

In the BD the addition of 1 wt% of CNT determines an excellent increase of the toughness (334%), while for 3% this increment is reduced to 152%. For 5 and 10 wt% of CNT content the increment drops down and this property is almost as high as that of the pure PP.

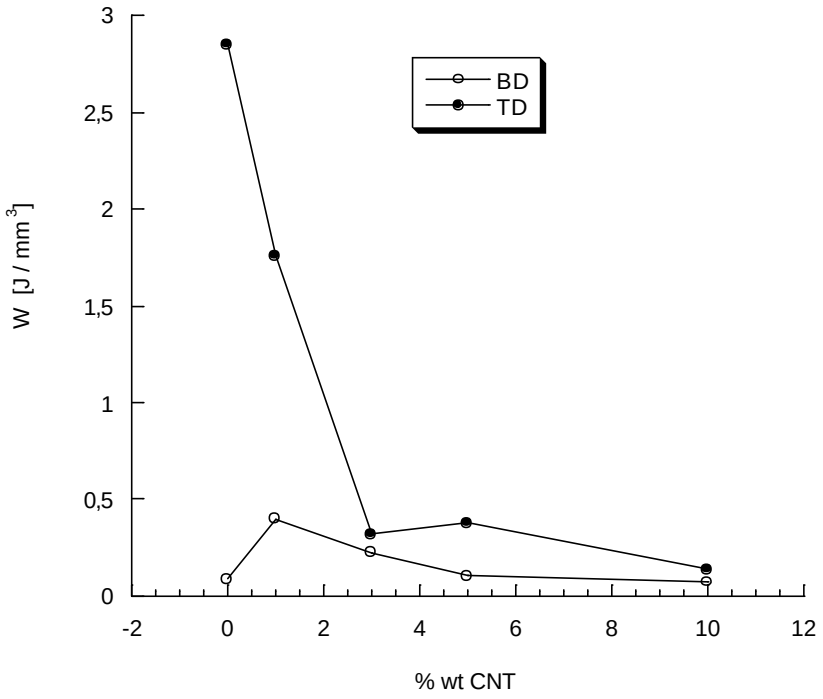

Figure 34: Comparison of Young's modulus versus wt.% CNT in the two direction TD and BD

The excellent improvement of the Young's modulus and strength occurred at 3 and 5 wt% may be related to the possible presence of a network structure (percolation) of the CNT occurring for a CNT content between these two compositions.

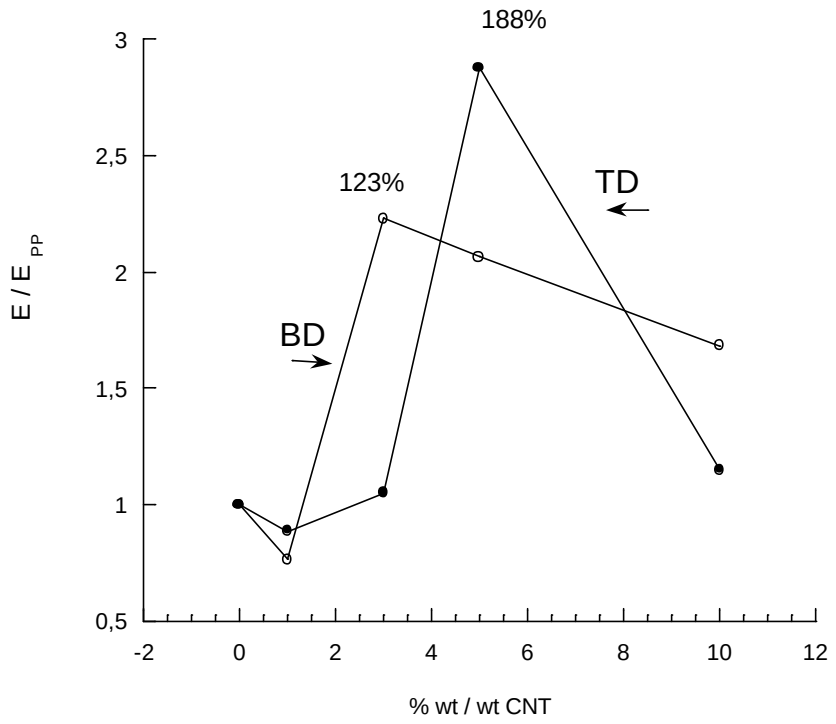

Figure 35: Increment relative to PP of Young's modulus against wt.% CNT for PP/CNT composite films

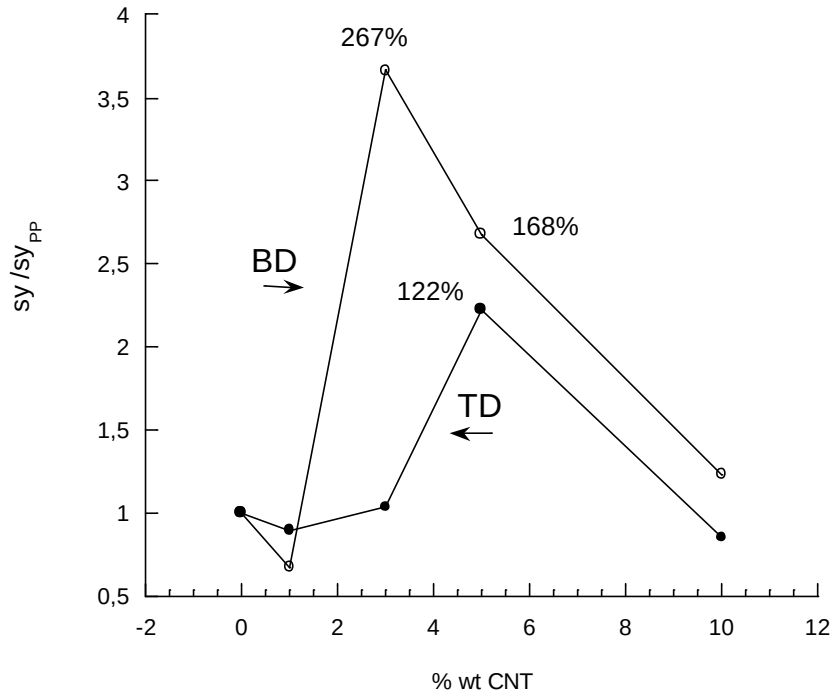

Figure 36: Increment relative to PP of strength at yield against wt.% CNT for PP/CNT composite films

In consideration of the phin thickness concerning the films, for too low concentration of CNT (1 wt%) the network might not form and the nanotubes might be randomly distributed inside the matrix, too far from each other to percolate and in too small amount to act as reinforcing phase. They can be assumed as local regions with higher concentration then the average volume fraction in the material. Their effect in the polymer is that of local defects, becoming “inclusions” or

holes in the PP which act as stress concentrators that lead to the observed strength and strain reduction relative to the pure PP. On the other hand, when the concentration of CNT reaches too high levels (10%) the agglomeration of CNT exerts a significant weakening effect to the reinforced composites, as can be observed in Figures 33-36.

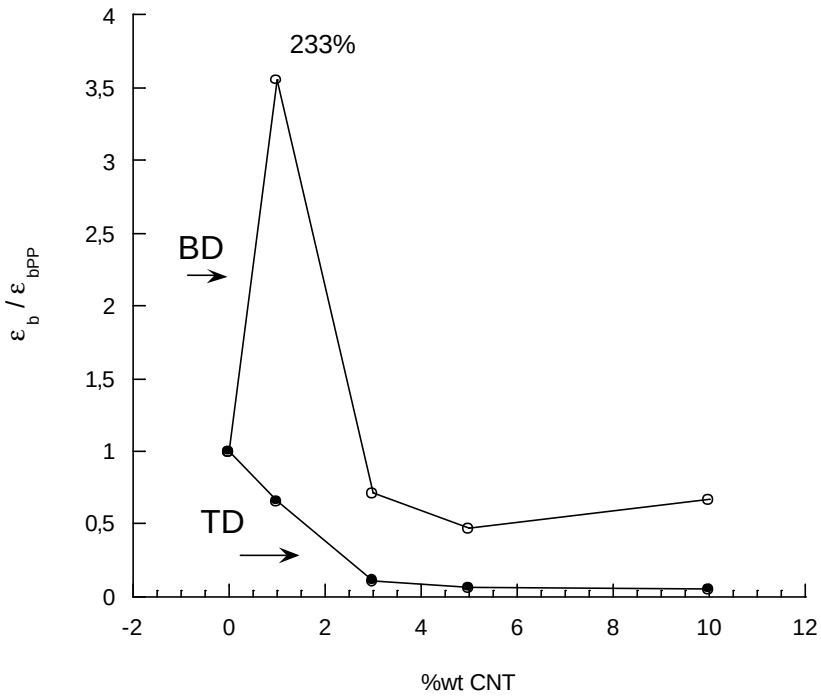

Figure 37: Increment relative to PP of strain at break against wt.% CNT for PP/CNT composite films

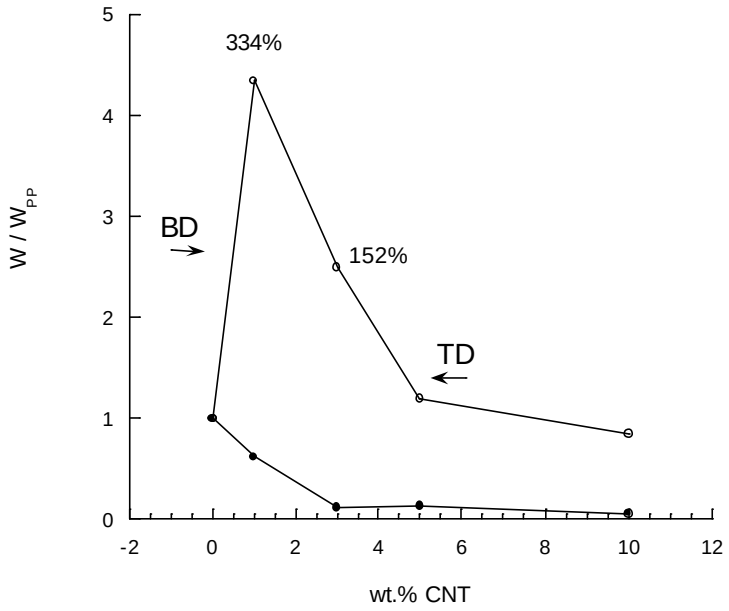

Figure 38: Increment relative to PP of strain at break against wt.% CNT for PP/CNT composite films

4.2.2 Dynamic-mechanical results

Dynamic mechanical analysis (DMA) is a powerful method to investigate the macromolecule chain movement of polymer materials exposed to variation of temperature.

Frequency scan at 1 Hz in the range –0÷110°C and frequency/temperature scan in the range 20÷80°C and 0.01÷35Hz were performed on pure PP matrix and carbon nanotubes composites. In the next paragraphs the results of these two types of measurements will be discussed.

4.2.2.1 Frequency scan

Figures 45 show a plot of the storage modulus E' at 1 Hz as a function of temperature for the various nanotubes compositions. Polypropilene is above its glass transition temperature at room temperature, thus it displays a typical behaviour of semi-crystalline thermoplastic polymer in its glassy state. At low temperature the polymer is in the glassy state and the modulus slightly decreases with increase in temperature but remains roughly constant (around 3.0E+09 Pa). Then the slope changes a the modulus rapidly decreases with the temperature up toa temperature of ~60°C where the slope changes again and the madulus continue to decrease but with less slope. The storage modulus of PP/CNT composites tends to increase with increasing CNT content. This implies the effectiveness of reinforcing effect of CNTs. The maximum value of the storage modulus is reached with 5 wt% CNT loading.

It is displayed in Figures 46,47 the loss modulus E'' and the concomitant relaxation process through the mechanical loss factor tanδ, where it is notable that the unfilled PP passes a maximum around 0°C. The tan δ peak is associated with the soft segment glass transition temperature (Tg). Below the glass transition temperature, the molecular chains of PP are frozen. Above Tg, the mobility of PP chains increases. It can be noticed that, beside the case of PP1%, the

introduction of MWNTs does not effect in a relevant extent the Tg and damping capacity. Two are the phenomena to be considered to better understand the effect of CNTs on the glass transition: on one hand the the well-dispersed SWNTs will restrict the molecular motion, and will lead to an increase in Tg. On the other hand, the increase in microphase separation with the introduction of MWNT will lead to a decrease in Tg because there are less hard segment present in the soft phase hindering the motion of soft segment. This result suggest that the latter play a predominant role in Tg shift. The temperature position of this relaxation process is known to depend on the frequency of the measurement.

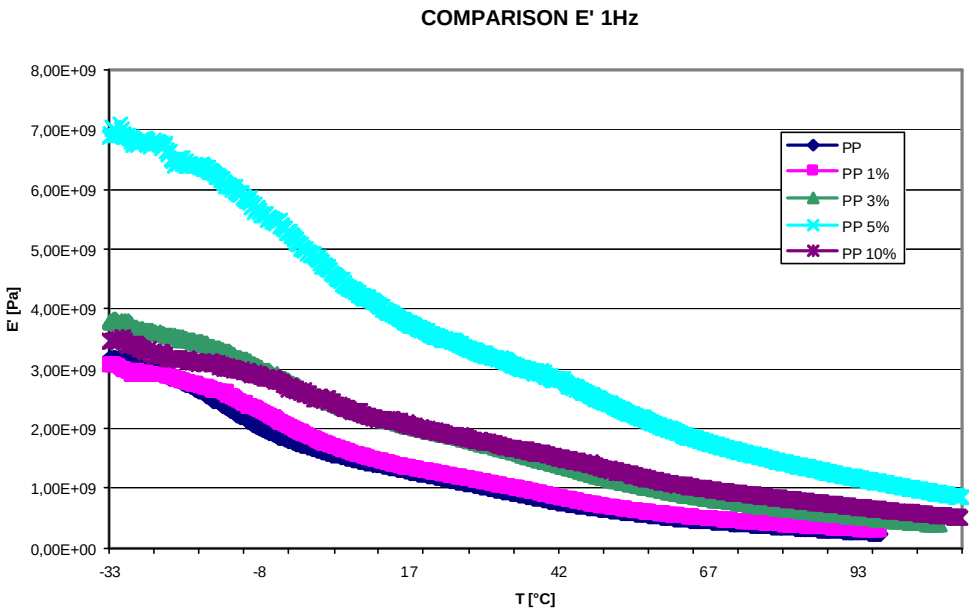

Figure 45: Storage modulus E' at 1 Hz as a function of temperature for PP/CNT composite plates

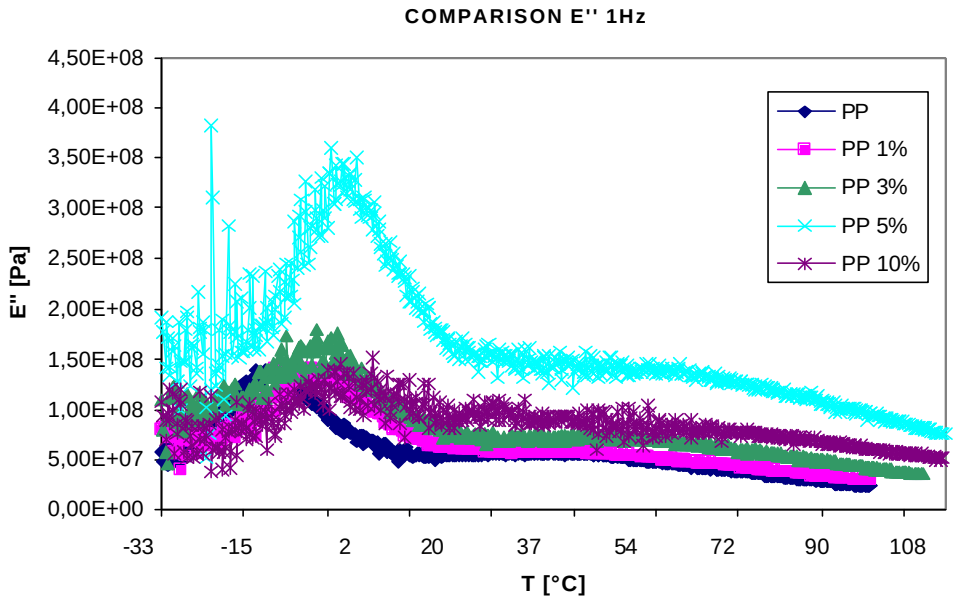

Figure 46: Loss modulus E'' at 1 Hz as a function of temperature for PP/CNT composite plates

Above Tg and highly filled materials, a relevant increase in the composite modulus is observed with 5% of weight fraction of carbon nanotubes. For less concentration the effect of CNT on the dynamic storage modulus is not relevant while, for example, at 5 wt% of CNT the relaxed modulus of the composite is at 25°C is ~3 times higher then that of the pure PP (Figure 48, 49). The increment of E' relatively to PP decreases with temperature, as can be observed in Figure 45 and 49 and at limit at high temperature the bundle of curve tend to overpose to a common plateau around 1,00E+09.

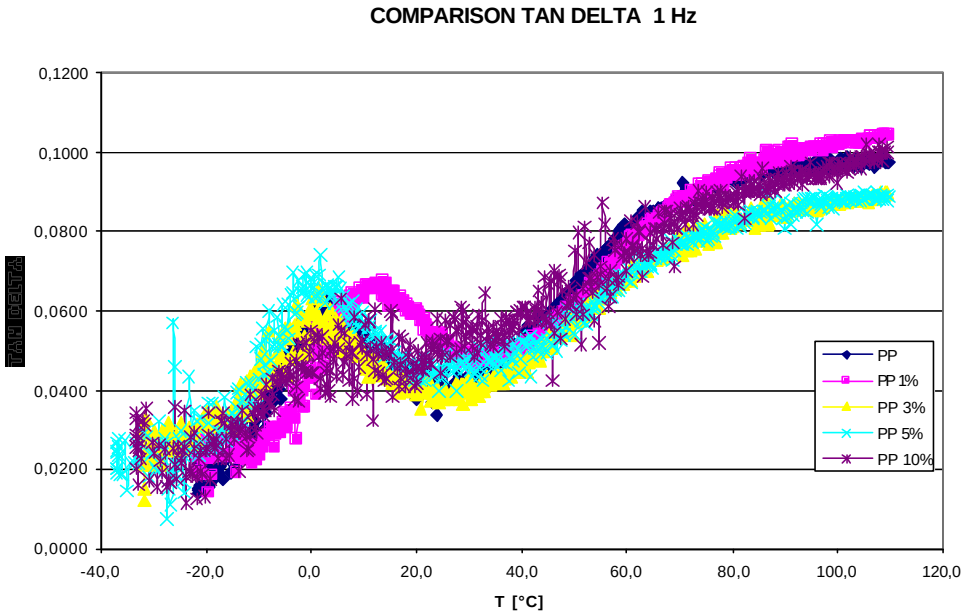

Figure 47: Tan delta at 1 Hz as a function of temperature for PP/CNT composite plates

In addition to their reinforcing effect at high temperature, carbon nanotubes improve the thermal stability of the composite materials. Indeed, whereas the stiffness of the non-reinforced matrix decreases with temperature, the relaxed modulus of composites remains roughly constant up to a temperature which value increases with the filler content. For instance, the modulus of the composite containing 3 wt% of nanotubes drops at –10 whereas the terminal zone occurs at –30°C for the unfilled material. This phenomenon can be most probably ascribed to good interfacial bonding between the filler and the matrix, which prevents irreversible flow of the matrix at high temperature.

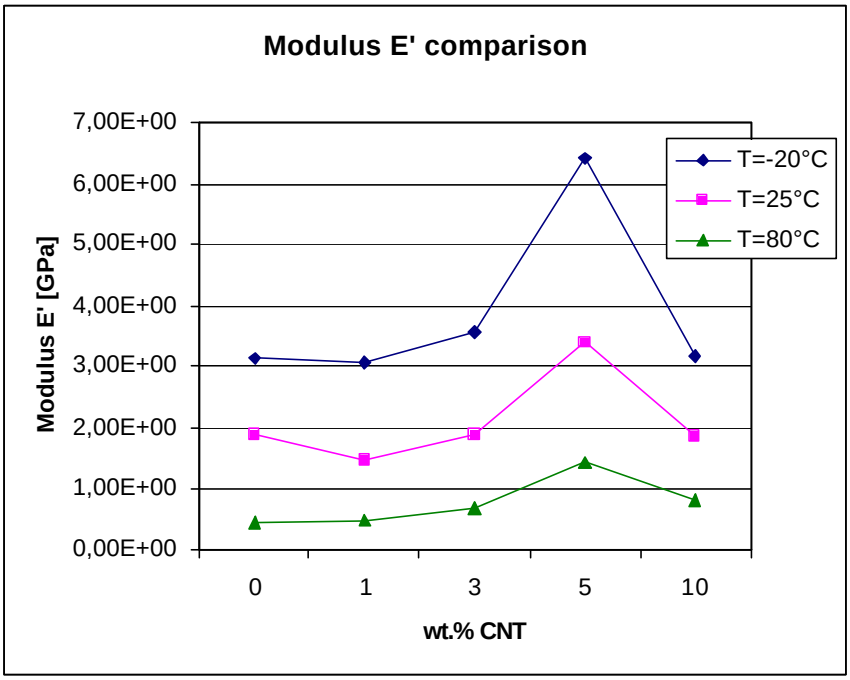

Figure 48: Storage modulus E' as a function of wt.% CNT at different temperatures

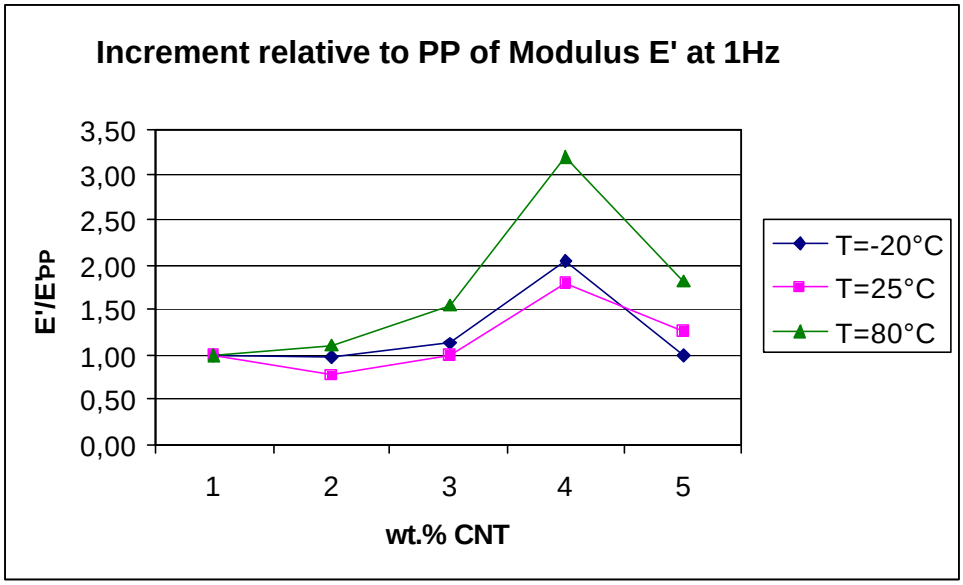

Figure 49: Increment relative to PP of the storage modulus E' as a function of wt.% CNT at different temperatures

4.2.2.2 Frequency/Temperature scan

Frequency/temperature scan in the range 20÷80°C and 0.01÷35Hz were performed on pure PP matrix and carbon nanotubes composites.

In Figures 50-59 the results of these tests are reported in terms of E' as a function of temperature and frequency. These graphs represent a simple visualization of the raw data before the maser-curves are building.

Furthermore, prior to create the master-curves, the values of E' resulted from the frequency scan at 1 Hz were compared to that resulted from the frequency/temperature scan to verify the concordance between the two type of experiments. This verification is showed in Figures 60-64, where the discrepancies between the two measurements are considered acceptable.

Finally, in Figures 65-69 the master curves are reported for each weight composition of CNT. The same curves are then compared with that of the unfilled PP in Figures 70-74.

4.2.2.2 Frequency/Temperature scan

Frequency/temperature scan in the range 20÷80°C and 0.01÷35Hz were performed on pure PP matrix and carbon nanotubes composites.

In Figures 50-59 the results of these tests are reported in terms of E' as a function of temperature and frequency. These graphs represent a simple visualization of the raw data before the maser-curves are building.

Furthermore, prior to create the master-curves, the values of E' resulted from the frequency scan at 1 Hz were compared to that resulted from the frequency/temperature scan to verify the concordance between the two type of experiments. This verification is showed in Figures 60-64, where the discrepancies between the two measurements are considered acceptable.

Finally, in Figures 65-69 the master curves are reported for each weight composition of CNT. The same curves are then compared with that of the unfilled PP in Figures 70-74.

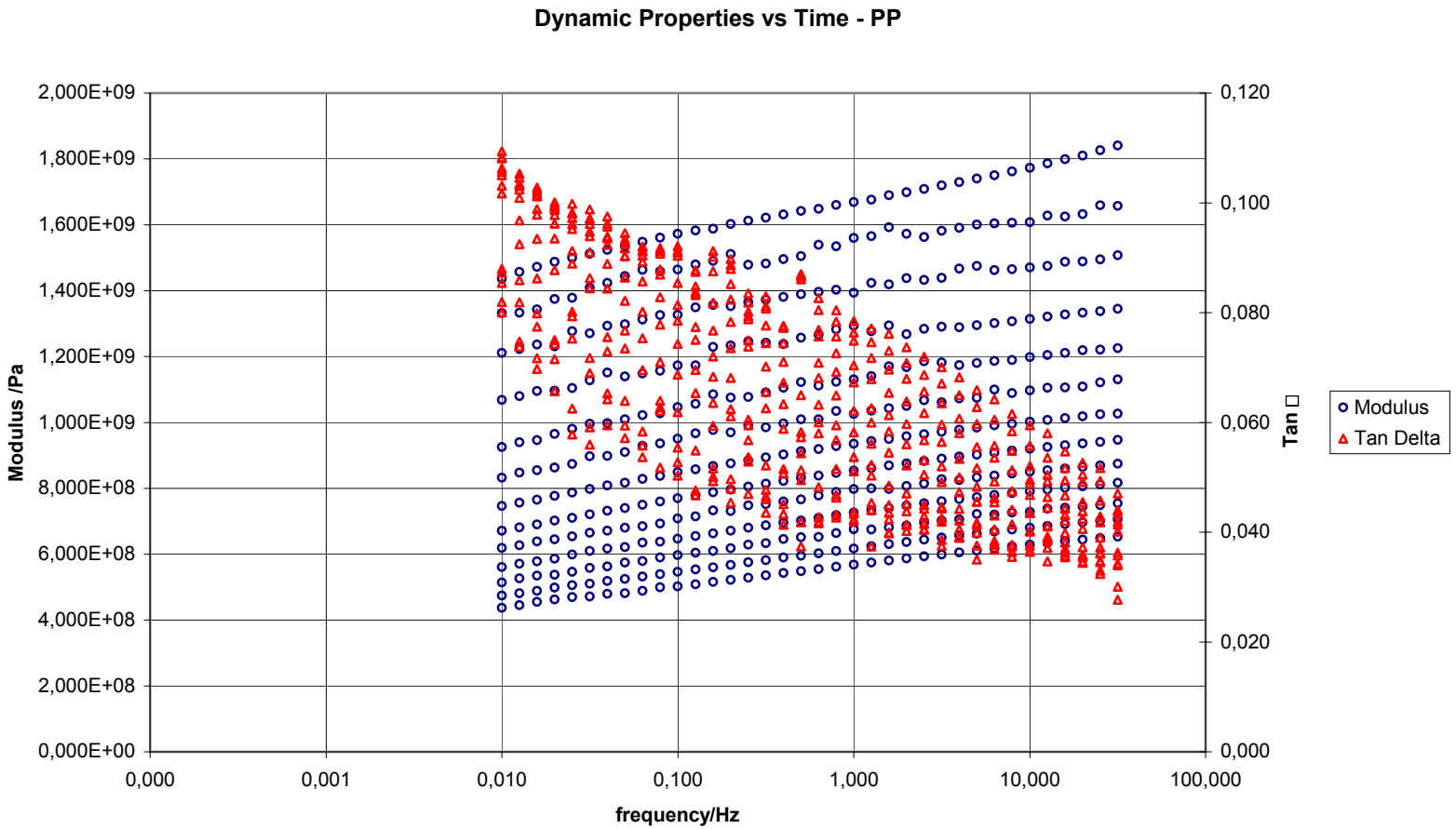
Dynamic Properties vs Time - PP
2,000E+09
1,800E+09
1,600E+09
1,400E+09
1,200E+09
1,000E+09
8,000E+08
6,000E+08
4,000E+08
2,000E+08
0,000E+00
Modulus /Pa
0,120
0,100
0,080
0,060
0,040
0,020
0,000
Tan □
0,000
0,001
0,010
0,100
1,000
10,000
100,000
frequency/Hz
Modulus
Tan Delta

Figure 50

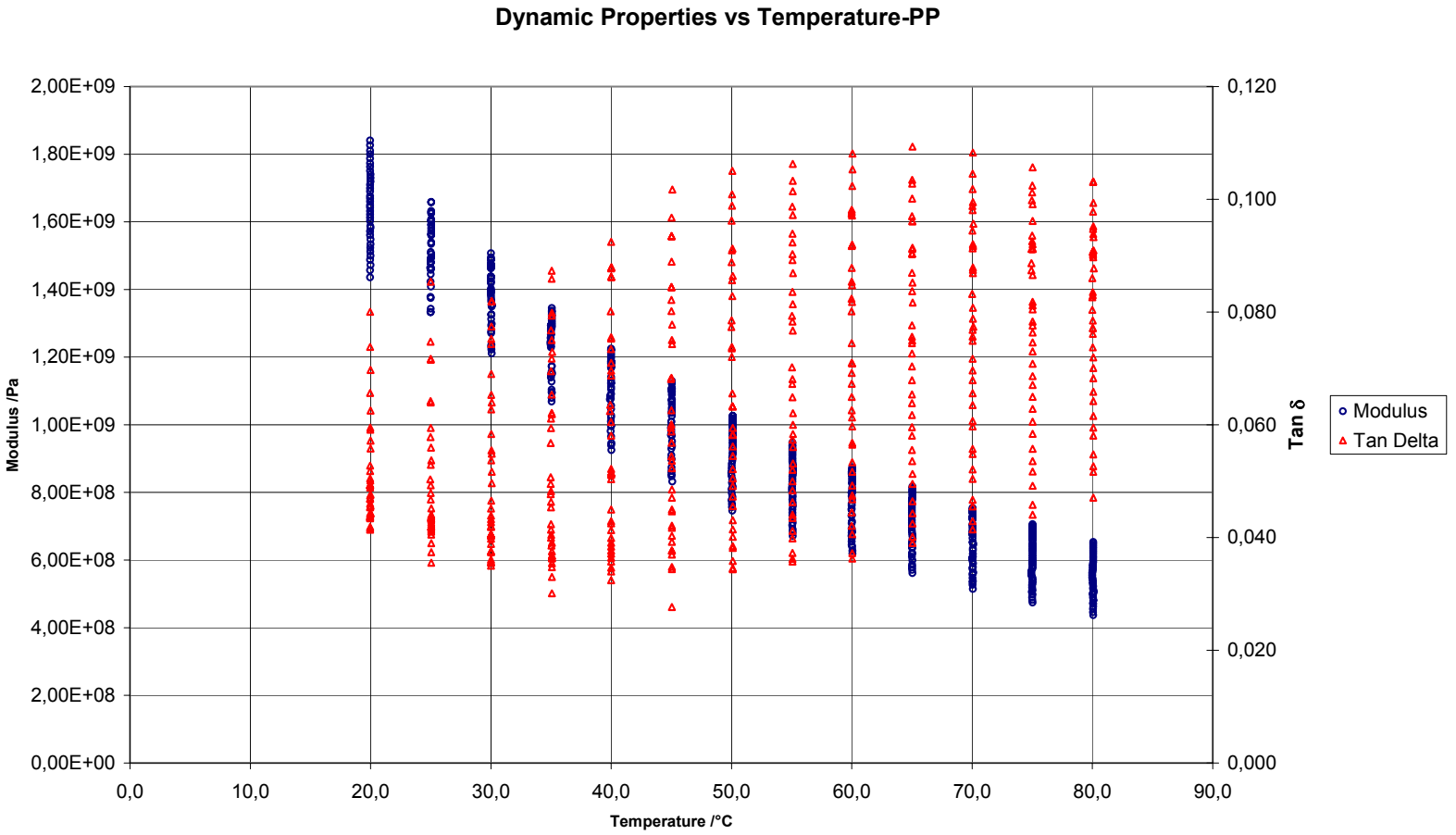
Dynamic Properties vs Temperature-PP
Modulus /Pa
2,00E+09
1,80E+09
1,60E+09
1,40E+09
1,20E+09
1,00E+09
8,00E+08
6,00E+08
4,00E+08
2,00E+08
0,00E+00
Tan δ
0,120
0,100
0,080
0,060
0,040
0,020
0,000
0,0
10,0
20,0
30,0
40,0
50,0
60,0
70,0
80,0
90,0
Temperature /°C
Modulus
Tan Delta

Figure 51

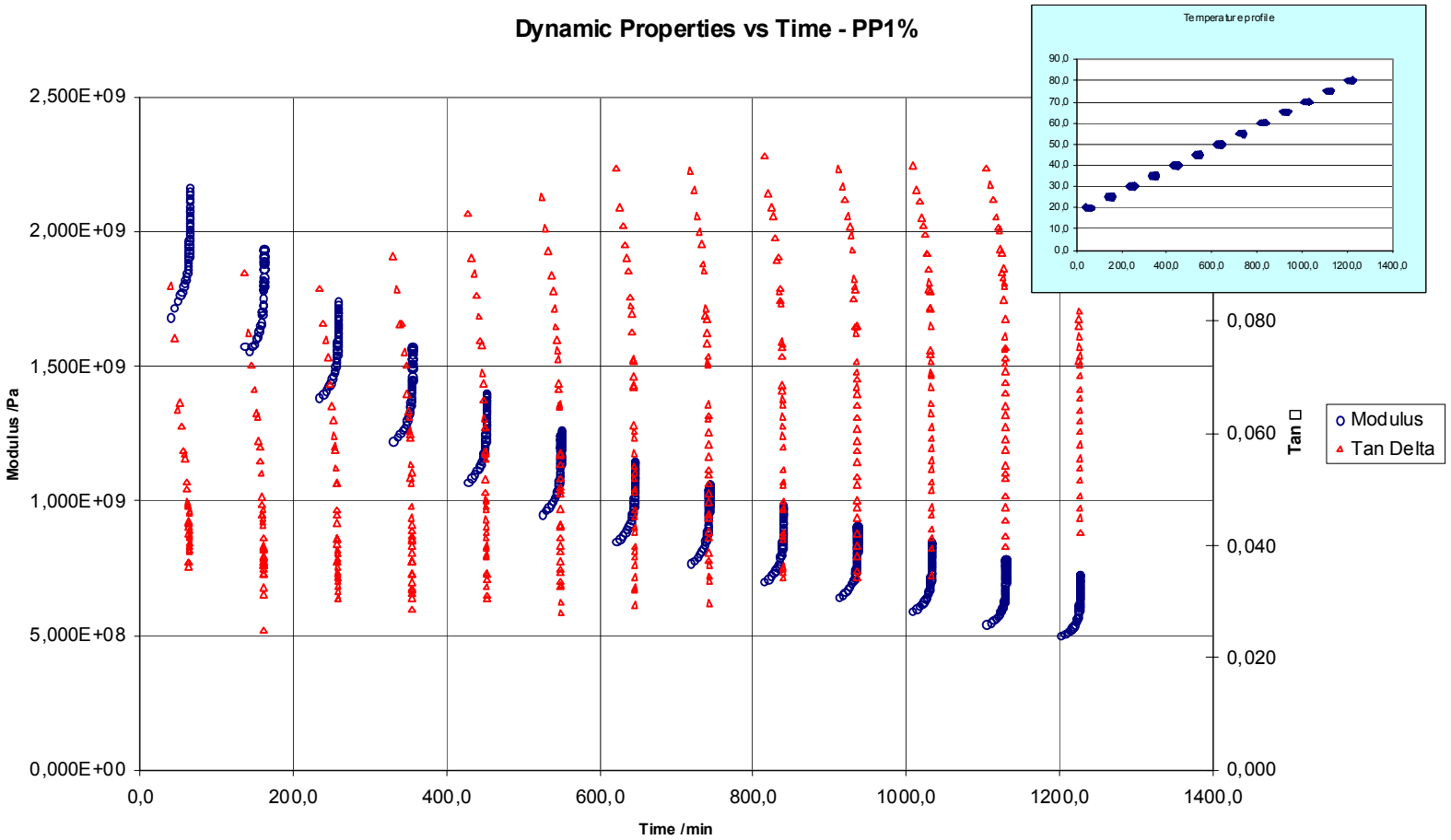
Dynamic Properties vs Time - PP1%
Temperature profile
90,0
80,0
70,0
60,0
50,0
40,0
30,0
20,0
10,0
0,0
0,0
200,0
400,0
600,0
800,0
1000,0
1200,0
1400,0
2,500E+09
2,000E+09
1,500E+09
1,000E+09
5,000E+08
0,000E+00
Modulus /Pa
0,080
0,060
0,040
0,020
0,000
Tan □
Modulus
Tan Delta
0,0
200,0
400,0
600,0
800,0
1000,0
1200,0
1400,0
Time /min

Figure 52

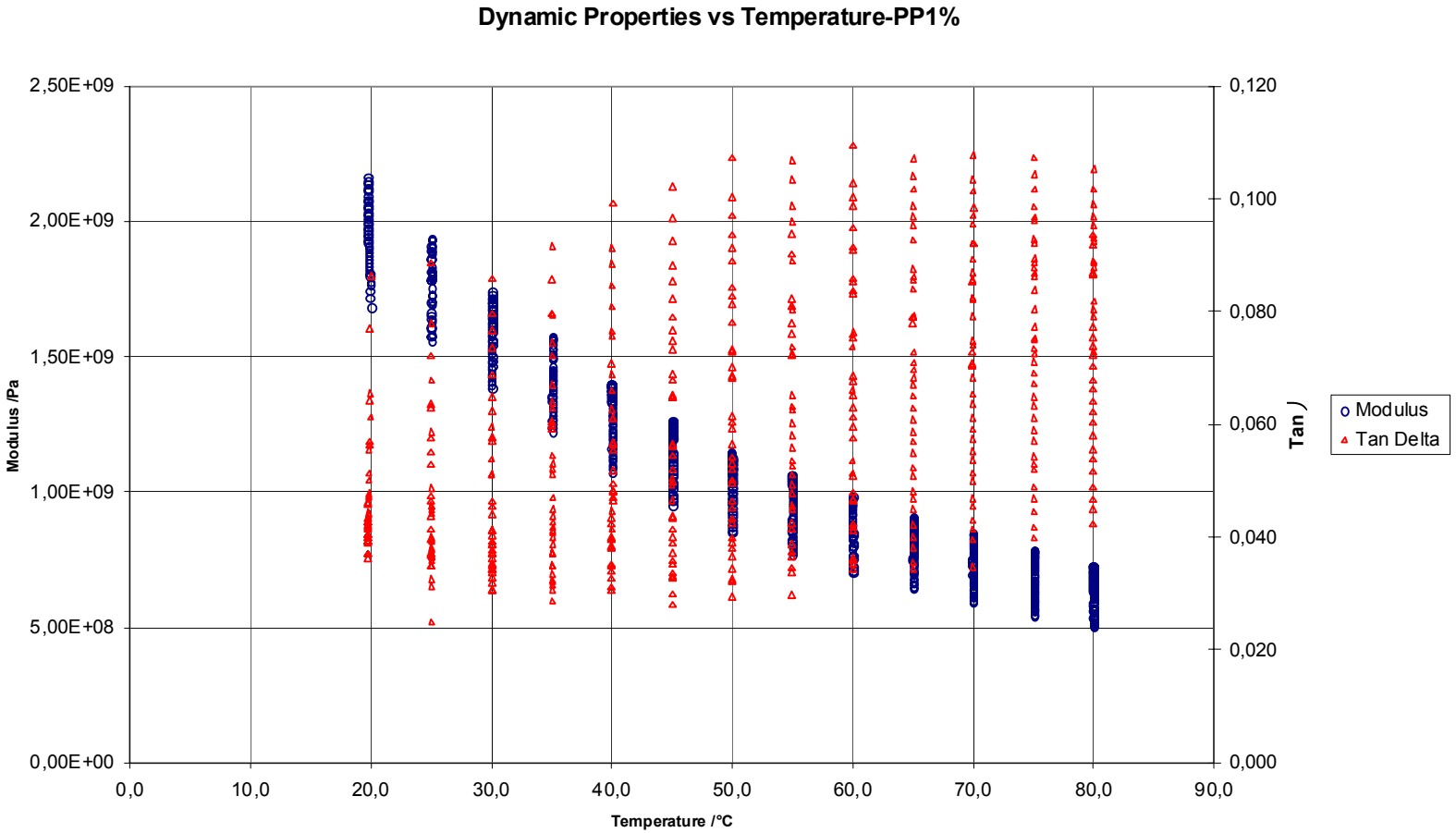
Dynamic Properties vs Temperature-PP1%
2,50E+09
2,00E+09
1,50E+09
1,00E+09
5,00E+08
0,00E+00
Modulus /Pa
0,120
0,100
0,080
0,060
0,040
0,020
0,000
Tan δ
0,0
10,0
20,0
30,0
40,0
50,0
60,0
70,0
80,0
90,0
Temperature /°C
Modulus
Tan Delta

Figure 53

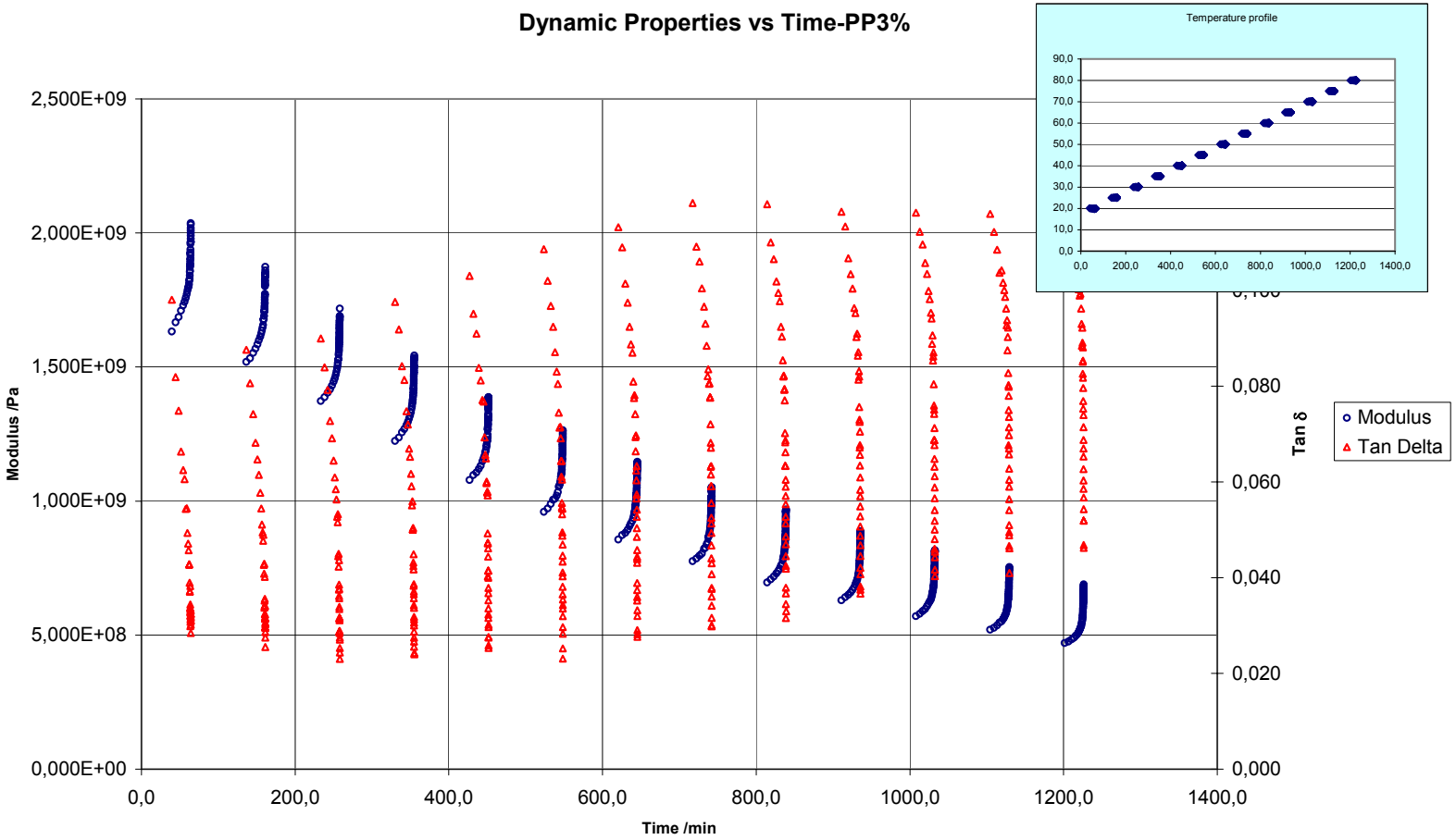
Dynamic Properties vs Time-PP3%
Temperature profile
90,0
80,0
70,0
60,0
50,0
40,0
30,0
20,0
10,0
0,0
0,0
200,0
400,0
600,0
800,0
1000,0
1200,0
1400,0
2,500E+09
2,000E+09
1,500E+09
1,000E+09
5,000E+08
0,000E+00
Modulus /Pa
0,080
0,060
0,040
0,020
0,000
Tan δ
Modulus
Tan Delta
Time /min

Figure 54

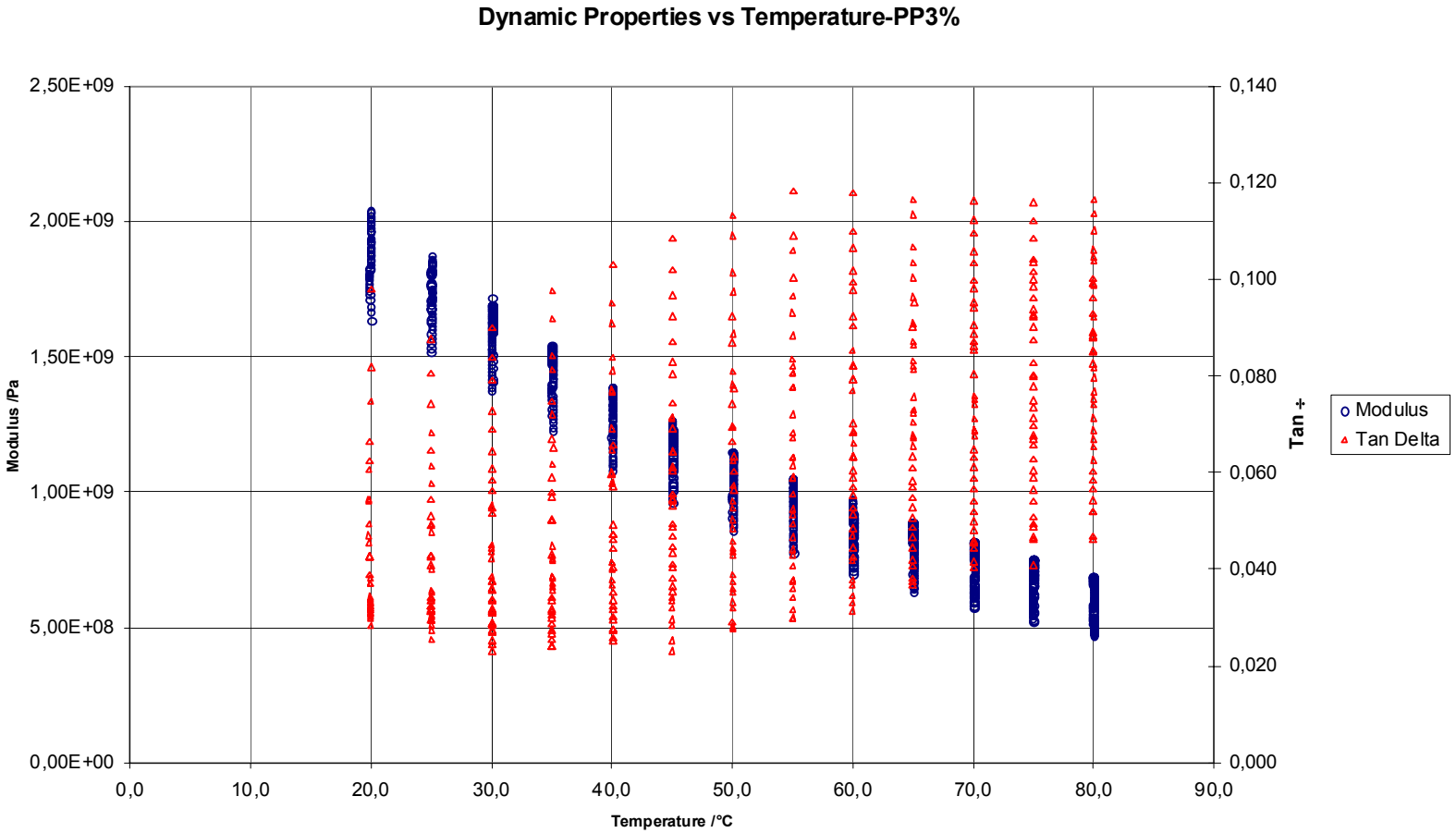
Dynamic Properties vs Temperature-PP3%
2,50E+09
2,00E+09
1,50E+09
1,00E+09
5,00E+08
0,00E+00
Modulus /Pa
0,140
0,120
0,100
0,080
0,060
0,040
0,020
0,000
Tan δ
0,0
10,0
20,0
30,0
40,0
50,0
60,0
70,0
80,0
90,0
Temperature /°C
Modulus
Tan Delta

Figure 55

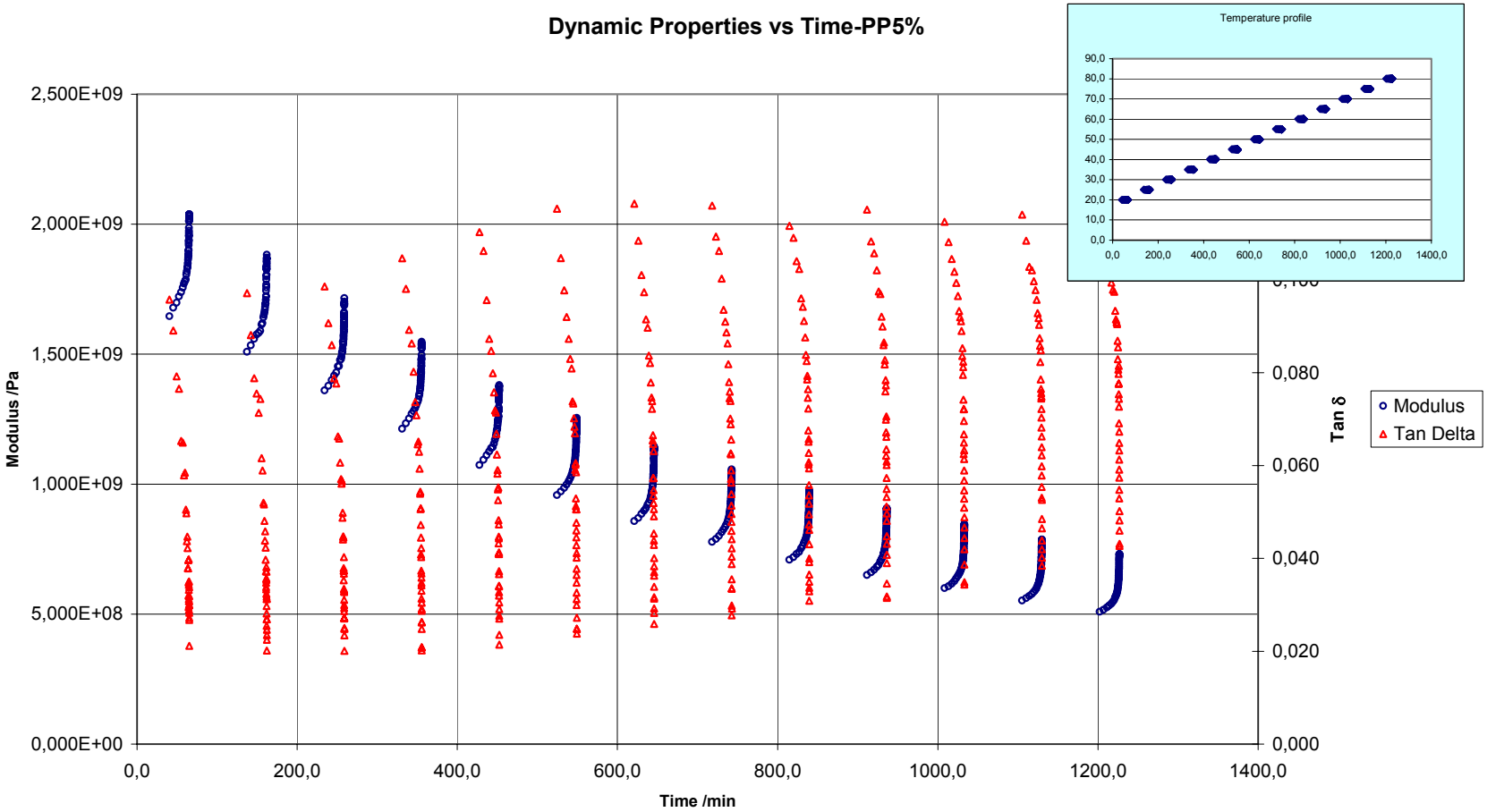
Dynamic Properties vs Time-PP5%
Temperature profile
90,0
80,0
70,0
60,0
50,0
40,0
30,0
20,0
10,0
0,0
0,0
200,0
400,0
600,0
800,0
1000,0
1200,0
1400,0
2,500E+09
2,000E+09
1,500E+09
1,000E+09
5,000E+08
0,000E+00
Modulus /Pa
0,080
0,060
0,040
0,020
0,000
Tan δ
Modulus
Tan Delta
Time /min

Figure 56

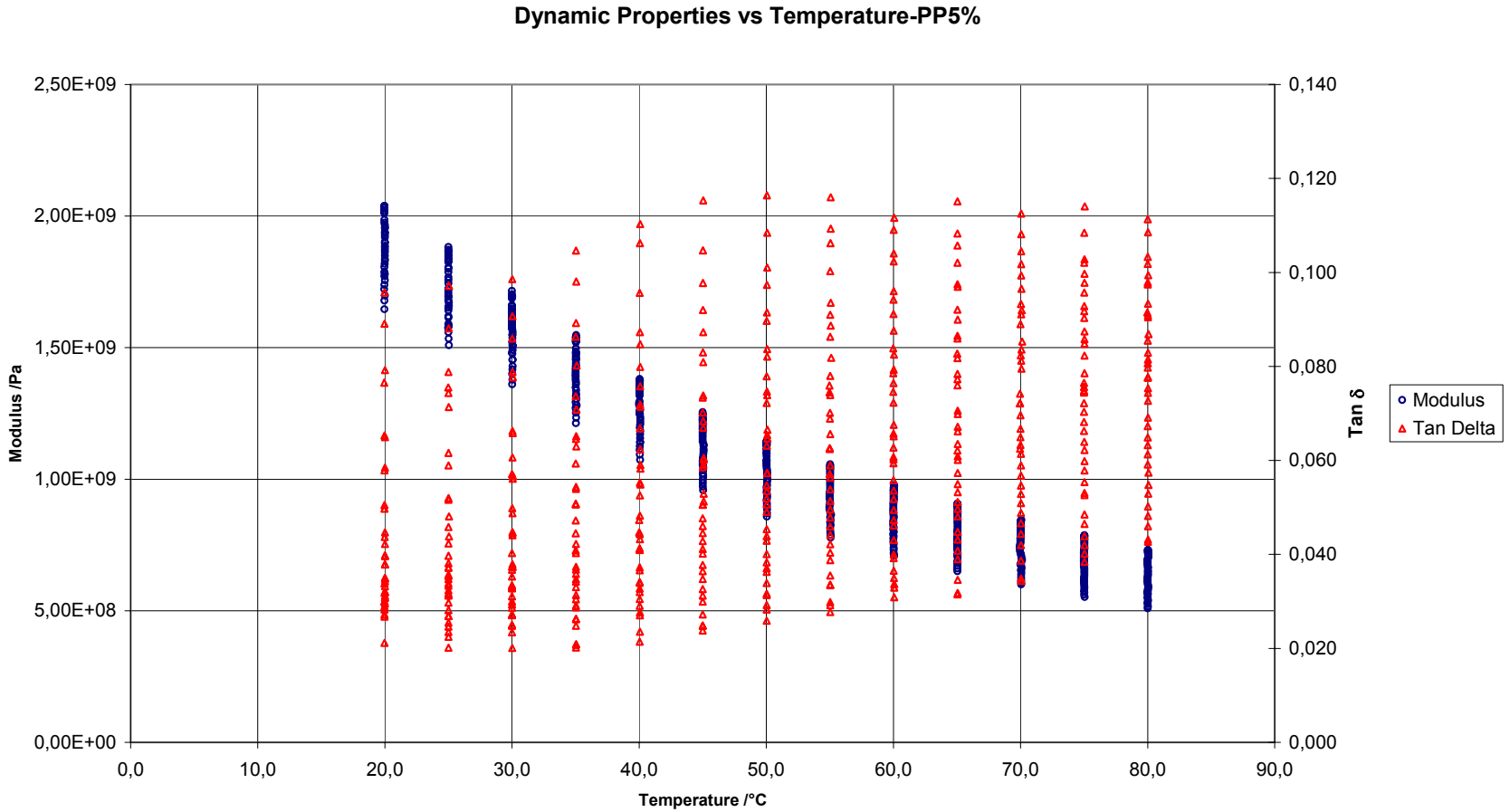
Dynamic Properties vs Temperature-PP5%
2,50E+09
2,00E+09
1,50E+09
1,00E+09
5,00E+08
0,00E+00
Modulus /Pa
0,140
0,120
0,100
0,080
0,060
0,040
0,020
0,000
Tan δ
0,0
10,0
20,0
30,0
40,0
50,0
60,0
70,0
80,0
90,0
Temperature /°C
Modulus
Tan Delta

Figure 57

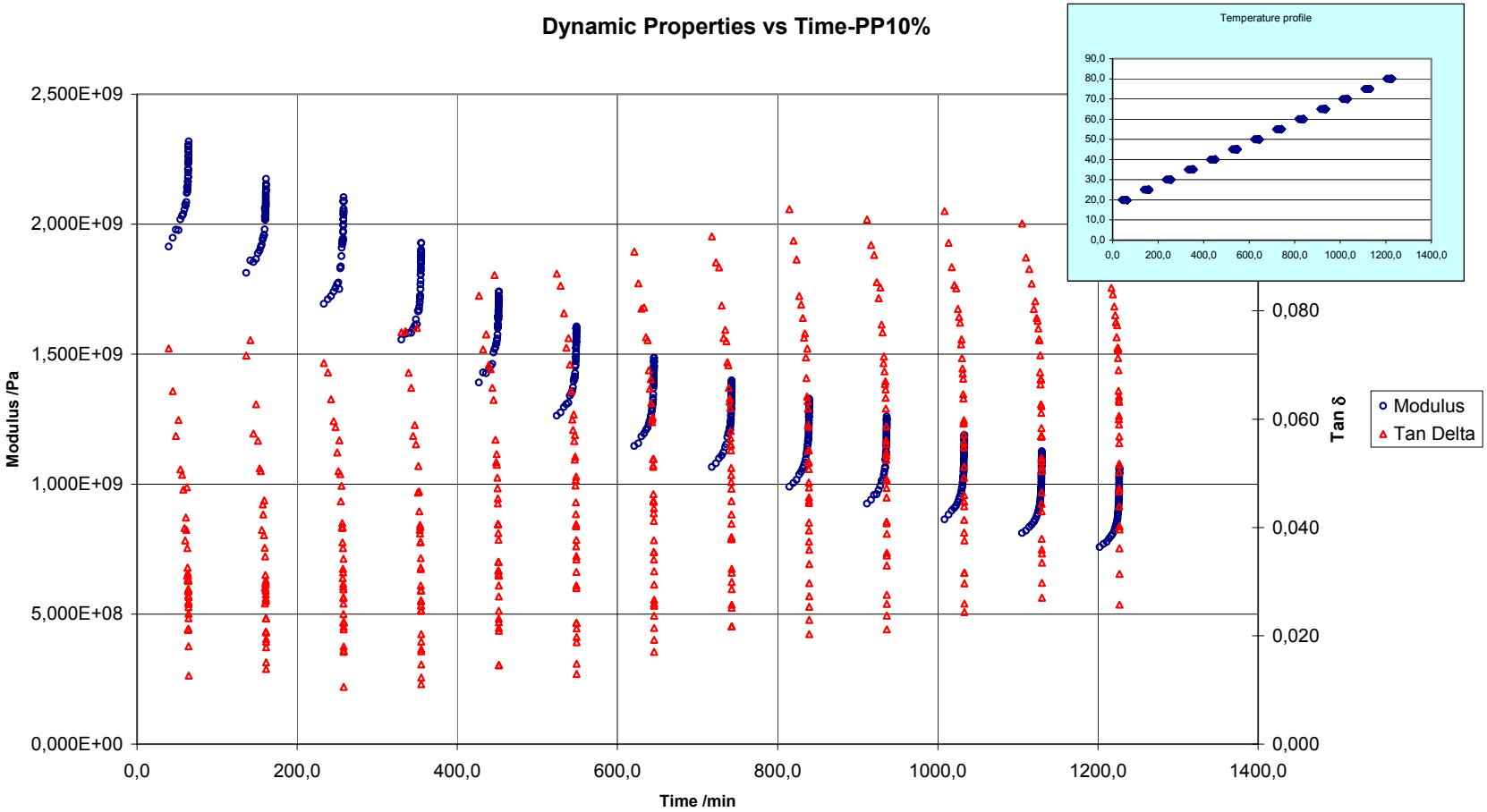
Dynamic Properties vs Time-PP10%
Temperature profile
90,0
80,0
70,0
60,0
50,0
40,0
30,0
20,0
10,0
0,0
0,0
200,0
400,0
600,0
800,0
1000,0
1200,0
1400,0
2,500E+09
2,000E+09
1,500E+09
1,000E+09
5,000E+08
0,000E+00
Modulus /Pa
0,080
0,060
0,040
0,020
0,000
Tan δ
Modulus
Tan Delta
Time /min

Figure 58

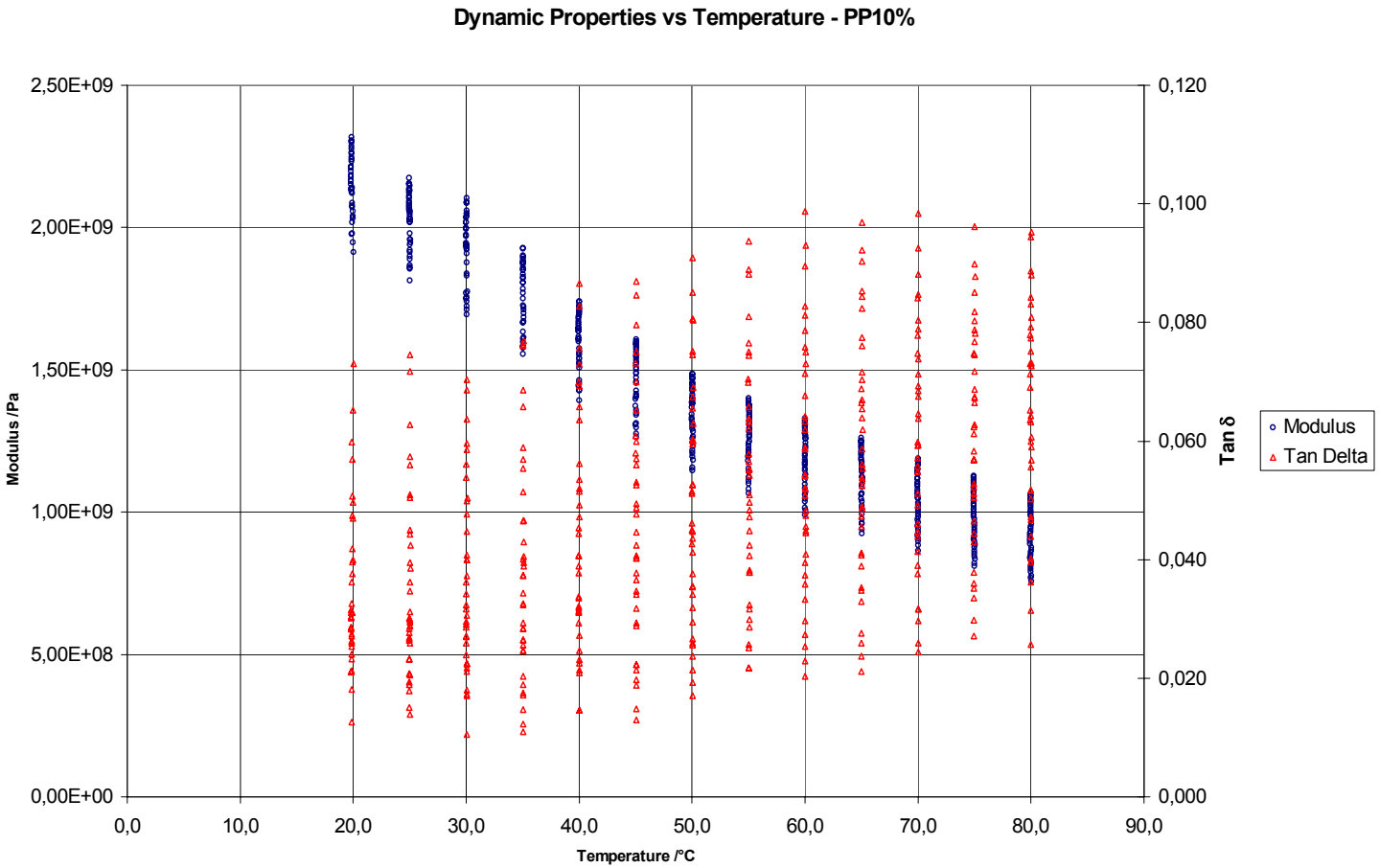
Dynamic Properties vs Temperature - PP10%
2,50E+09
2,00E+09
1,50E+09
1,00E+09
5,00E+08
0,00E+00
Modulus /Pa
0,120
0,100
0,080
0,060
0,040
0,020
0,000
Tan δ
0,0
10,0
20,0
30,0
40,0
50,0
60,0
70,0
80,0
90,0
Temperature /°C
Modulus
Tan Delta

Figure 59

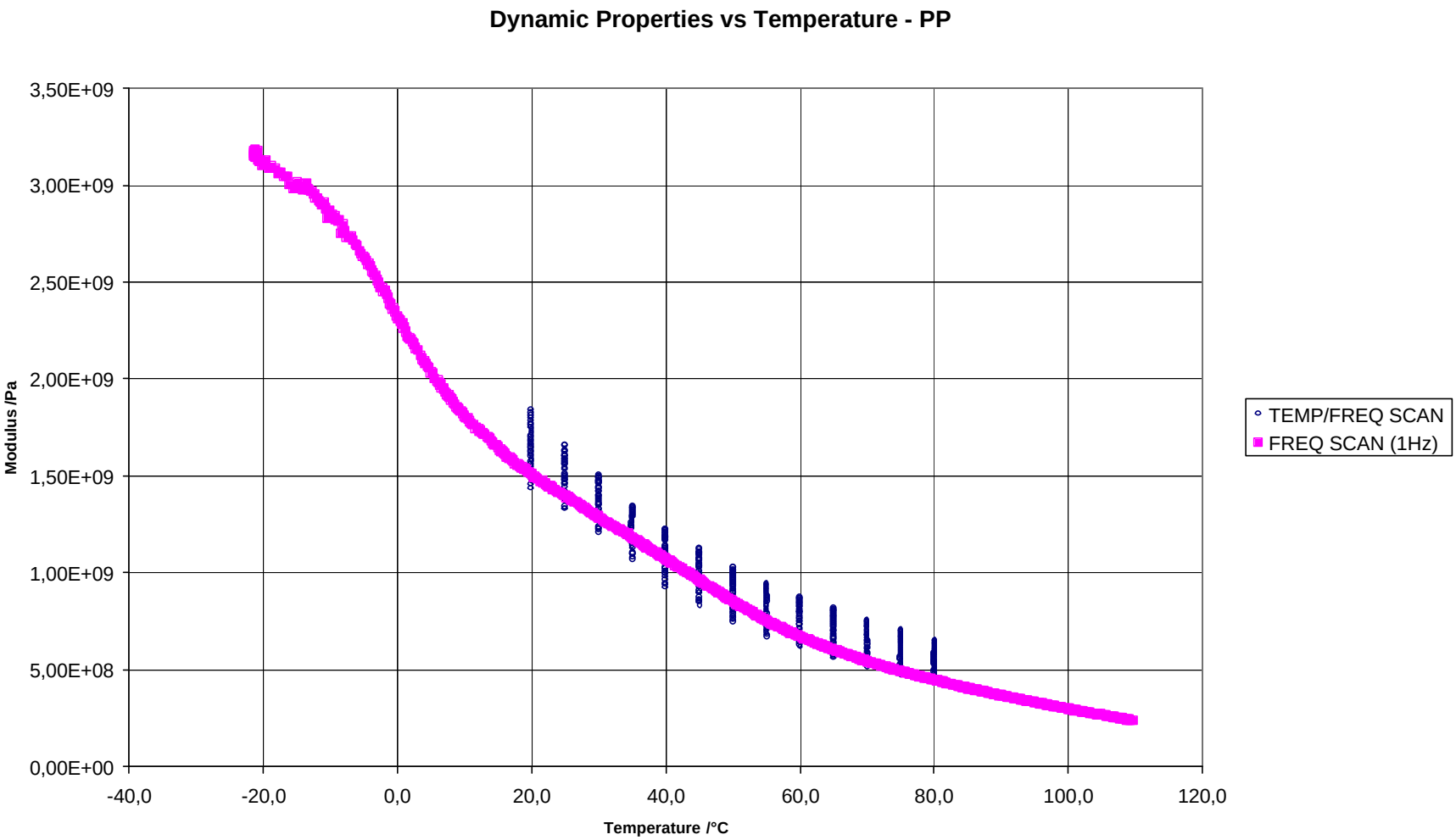
Dynamic Properties vs Temperature - PP
3,50E+09
3,00E+09
2,50E+09
2,00E+09
1,50E+09
1,00E+09
5,00E+08
0,00E+00
Modulus /Pa
-40,0
-20,0
0,0
20,0
40,0
60,0
80,0
100,0
120,0
Temperature /°C
TEMP/FREQ SCAN
FREQ SCAN (1Hz)

Figure 60

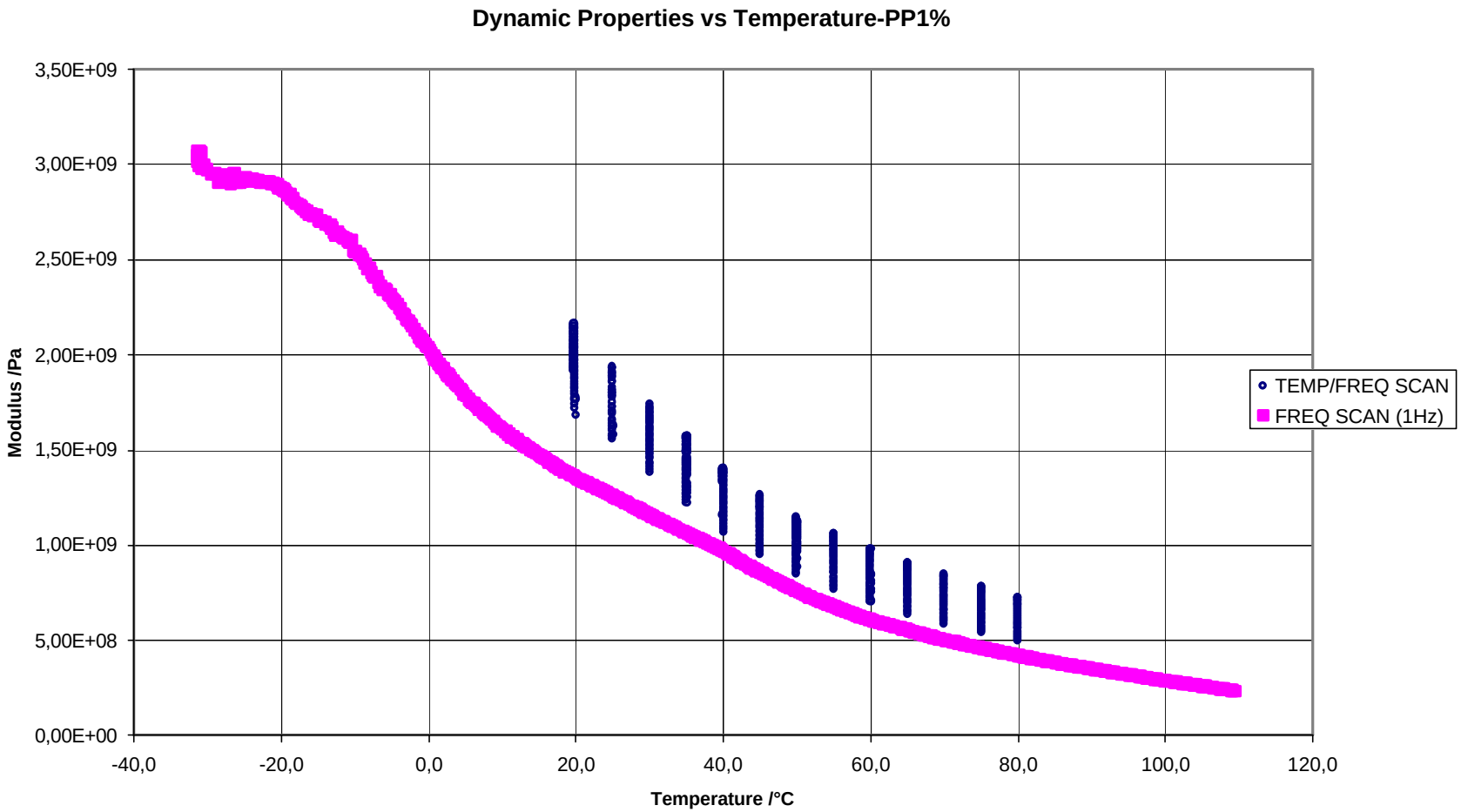
Dynamic Properties vs Temperature-PP1%
3,50E+09
3,00E+09
2,50E+09
2,00E+09
1,50E+09
1,00E+09
5,00E+08
0,00E+00
Modulus /Pa
-40,0
-20,0
0,0
20,0
40,0
60,0
80,0
100,0
120,0
Temperature /°C
TEMP/FREQ SCAN
FREQ SCAN (1Hz)

Figure 61

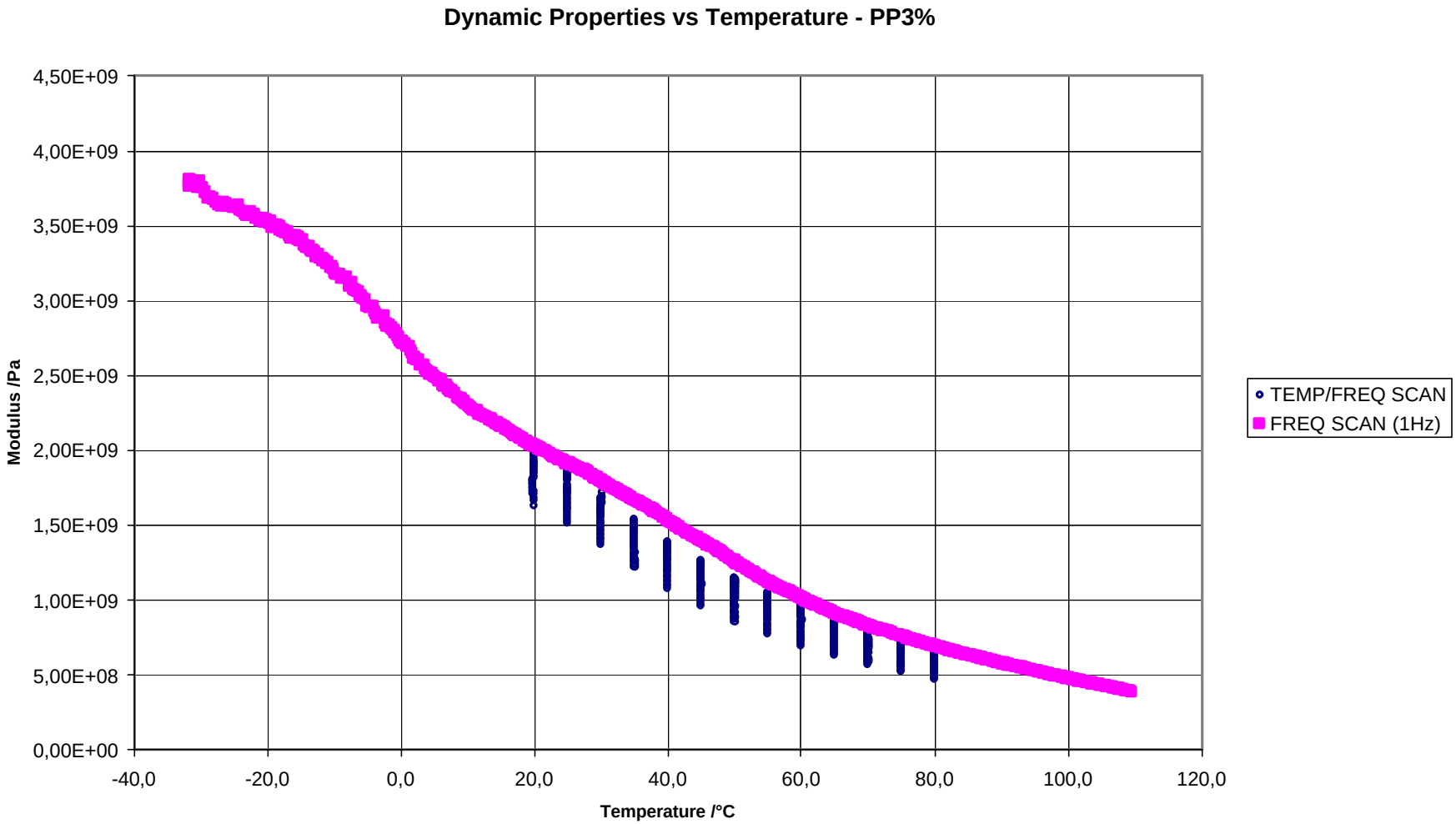
Dynamic Properties vs Temperature - PP3%
4,50E+09
4,00E+09
3,50E+09
3,00E+09
2,50E+09
2,00E+09
1,50E+09
1,00E+09
5,00E+08
0,00E+00
Modulus /Pa
-40,0
-20,0
0,0
20,0
40,0
60,0
80,0
100,0
120,0
Temperature /°C
TEMP/FREQ SCAN
FREQ SCAN (1Hz)

Figure 62

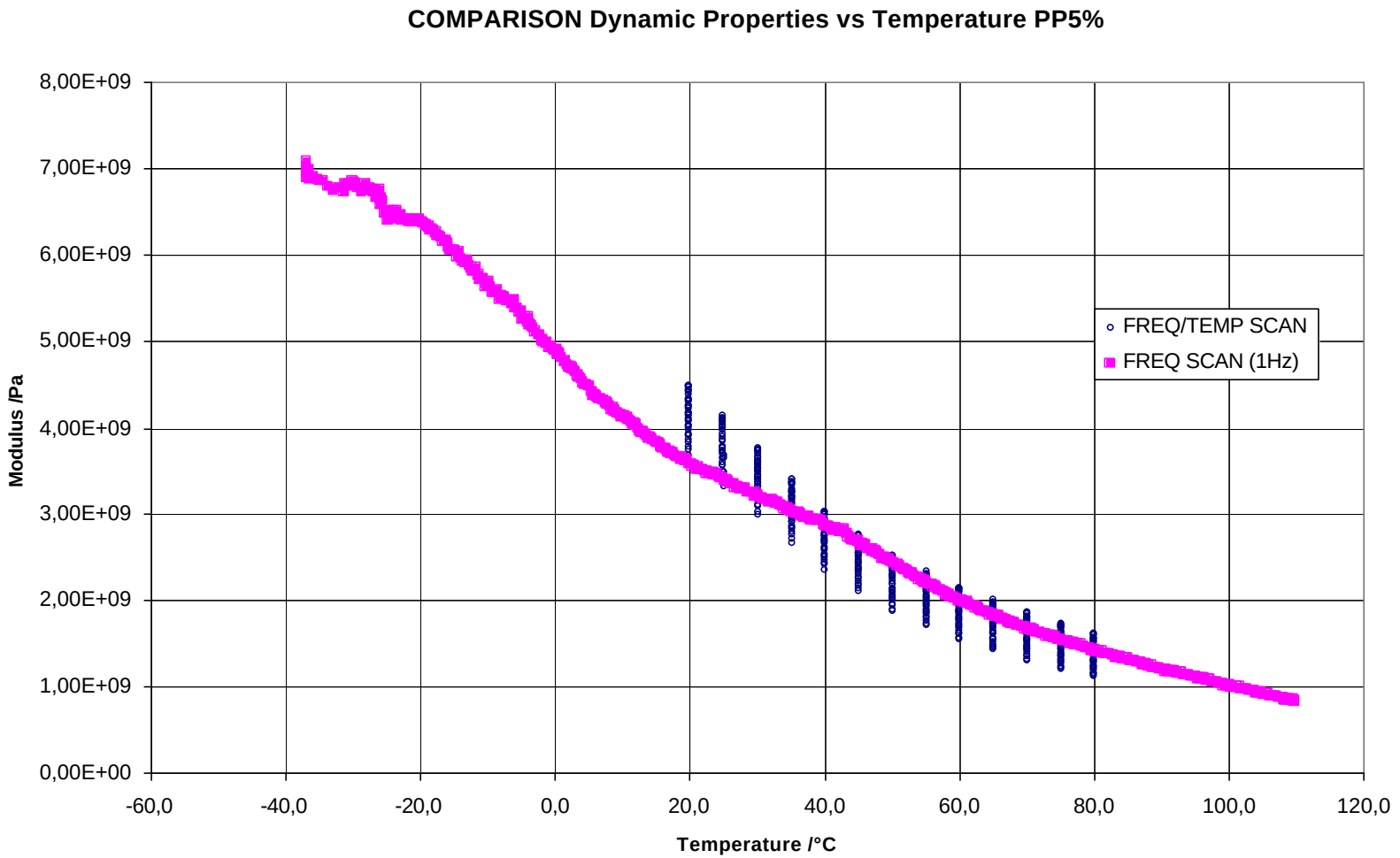
COMPARISON Dynamic Properties vs Temperature PP5%
8,00E+09
7,00E+09
6,00E+09
5,00E+09
4,00E+09
3,00E+09
2,00E+09
1,00E+09
0,00E+00
Modulus /Pa
-60,0
-40,0
-20,0
0,0
20,0
40,0
60,0
80,0
100,0
120,0
Temperature /°C
FREQ/TEMP SCAN
FREQ SCAN (1Hz)

Figure 63

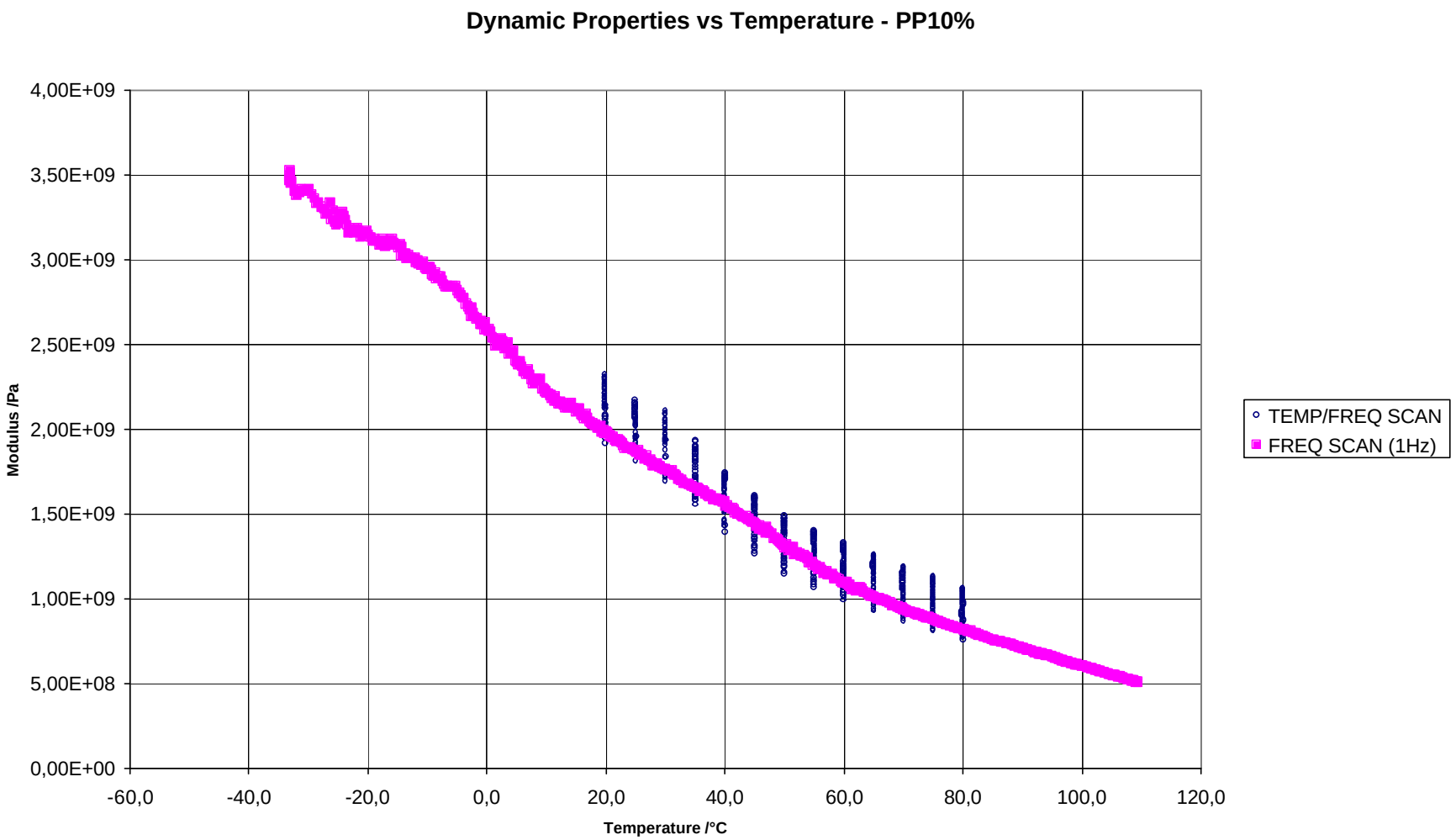
Dynamic Properties vs Temperature - PP10%
4,00E+09
3,50E+09
3,00E+09
2,50E+09
2,00E+09
1,50E+09
1,00E+09
5,00E+08
0,00E+00
Modulus /Pa
-60,0
-40,0
-20,0
0,0
20,0
40,0
60,0
80,0
100,0
120,0
Temperature /°C
TEMP/FREQ SCAN
FREQ SCAN (1Hz)

Figure 64

The master curves have revealed consistent differences in the conservative modulus E' with respect to the pure PP for 5 and 10 wt% of CNT, in accordance with the results from the frequency scan at 1Hz. In the following Figure the master curves are reported all together for comparison, while in Figures 75-79 each CNT composite is compared with the pure PP. It is visible the remarkable increase of the conservative modulus E' for 5 wt% with respect to the other weight composition of CNT for which the differences with the unfilled PP are less remarkable.

Finally, Figure 80, 81 the comparison of Young's modulus from quasi-static mechanical tests and the conservative modulus E' from the dynamic-mechanical tests as well as the increment relative to PP are showed are showed. It can be noticed that for all weight compositions of CNT the values of Young's modulus E are always lower than those of the conservative modulus E'. This behavior was expectedin consideration of the level of strain rate adopted in tensile experiments (50mm/min) which corresponds to 10^{-2} s^{-1}, thus two order magnitude lower than the time adopted for the frequency scan in the dynamic tests (1Hz).

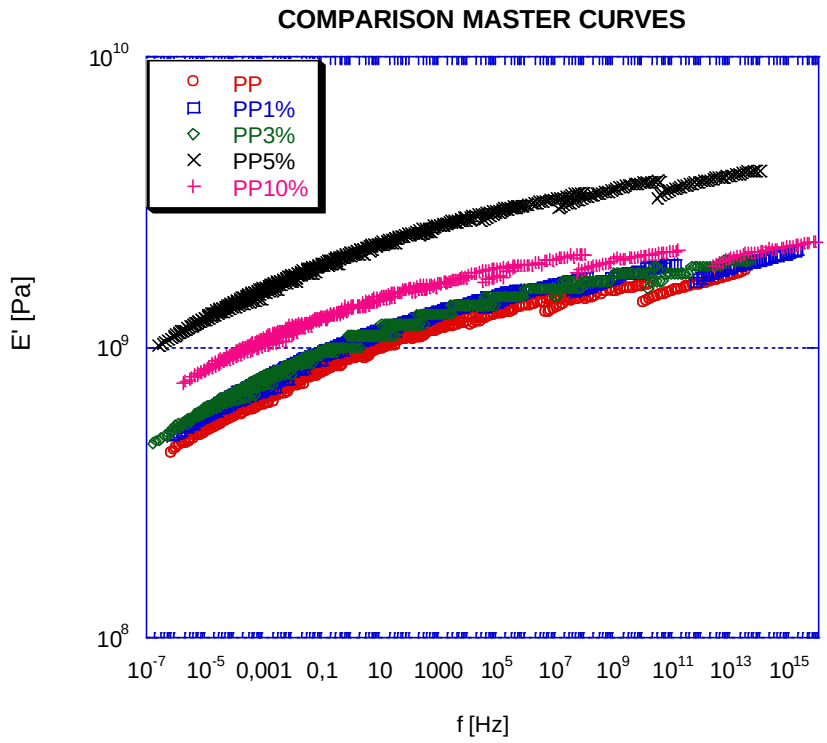

Figure 75: Comparison master curves for PP and PP/CNT composites

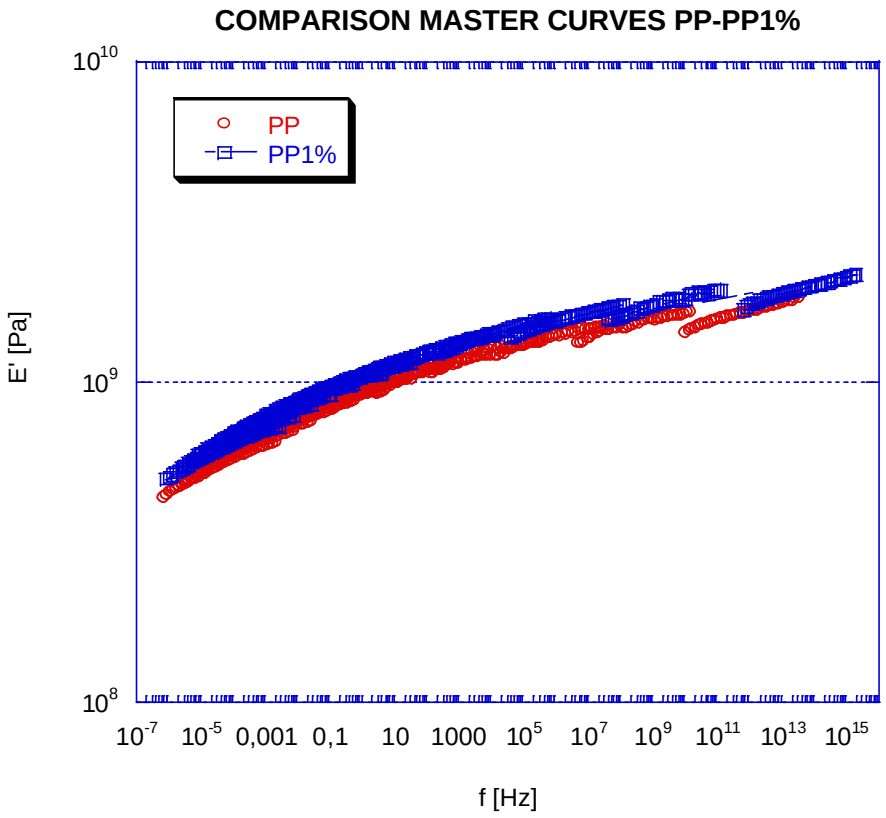

Figure 76: Comparison master curves for PP and PP1% composites

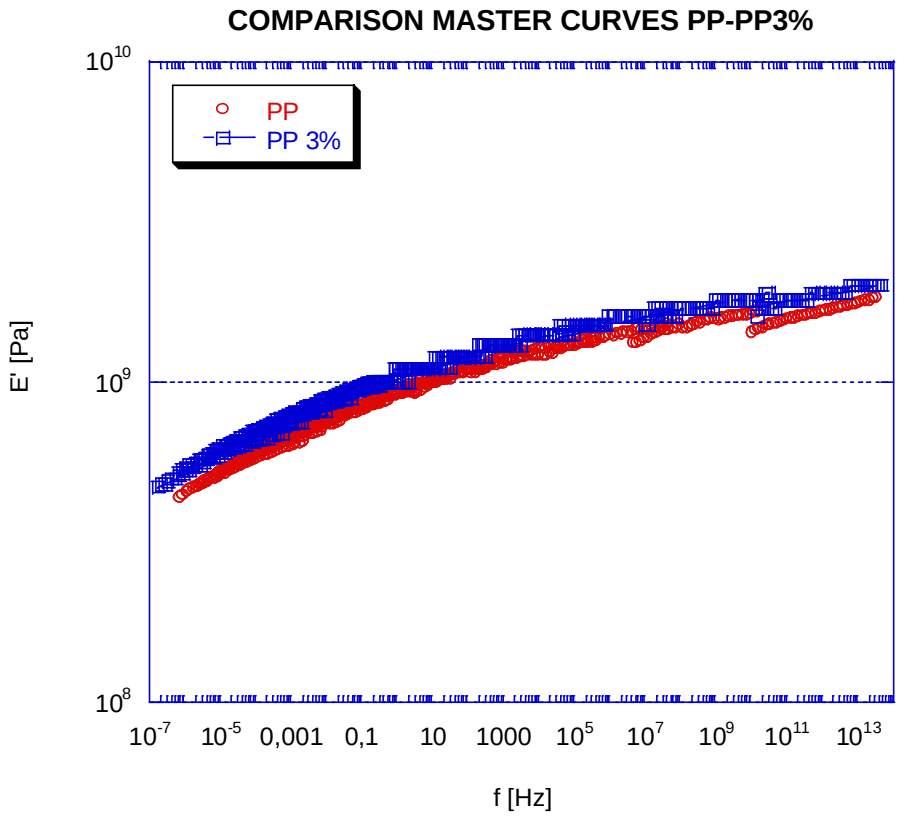

Figure 77: Comparison master curves for PP and PP3% composites

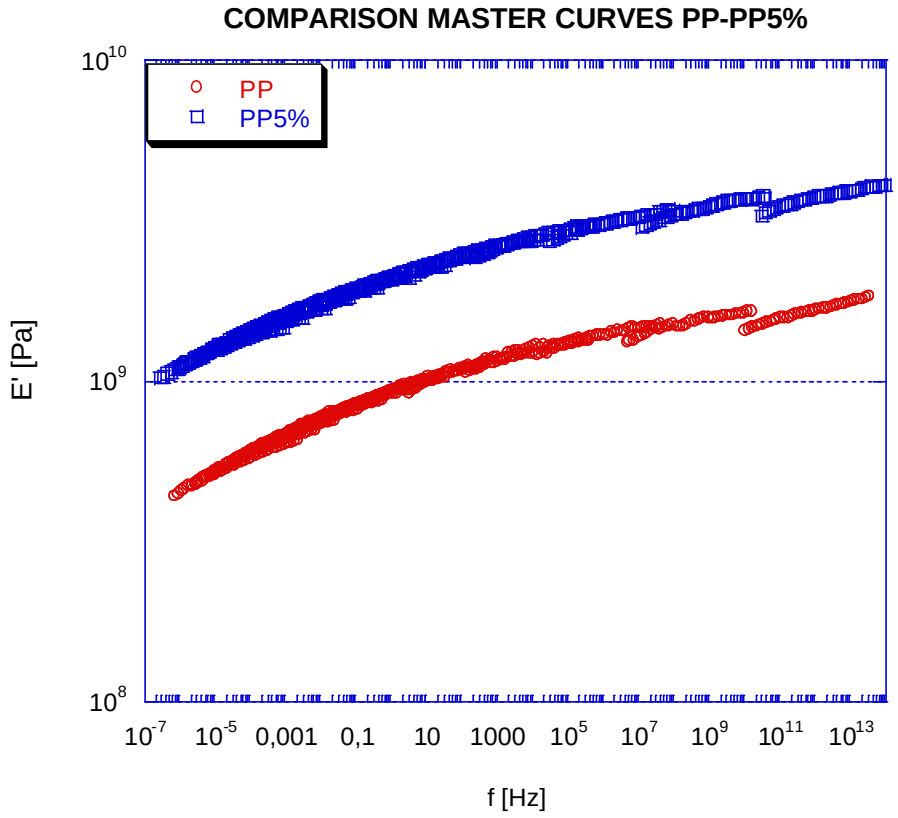

Figure 78: Comparison master curves for PP and PP5% composites

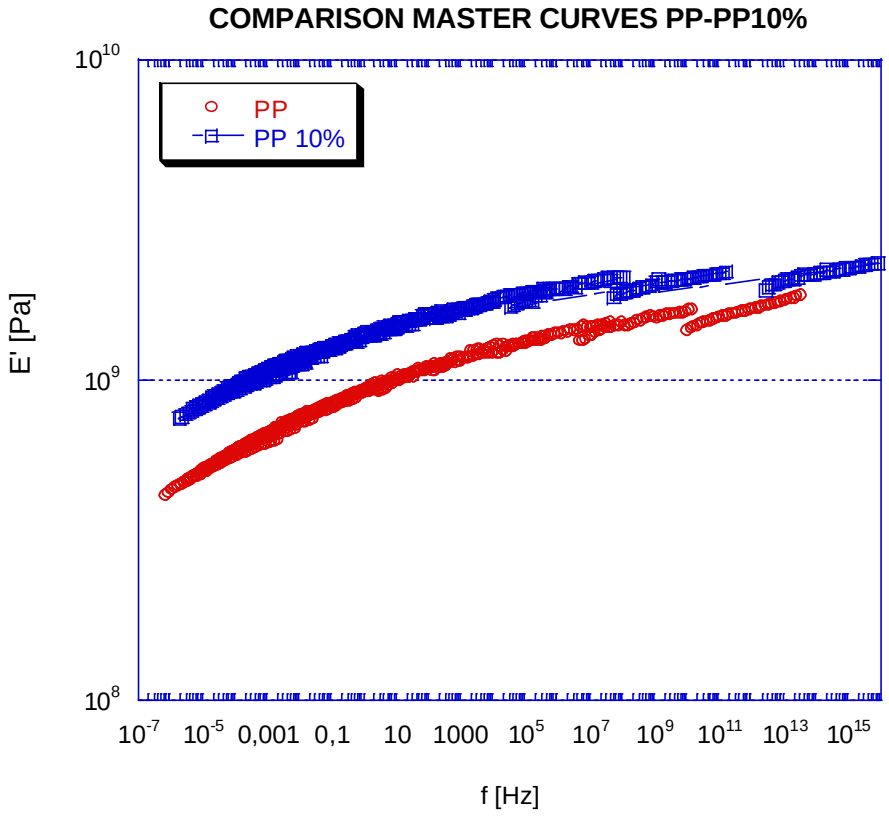

Figure 79: Comparison master curves for PP and PP10% composites

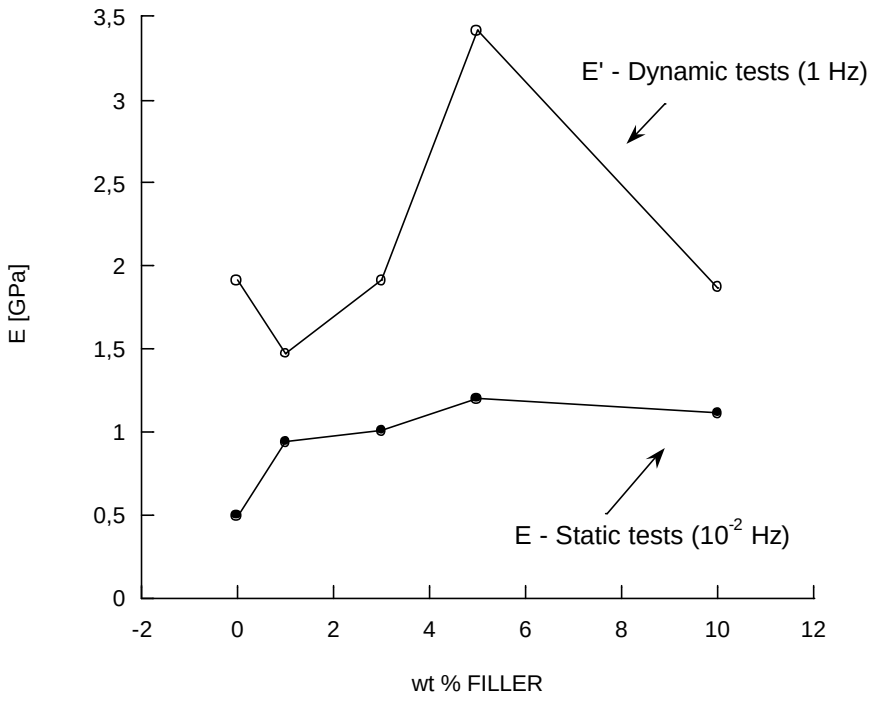

Figure 80: Comparison of the elastic properties of PP/CNT composite plates for static and dynamic tests

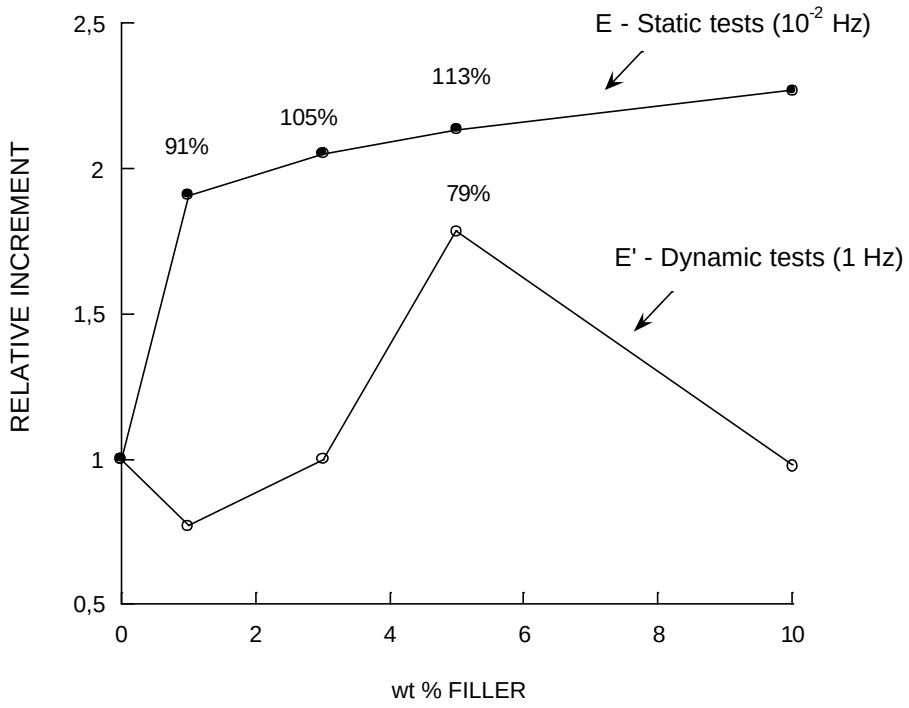

Figure 81: Comparison of the increment relative to PP elastic properties of PP/CNT composite plates for static and dynamic tests

4.1 Rheological characterization

As also discussed in the previous chapter, the rheological analysis was conducted at 220°C in nitrogen atmosphere and run with 25 mm parallel-plate geometry and 1 mm sample gap. The dynamic viscoelstic properties were determined using low strain values (1 %) with frequency range from 0.1 to 100 rad/s, which were within the linear viscoelastic region for these materials.

In Figure82-86 the storage and the loss modulus G’ and G’’ of polypropylene and the nanotube composites are shown. Rheological behaviour at high frequencies can be related to the effect of the filler on processing properties, while low frequency behaviour is sensitive to the structure of the composites and can be used to have information about the percolation state of the MWNTs within the composite.

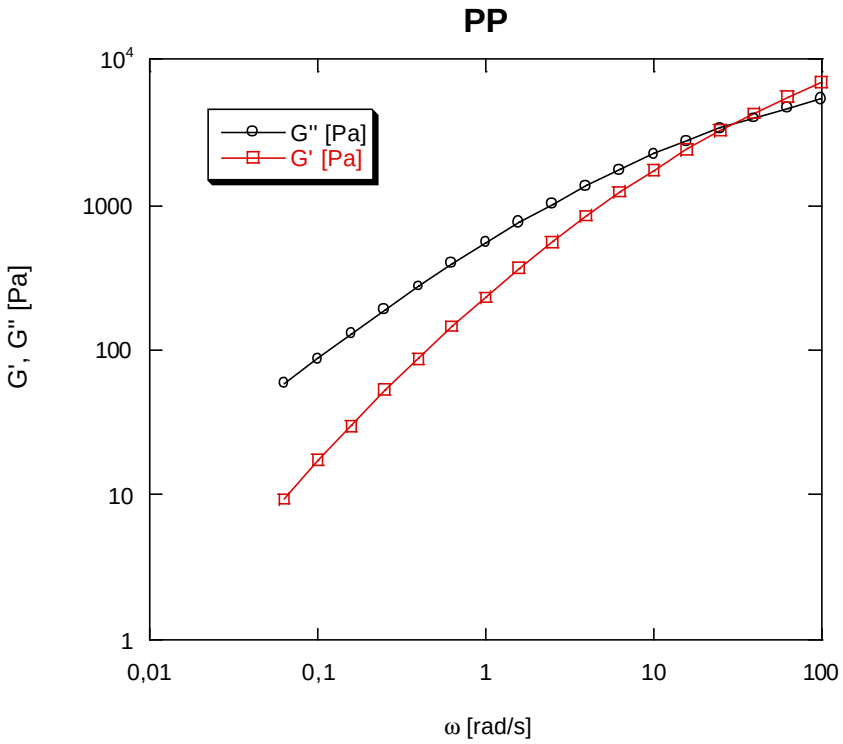

Figure 82: Storage and the loss modulus G’ and G’’ of PP

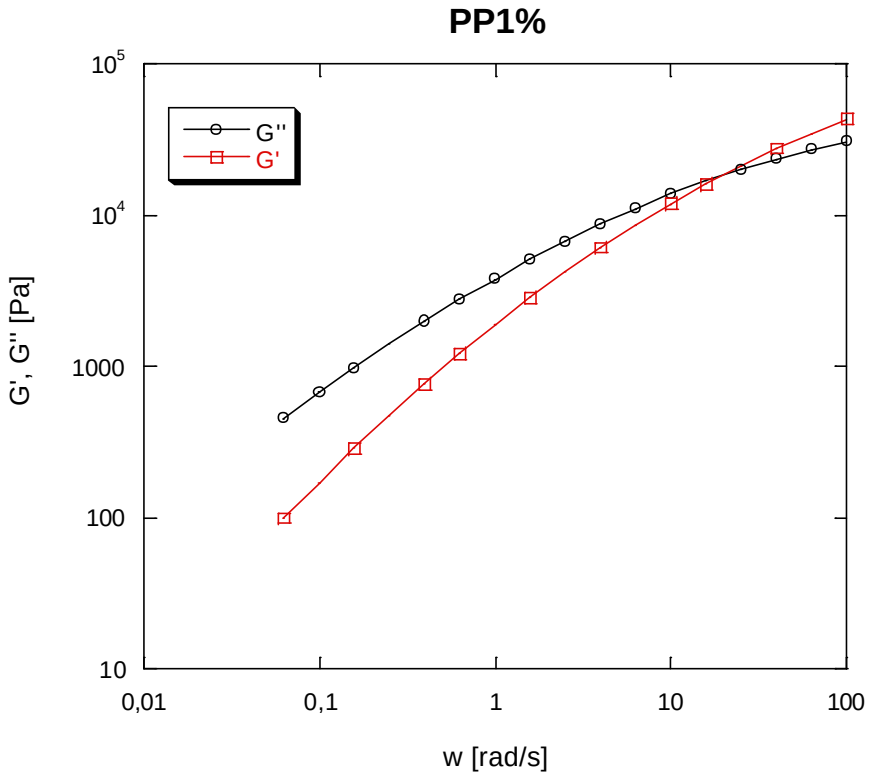

Figure 83: Storage and the loss modulus G' and G'' of PP1%

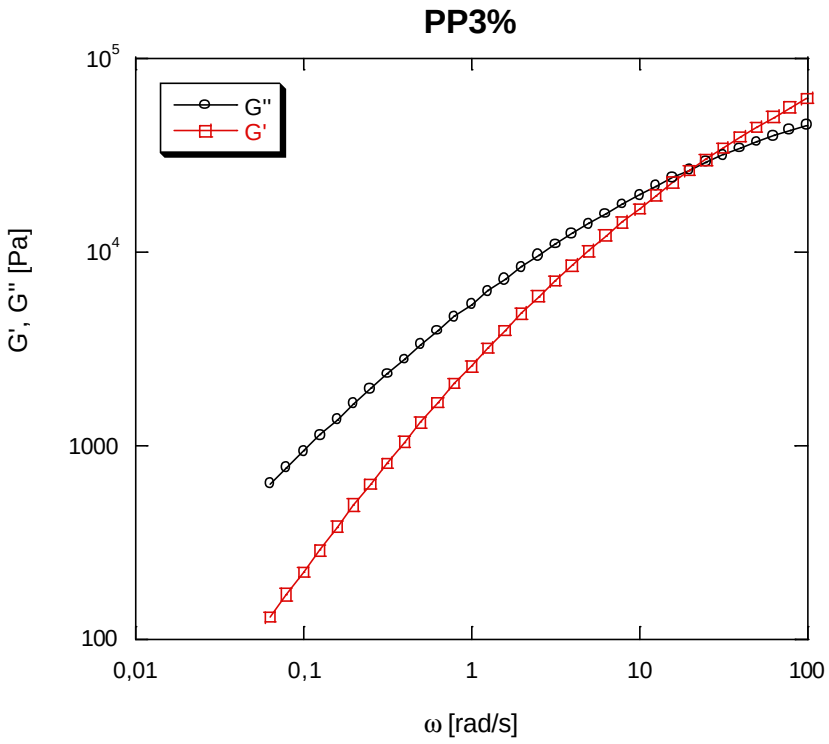

Figure 84: Storage and the loss modulus G' and G'' of PP3%

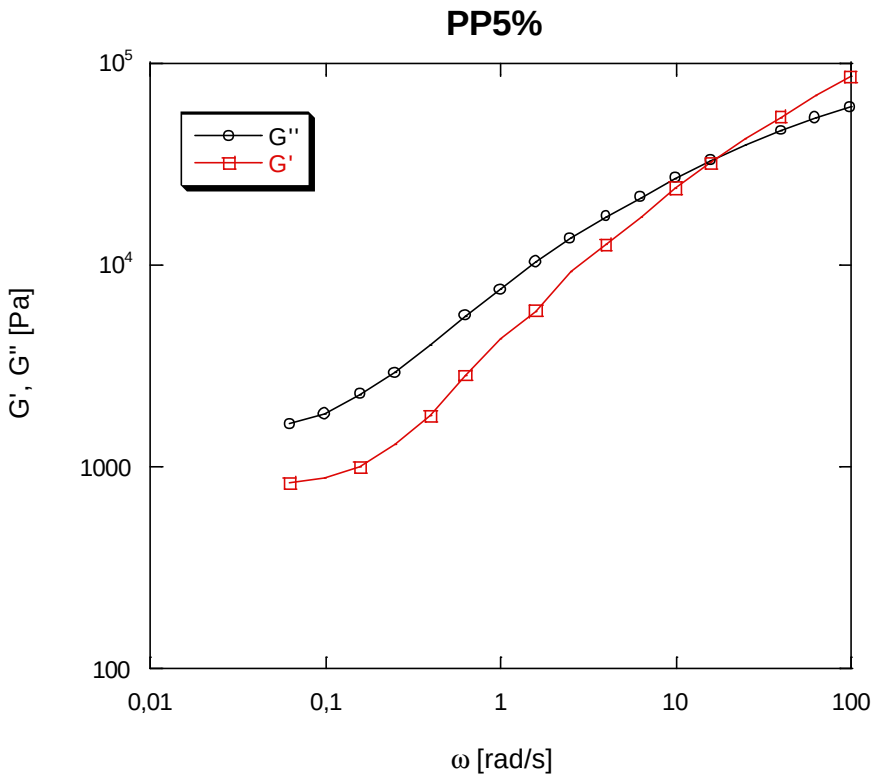

Figure 85: Storage and the loss modulus G' and G'' of PP5%

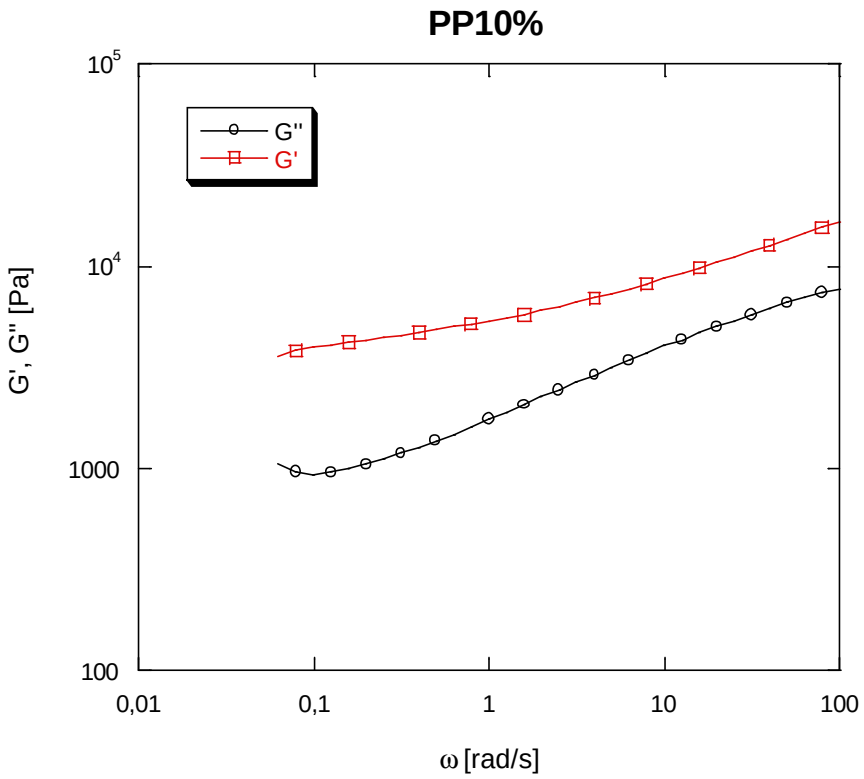

Figure 86: Storage and the loss modulus G' and G'' of PP10%

The complex viscosity η* of the pure polypropylene and the nanotube composites is shown in Figure 87. As can be observed, the nanotubes have a dramatic effect on the rheological behaviour even 1 wt%, at which the viscosity of composites is order of magnitude more viscous than the pure PP especially at low frequency and exhibits a strong shear thinning effect whereas the neat PP shows only a small

frequency dependence at high frequencies. The complex viscosity increases with the nanotubes weight content; the effect of the nanotubes is more pronounced at low frequency and the relative effect diminishes with frequency due to shear thinning. This is in accordance with the theoretical expectations and experimental investigations for fiber-reinforced composites [140,141]. It is worth noticing that the viscosity curves for 1 wt% nanotubes have a similar frequency dependence as the pure PP, revealing a newtonian plateau at low frequencies. However, above 1 wt% the viscosity curves have a much steeper slope at low frequencies and there in no newtonian plateau within the frequency range studied. At 5 wt% nanotubes, the frequency dependence is nearly identical to that of 3 wt%, while for 10 wt% CNT the viscosity curve is nearly linear over the range of frequencies shown.

The rheological behaviour of PP/CNT composites at different frequencies is maybe ascribed to the following reasons: if nanotubes form a nanoscale network structure, then the rheological behaviour of composites should be solid-like with only minor influence of temperature at low shear rates. At high shear rates the rheology will be determined by the polymer matrix. Thus the composites will behave more like a

liquid with the well-known strong temperature influence on viscosity. Figure 86 shows that the viscosity increases sharply at even 1 wt.% loading, indicating that there is a change in the material structure. This sudden change in the complex viscosity means that the composites have reached a rheological percolation at which the nanotubes impede the motion of the macromolecule and form a nanoscale network structure.

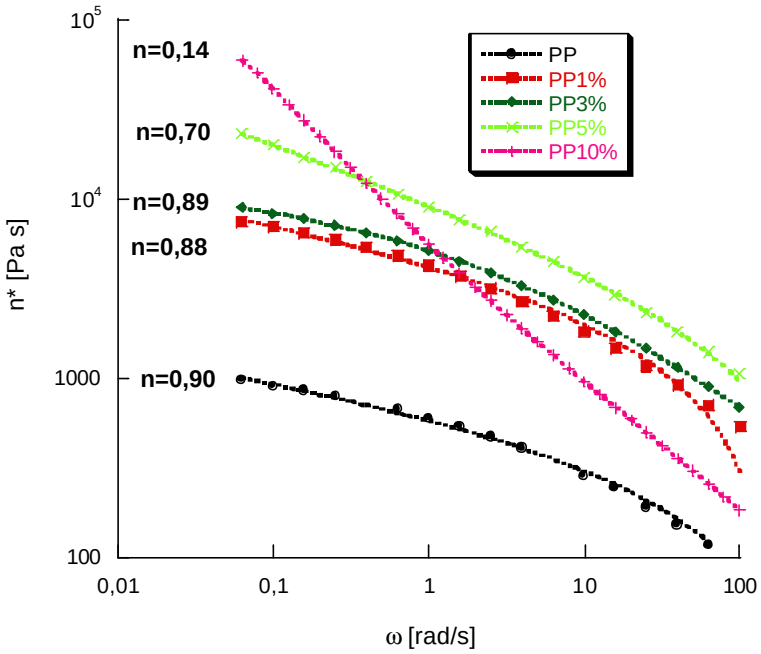

Figure 87: Complex viscosity η* of pure PP and the PP/CNT composites fitted with the Herschel-Bulkley model

The data of complex viscosity can be fitted very well with the Herschel-Bulkley model [147]. The complex viscosity (η∗) can be calculated according to the equation for Herschel-Bulkley suspensions to be modified for the case of dynamic measurements:

$$h^* = h_0^* + kw^{n-1} \qquad (4.1)$$

where k and h_0^* are two constants, n is the flow behaviour index. When n>1, the fluid exhibits a shear thickening behaviour, when n=1, the fluid exhibit a Bingham plastic behaviour; when n<1 the fluid exhibit a shear thinning behaviour. The n value can be denoted as *shearing-thinning exponent*. When τ_0 is equal to zero, eqn. (4.1) is equal to a power low model. It is believed that the n, k, t_0 values are related to the state of dispersion of carbon nanotubes through the matrix. Due to their high aspect ratio, if carbon nanotubes are in a state of a good dispersion, high shearing will make the nanotubes align with the flow direction, and thus make the viscosity decrease, while if the carbon nanotubes existed in an aggregation state then shear thinning behaviour will be very

weak. The better the state of dispersion, the lower the shear thinning exponent *n*.

In Figure 87 the scatter points are the experimental data, the solid lines are the fitted curve according to the Herschel-Bulkley model. The shear thinning exponent decreases with increasing the wt.% of CNT, which means a more significant shear thinning behaviour.

In Figure 88 a) the complex viscosity is reported against nanotube content at different frequencies. At all frequencies, it is visible a fast rise at 1 wt% CNT and then the increase in viscosity is almost linear with the composition up to 5 wt.% CNT. At 10 wt% CNT the increase in viscosity is present only at low frequencies, while even at 1 rad/s the slope becomes slower to evenmore negative (the viscosity diminuishes) at 10 and 100 rad/s.

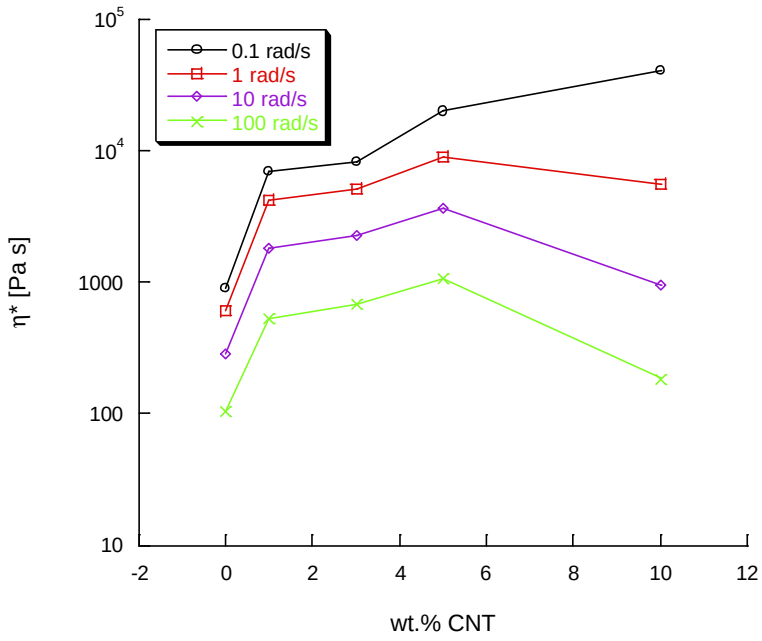

a)

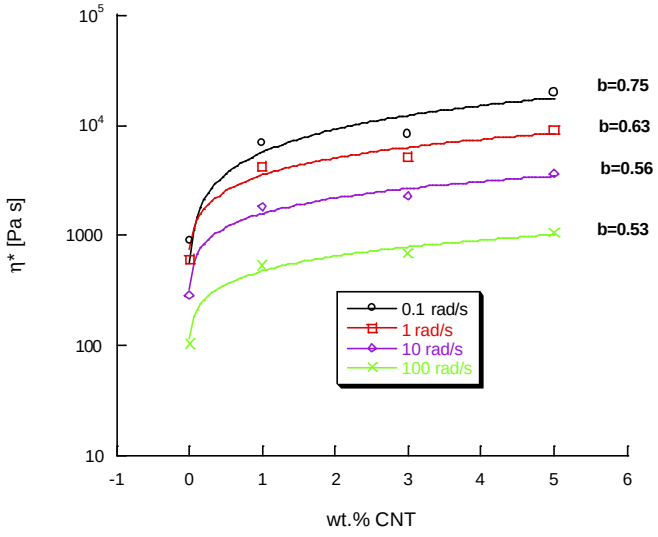

b)

Figure 88: Complex viscosity η* against CNT weight content at different frequencies. Scatter data a) and b) comparison with fitted data up to 5 wt.% CNT with eqn. 4.2

The values of viscosity as a function of CNT loading can be fitted through the following modified power low relation:

$$h \propto b_h m^{c_h} \qquad (4.2)$$

where η is the viscosity, m is CNT loading, b_η is constant and c_η is a critical exponent. The critical exponent, resulted from fitting, decreases with increasing the CNT content(Figure 88b)).

In Figure 89 the increment of complex viscosity standardized against PP value is reported as a function of CNT content for different frequencies. A rapid relative increment is visible already at 1 wt%CNT, with little differences for the single frequencies. In all cases, for each CNT content the increment relative diminuishes with the frequency and the highest increment is reached at low frequency (0.1 rad/s) with 5 wt% CNT.

The increase in complex viscosity with nanotubes composition is primarily due to the dramatic increase in the storage modulus G', as may be seen in Figure 89, where all the curves are reported as a function of frequency for different weight composition CNT. The corresponding increase in the

less modulus G'' is much lower as seen in Figure 91. Both moduli increase with frequency, but the rate of increase in the loss moduli becomes less the higher the nanotubes content. Thus, the effect of nanotubes concentrations is much higher at low frequencies than high frequencies. All G' curves for PP composites, display a monotone behaviour at any frequency, with the slope decreasing with increasing the amount of CNT. At low frequencies, PP chains are fully relaxed and exibit a typical homopolymer –like terminal behaviour. However, at nanotube loading higher than 1 wt.% this terminal behaviour disappear and the dependence of G' and G'' on ω at low frequency is weak. Thus, large-scale polymer relaxation in the composites are effectively restrained by the presence of MWNTs. As shown in Figures 90, at low frequencies, G' is almost frequency independent for nanotubes loading higher than 1 wt.%, which is indicative of a transition from liquid-like to solid-like behaviour. This non-terminal low frequency behaviour can be attributed to a nanotube network, which restrains the long motion of polymer chains.

Table 4: Slopes of G’ and G’’ versus w for different wt.% CNT

CNT wt.%	**Slope of G’ versus** w	**Slope of G’ versus** w
0	1.22	0.78
1	1.15	0.76
3	0.60	0.76
5	0.20	0.60
10	0.15	0.24

As a result, in Figure 91 the low frequency dependence of G’’ have a similar trend. However, the corresponding increase in the loss modulus G’’ is much lower than that of the in the storage modulus G’ at fixed nanotube content.

While the values of G’ and G’’ for the composites containing 1 wt% nanotubes are significantly higher than that of the pure PP, the shape of the curve does not differ very much from each other indicating that the two materials have the same frequency dependence. Above 1 wt%, the slopes of the modulus curves change significantly at low frequency with an initial plateau for 3 and 5 wt.% CNT and above 5 wt% nanotubes, G’ is nearly independent of frequency.

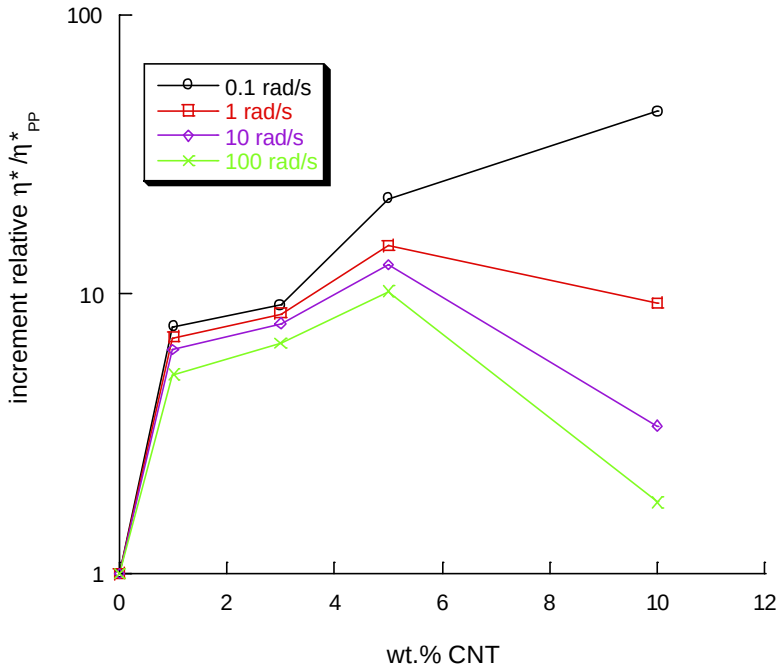

Figure 89: Increment relative to PP of complex viscosity η* at different shear rate

This behaviour shows a less remarkable frequency dependence of the composites, and thus a pseudo-solid behaviour of G' when the amount of CNT is in the range 1÷5 wt.%.

Up to 5 wt.% CNT, in fact, the improvement in G' in the left part of the plot is very relevant. After 5% , the degree of improvement decreases.

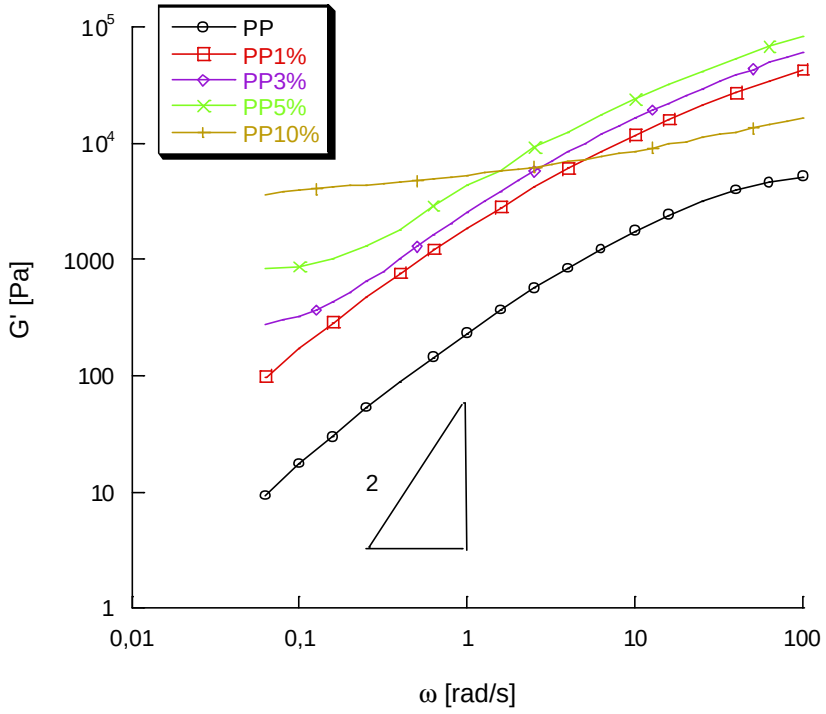

Figure 90: Storage modulus G' versus frequency for PP/CNT composite plates

The power low dependence of G' and G'' on frequency is listed in Table 4. Values of 2 for $G' \propto w^2$ and 1 for $G'' \propto w^1$ are expected for the noncrossedlinked linear polymer melts, but large deviations occur, especially when network structures are formed in the molten state. At molten state, in the case of pure PP, polymer chains exhibit terminal behaviour like linear

polymers with scaling properties of approximately $G' \propto w^{1.2}$ and $G'' \propto w^{0.8}$. When CNT loading exceeds 1 wt.% the terminal behaviour disappear, and the dependence of G' and G'' on ω weakens. This nonterminal behaviour suggests that CNTs not only cause the restriction of PP chains relaxation but also influence the short-range dynamics or local motion of the PP chains in the nanocomposites which can be attributed to existence of CNT network.

The power law dependence of G' and G'' of frequency weakens monotonically with increasing CNT loading from $w^{1.2}$ to $w^{0.15}$ and from $w^{0.78}$ to $w^{0.24}$, respectively. This is an indicator to transition from liquid-like to solid-like viscoleastic behaviour. The nonterminal behaviour in the composites should be caused by formation of nanotube network, which confines long-range motions of PP chains.

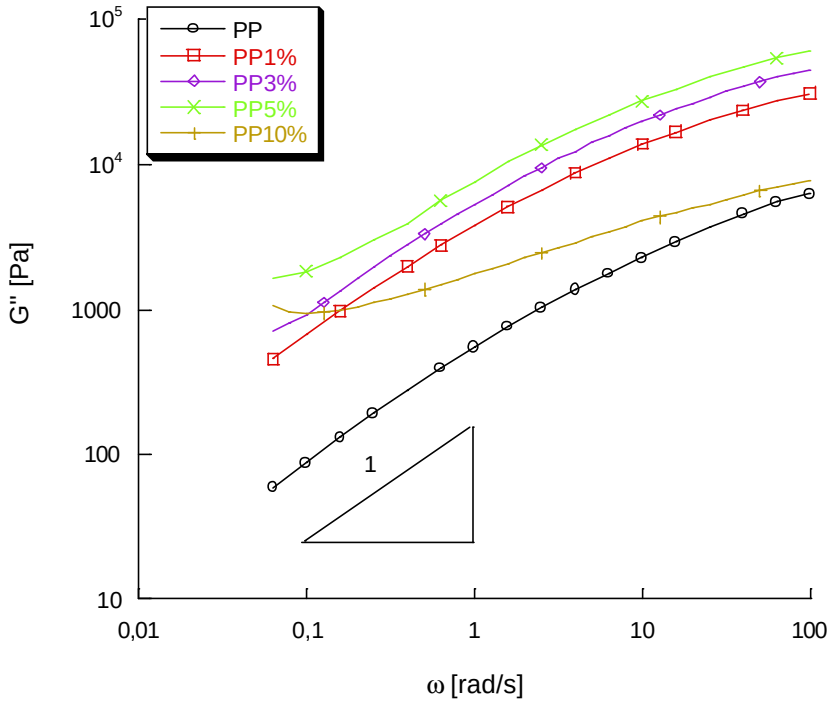

Figure 91: Storage modulus G' versus frequency for PP/CNT composite plates

It is known from the literature that interconnected structures of anisometric fillers result in an apparent yield stress which is visible in dynamic measurements by the presence of a plateau at low frequencies [142-144]. This effect is more pronounced in G' than in G'' [142]. As the nanotubes content increases in this composite system, nanotube-nanotube interactions begin to dominate and eventually lead to

percolation and the formation of an interconnected structure of nanotubes. Starting at about 3 wt% nanotubes, G' seems to reach such a plateau at low frequencies (solid-like behaviour). Therefore, an interconnected structure is assumed to form. This critical composition is regarded as a rheological percolation composition. At high concentrations of nanotubes, connectivity is more pronounced, as seen in the enhanced elasticity.

Figures 92, 93 show a plot of the storage modulus G'and the loss G'' against carbon nanotube content at different frequencies. These graphs again show that the increase in G' with carbon nanotube contents much higher than that of G'' and a strong increase at already 1 wt.%CNT. At all frequencies the increase with composition is almost linear up to 5 wt.% CNT; this phenomena is especially evident at low frequencies. For 10 wt.% CNT the slope becomes negative (G' diminueshes), also in accordance with the results from the mechanical and dynamic-mechanical tests, indicating the weakening effect effect of the CNT on the polypropylene when the CNT is too high.

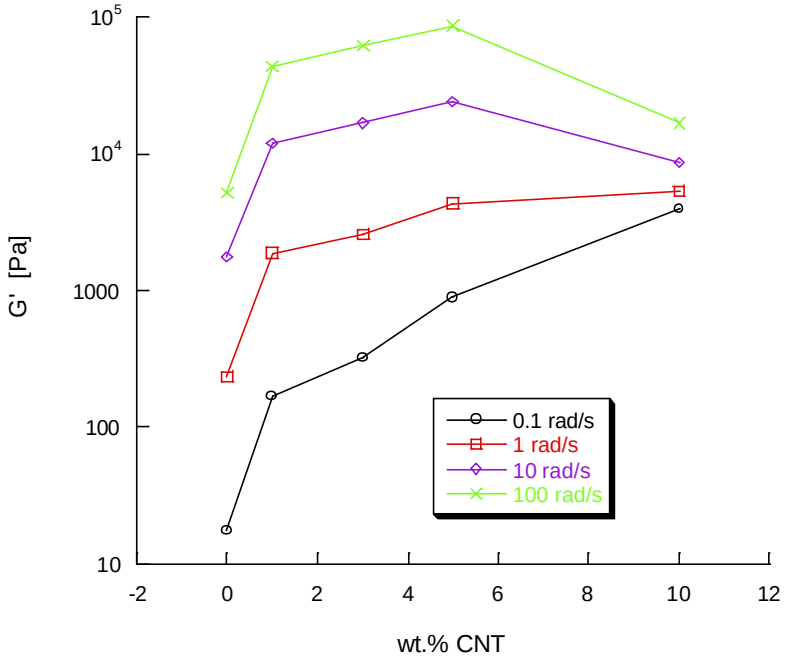

a)

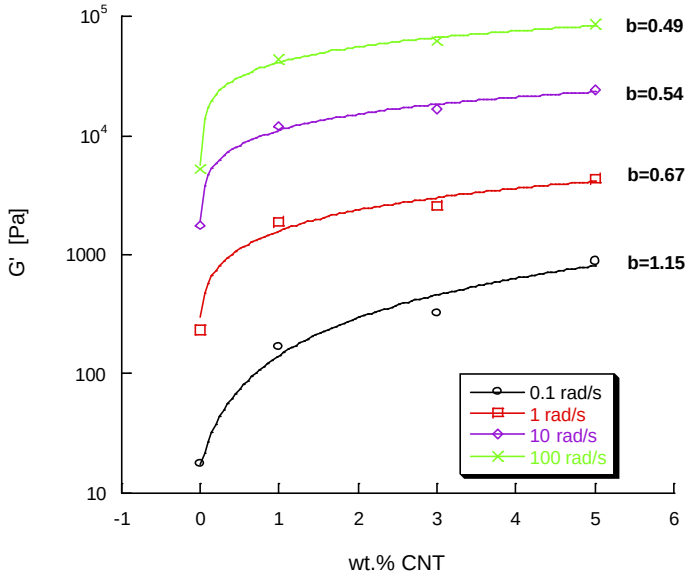

b)

Figure 92: Storage modulus G' against CNT weight content at different frequencies. Scatter data a) and b) comparison with fitted data up to 5 wt.% CNT with the indication of the critical exponent b

A rapid relative increment is visible already at 1 wt%CNT, with little differences for the single frequencies. In all cases, for each CNT conten the increment relative diminuishes with the frequency and the highest increment is reached at low frequency (0.1 rad/s) with 5 wt% CNT.

In analogy with the complex viscosity, G' values as a function of CNT loading can be fitted through the following modified equation:

$$G' \propto b_{G'} m^{c_{G'}}$$

where G' is the storage modulus, m is CNT loading, $b_{G'}$ is constant and $c_{G'}$ is a critical exponent (Figure 92b)). Also in this case, the critical exponent, resulted from fitting, decreases with increasing the CNT content.

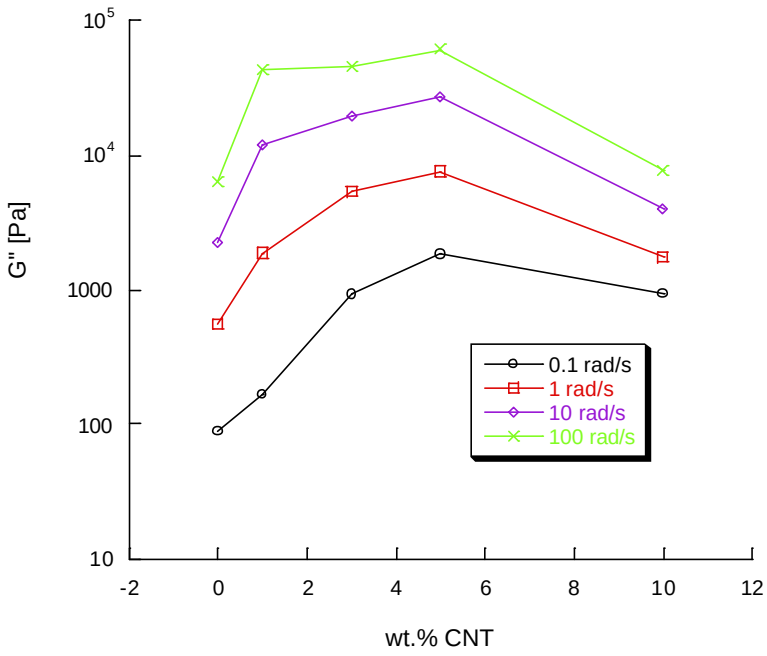

Figure 93: Storage modulus G' against CNT weight content at different frequencies.

In Figures 94, 95 the log-log plot of increment G' and G'' standardized against PP value is reported as a function of CNT content for different frequencies. For all frequencies, a relevant increment is present at 1 wt% CNT, then, at low frequency (0.1 and 10 rad/s) the increment is almost linear wth the slope lower the higher the frequency. For higher values of frequency the increment is again linear up to 5 wt%, while for

10 wt.% CNT the slope become negative as the relative increment of G' diminueshes.

With regarding to the relative increment of G'', beside the rapid increment which occours again for 1 wt% CNT, for all frequencies it is again almost linear up 5 wt% CNT with the slope strongly decreasing with frequencies and then at 10 wt% CNT the slope becomes again negative, as G'' decreases with the frequency.

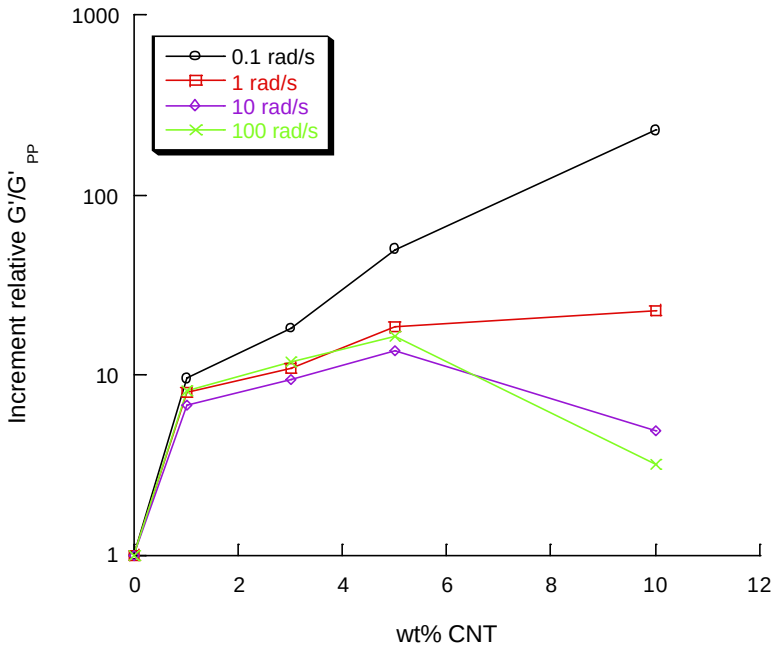

Figure 94: Increment relative to PP of storage modulus G' at different shear rate

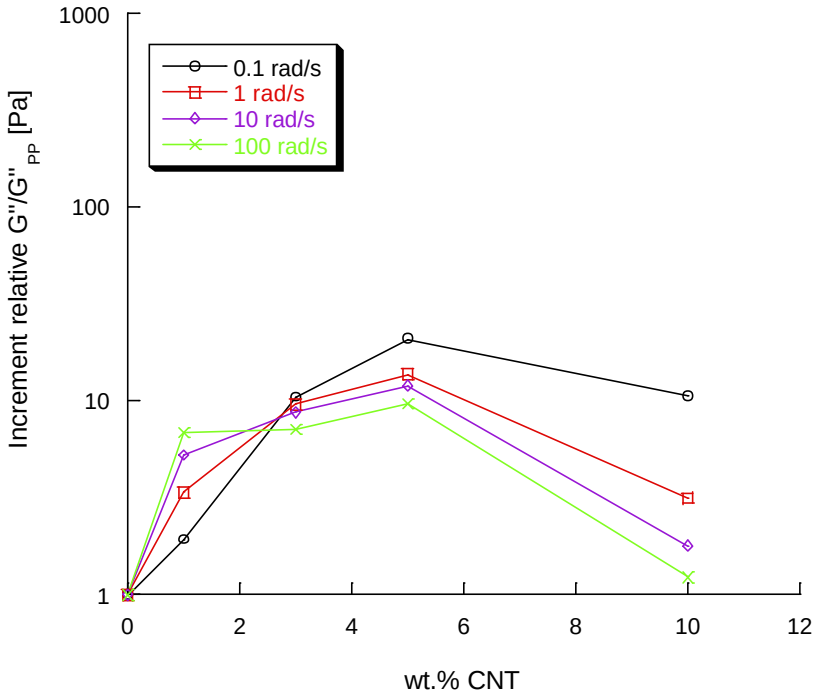

Figure 95: Increment relative to PP of loss modulus G'' at different shear rate

4.4 Morphological characterization

It was of interest to analyze the morphology of PP/CNT composite plates and films. The morphology was observed through SEM and OM, and important information were deduced from both of them.

4.4.1 SEM

Figure 96 shows a SEM photomicrograph of masterbatch containing 20 wt% nanotubes. As can be observed, the nanotubes are randomly oriented and form interconnected structures. Due to the complexity of nanotube network, it is virtually impossible to obtain any information from SEM photomicrographs about the fiber length. By the way, several interesting information can be deduced from the observation of the microphotograph concerning the nanotube diameter of the masterbatch system.

Because of the pronounced curved structure, it is not unexpected that during the sample preparation part of the nanotubes being cut and appear as different individual tubes rather than part of an individual tube which as been fractured, as shown schematically in Figure 97

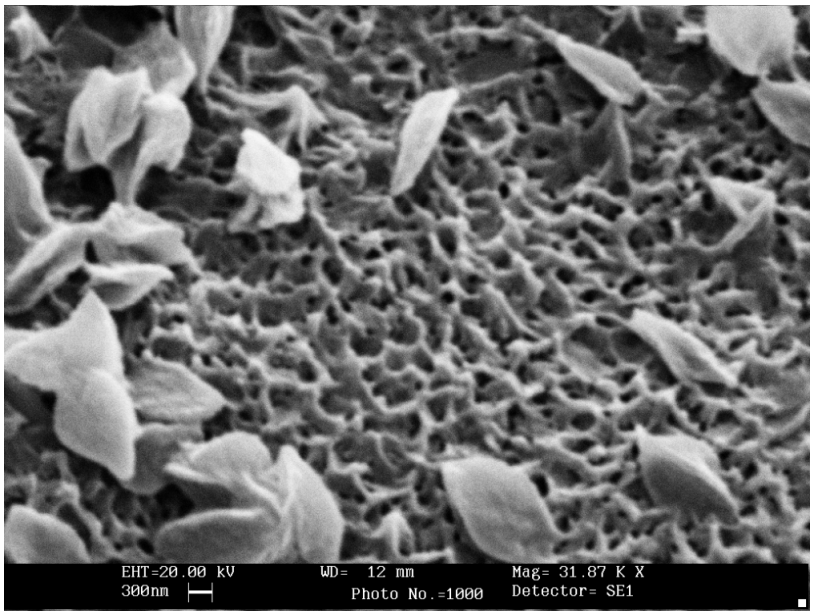

Figure 96: SEM microphotograph of PP/CNT masterbatch

Furthermore, the morphology shows that the MWNTs are randomly oriented and form a highly entangled and interconnected structure in the PP matrix. The MWNT used in this research exhibit a clear curved shape in all three dimensions which can described as “spaghetti” like structure forming an interlocked structure of MWNT in the agglomerate state. A similar type of interconnected structure has been reported in poly(vinyl alcohol)-MWNT composite with 50 wt% MWNT content [145]. As mentioned before, the Hyperion reports that their nanotubes typically range between 10 and

15nm. Here, we have to consider that the diameter visible in the micrographs represents the contact area between the tube and the very end of the tip, and, therefore is slightly higher then the true tube diameter. In contrast, the photomicrograph for the masterbatch system depicted in Figure 96 reveals that the diameters are in the range between 10 and 50nm which is significantly higher than the values reported by the supplier. This results indicates the formation of an adsorbed layer of polypropylene exists on the surface on nanotubes, indicating some degree of wetting and phase adhesion with the nanotubes, unlike the hydrophobic polymer system.

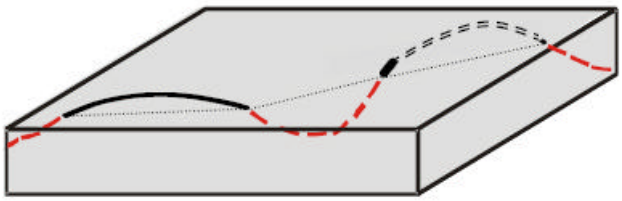

Figure 97: Schematic of spaghetti-like structure where is visible parts at cut surface (solid line) or in a phin section (dashed line)

Figure 98-101 show the SEM microphotographs of the fracture surface of PP/CNT composites. In the fracture surface of PP1%, containing 1 wt% CNT, carbon nanotubes appear to

be disperse in the form of 1 µm diameter cluster and seems to be the center for PP crystal growth. They are observed as white spots dispersed independently through the matrix, although some of them entangled toghether in the form of random arrays. With further increasing CNT content, a network of CNT particles is gradually formed within the matrix of the composite leading to a sharp increase in the mechanical properties: a pronounced CNT network is formed in PP5% and PP10% composites.

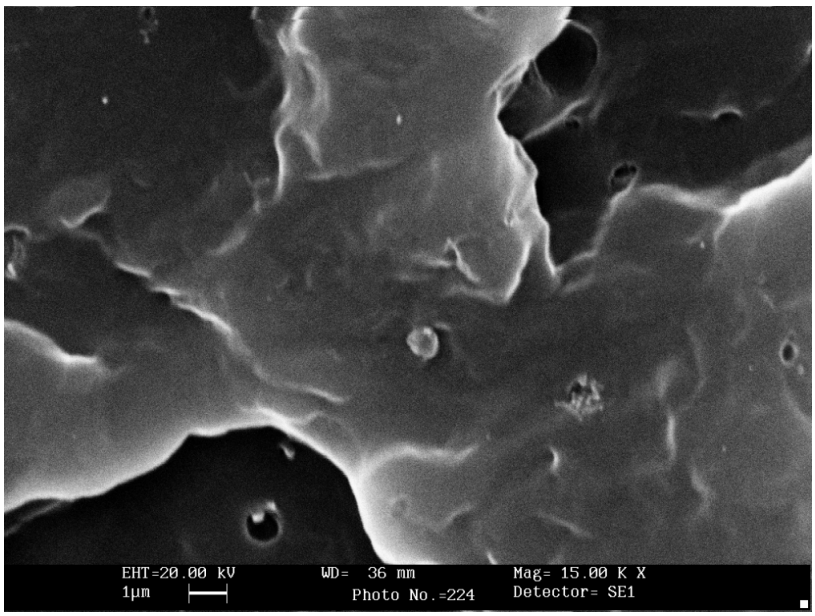

Figure 98: SEM microphotograph of fracture surface of PP1%

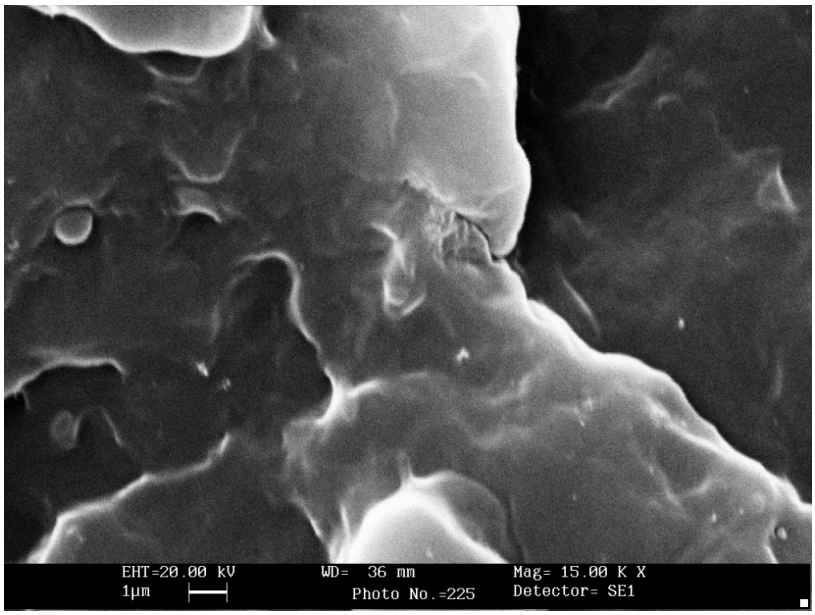

Figure 99: SEM microphotograph of fracture surface of PP3%

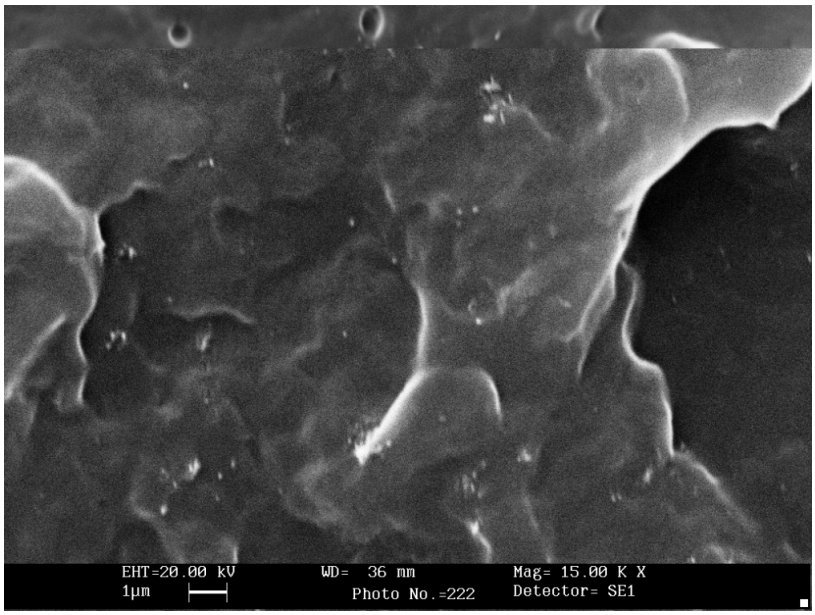

Figure 100: SEM microphotograph of fracture surface of PP5%

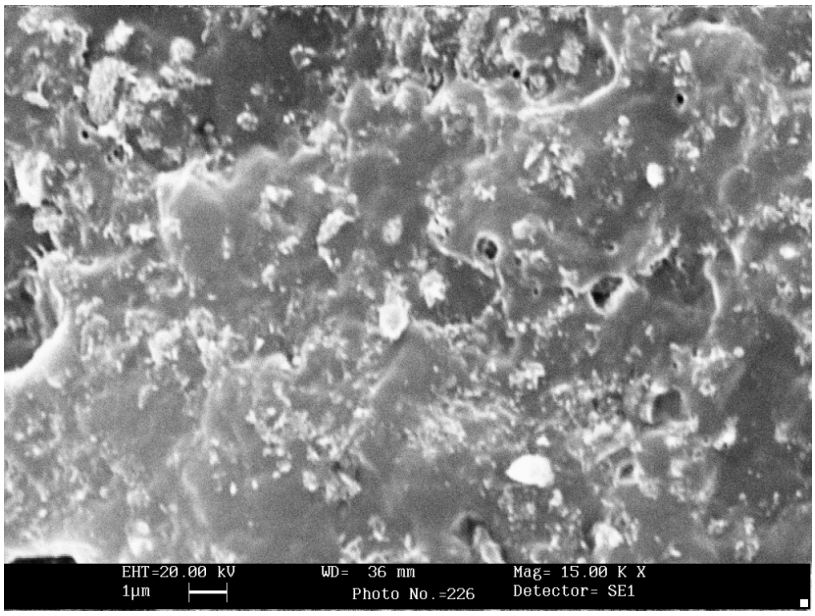

Figure 101: SEM microphotograph of fracture surface of PP10%

SEM microphotograph were also made on plane surface of PP/CNT composite film samples.

In Figures 102-104, typical SEM microphotographs of PP/CNT composite films containing 1, 3 and 5 wt.% CNT respectively are shown, where in particular Figure 104b) represents a zoom into the sample depicted in Figure 104a).

For 1 wt.% CNT the nanotubes appear again as separate white spots indicating local regions of aggregated nanotubes.

Anyway, even at this weight content of CNT it is possible to individuate an ordered positioning of nanotubes, almost equidistant from each other and in a preferred alignment almost parallel to the Take-up direction (TD). This configuration, while on one hand it prefigures already the potential network structure that will in fact be formed with the addition of higher amount of CNT, like it happens with 3 and 5 wt% CNT (Figure 103, 104), on the other hand is not yet a network itself. At 1 wt.% CNT the concentration of CNT in the composite films is probably too low and nanotubes are too far from each other to form an interconnected structure and thus in too small amount to act as reinforcing phase. In this situation, the nanotubes only form local regions of "aggregated" nanotubes which, in consideration of the phin thickness of the films, have the effect of local defect, becoming "inclusions" or holes in the film which act as stress concentrators that lead to a detriment in the mechanical properties with respect to the pure PP, as revealed also by the results of the tensile tests conducted on the composite films.

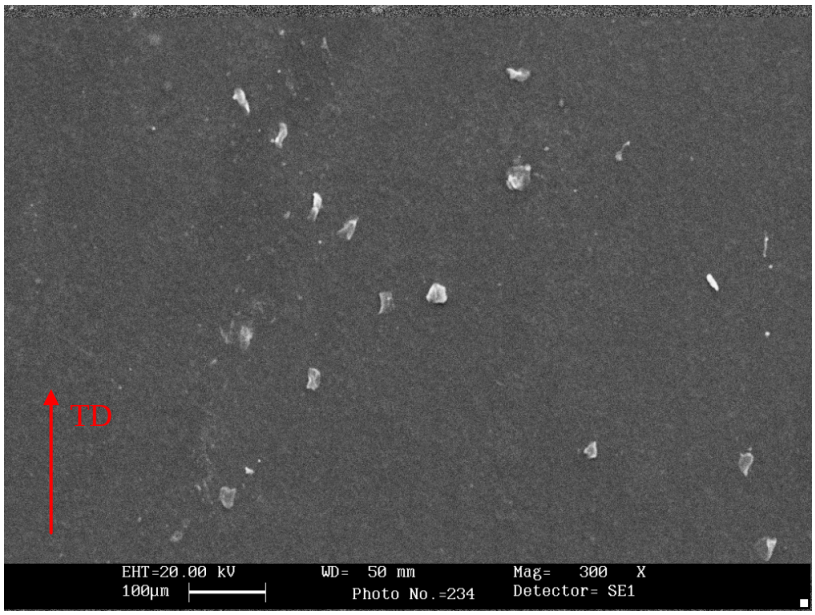

Figure 102: SEM microphotograph of plane surface of PP1L

With further increasing CNT content (Figures 103-105), a relevant interconnected structure with a preferred orientation in Take-up Direction (TD) is formed within the composite, leading to a remarkable improvement in the stiffness and strength, as also observed in the results of the tensile tests.

Other key issues can be discussed while observing Figure 104b) where it is depicted a zoom of the same film containing 5 wt.% CNT reported in Figure 104a). Two are the most important questions which are worth noticing in this picture: first the presence of a typical region of “agglomerated”

nanotubes, which in particular represent “knot and side” of part of the complex CNT array reported in Figure 104a). Furthermore, the nanotubes appear aligned in a preferred orientation almost parallel to TD. Second, there is apparently a pretty good adhesion with the matrix at the interface, while nearly nothing can be said about nanotubes waviness, since SEM technique is not suitable for this type of analysis. This concerns are fundamental for a deep understanding of the mechanical behaviour of our CNT reinforced composites since, beside the formation or not of a nanotubes array in the polymer matrix, three are the main effects on the stiffening mechanisms of carbon nanotubes, as also discussed in the previous paragraph: the waviness effect, the agglomeration effect and the interface effect.

With regarding to the waviness effect, because CNTs have very low bending stiffness due to the small tube diameter (~ 1 nm), most CNTs in composites exist in a curved state. I was observed [146] that the modulus of carbon nanotubes composites decreases rapidly as waviness increases. By the way, from SEM pictures it is quite impossible to get information about the nanotubes waviness.

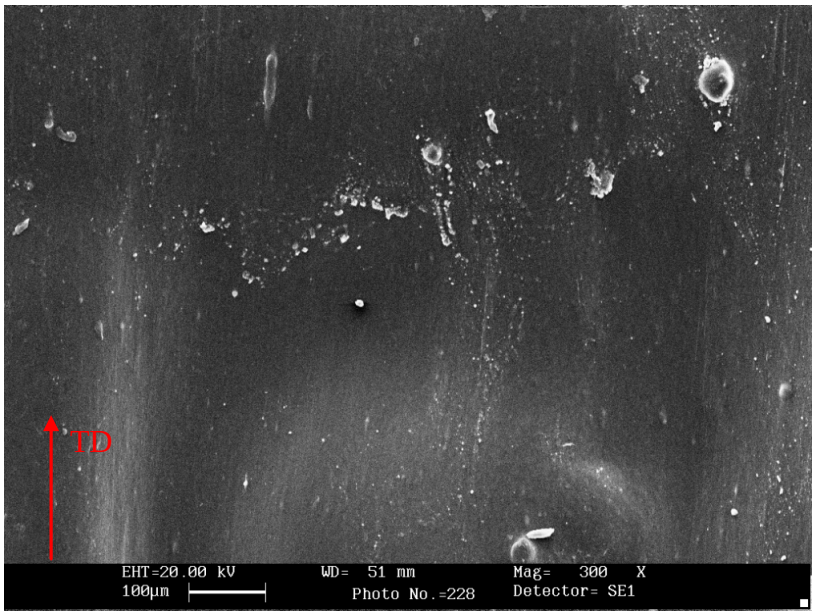

Figure103: SEM microphotograph of plane surface of PP3L

Concerning the agglomeration problem of CNTs in the polymer matrix, it represent a big challenge irrespective of the method of composite preparation. Anyway, in context with industrial application of polymer/nanotubes systems, melt mixing is in general the preferred method since applying shear is described to be very efficient in order to minimize nanotube aggregate formation [38, 42-44] and, thus, to enhance nanotube dispersion.

For the case of the present study, the situation revealed in the SEM micrograph of Figure 104b) indicates that the melt-

mixing process at which the PP/CNT reinforced composites were subjected to was not itself enough to control the dispersion of CNTs in the polymer matrix as well as the deagglomeration, i.e. the tubes tendency to form agglomerate, due to the intermolecular van der Waals interactions between them, their low bending stiffness and high aspect ratio.

The studies on CNT reinforced composites have demonstrated that the agglomeration of CNTs can exert a significant weakening effect to these composites [146]; but, on the other hand, the results of our tensile tests for 3 and 5 wt.% CNT have showed, instead, a relevant increase in the Young's modulus and strength.

These two events are only apparently in contrast with each other. Indeed, the contribution to the reinforcing effect of a network within the polymer matrix is exerted especially in terms of stiffness (Young's modulus) and strength, while the presence of agglomerated nanotubes, although being part of interconnected "sopramolecular" structure, during the tensile test may act as local defects and thus as stress concentrators which render the composite weaker, in terms of toughness and ductility.

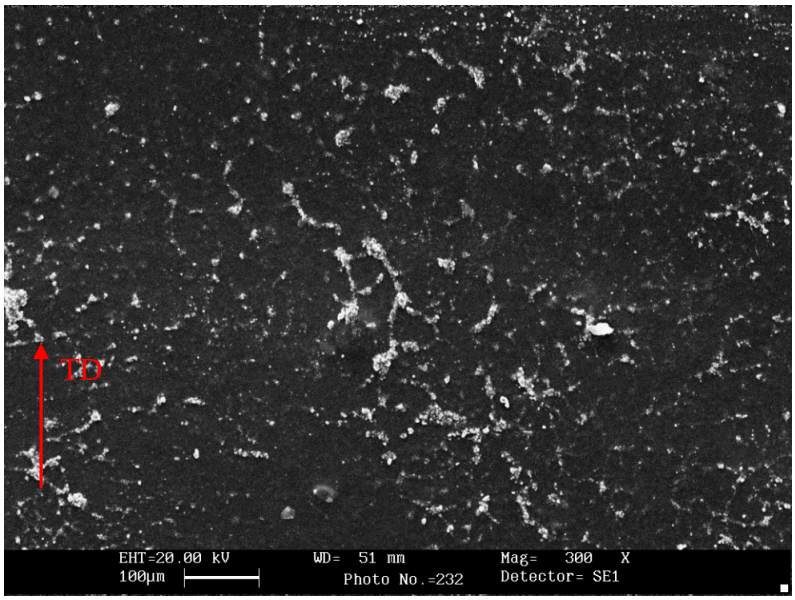

a)

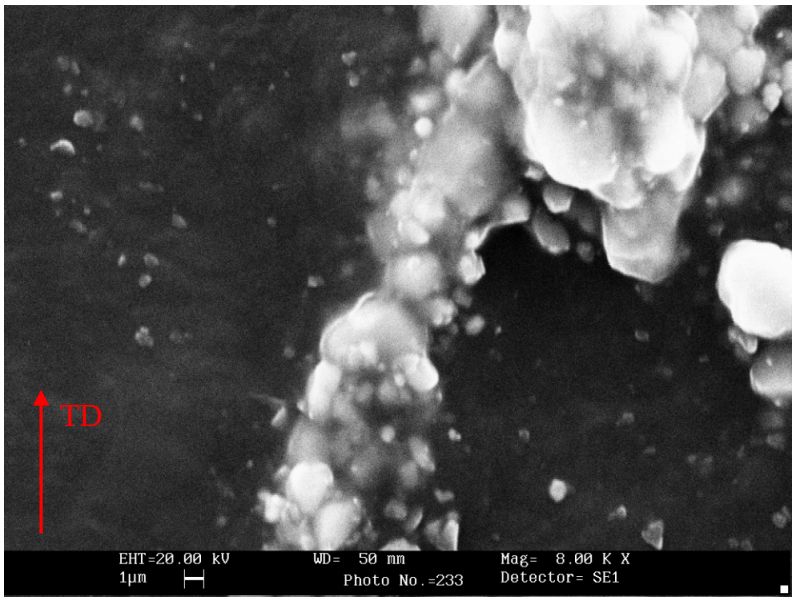

b)

Figure 104: SEM microphotograph of plane surface of PP5L

In this situation, a “solid-like behaviour” is thus a useful and summarizing analogy to describe this change in the mechanical response of the CNT reinforced composite with respect to the pure PP. In analogy, in fact, with the mechanical behaviour of a solid, the material has become much more rigid and resistant, but also more fragile, and less tough, in accordance also with results of the tensile tests.

A significant role in mechanical and physical properties of CNT reinforced composites is played by nterfaces also. The high surface area of CNTs creates a large interfacial region, with properties different from the bulk matrix. SEM micrograph reported in Figure 104b) shows a pretty good adhesion between the matrix and the nanotubes at the interface, which may act as a positive contribution the stiffening effect of CNTs. The good adhesion at the interface may probably related to the way that has been adopted in the present study to introducing nanotubes in polymer matrix.

As also described above, commercially available masterbatches of polymer/carbon nanotubes composite at 20 wt.% MWNT were used as starting material which were diluted by pure polymer in a subsequent melt mixing process.

At 20 wt.% MWNT, structure consists of highly entangled and "percolated" nanotubes in the PP matrix which are well wetted by the polymer matrix, very likely due also to the presence of chemical bonding between the polymer and the nanotubes. With the addition of PP into the masterbatch the network structure is being gradually expanded by incorporating the PP chains between the individual tubes while maintaining the "tube percolation" and, moreover, where present, the chemical bonding with polymer. Very high amount of PP added (and therefore, low amount of MWNTs) may break the percolated structure of the tubes and eventually interfere with the physical and chemical bonding of MWNTs with matrix.

By observing Figure 104a) one may surely assess that, for the particular case of PP/CNT composite films, 5 wt.% CNT is still an acceptable level of dilution, such that the percolated structure still exists, with MWNTs touching each other while maintaining a good adhesion nanotubes-matrix, with the consequence of a positive contribution to the improvement of the mechanical and physical properties of the PP/CNT composites.

In conclusion, the stiffening mechanics played by agglomerate, interface and waviness effects, are fundamental keys for improvement of the mechanical and physical properties of the base materials, whether or not the formation of a percolated structure in the matrix. If good adhesion, fine dispersion and low waviness of CNTs is guaranteed (and it is indeed a big challenge), than a relevant improvement in the mechanical and physical behaviour may in potential be achievable even if the network is not formed within the matrix. If at least one of these effects is not perfectly controlled, then the presence of CNTs in the polymer matrix may probably have no positive effects or at limit have negative effects on the mechanical properties of the base material. As soon as the percolation exists, then an increase in terms of “stiffness” and “strength” is usually exerted with respect to the pure polymer, but if, at the same time, adhesion and/or dispersion is not being well controlled, then the presence of CNTs gives a parallel negative contribution to the reinforcement of the composite with a consequence of a detriment of especially “ductility” and “toughness”. For this reasons, in summary, as long as the issue of aggregation and dispersion of CNTs will be out of control when introducing them within the polymer

matrix, then the addition of CNTs is likely to give birth to a much more “rigid” and “resistant” material, but, on the other hand, also more “fragile” and less “tough”.

4.4.2 OM

Many interesting information can be also discussed through the observation of OM photographs, which were taken on CNT composite films.

In Figures 105a) and b), it is depicted a PP1L sample film after the tensile deformation, in the necking and the failure zone respectively, while in Figure 106 the failure zone of a PP3L sample film is showed. In these Figures it is possible to distinguish the presence of either big regions of one ore more separate aggregate nanotubes either smaller local aggregation of nanotubes, clearly oriented along the take up direction (TD).

Furthermore, it also worth noticing the trace of the polymer’s “cold flow”, which occurs through a tortuous path around the region of nanotubes. It is known that a

thermoplastic polymer, under static load, is subjected, at room temperature, to continuing dimensional change, reversible or non reversible, that follows initial instantaneous deformation (necking). This phenomena is named “cold flow” and lead to a molecular flow which allow molecule to be oriented in the direction of to the applied load.

In this particular type of “energy dissipating flow”, the regions of aggregated nanotubes move relatively to each other and arrange themselves in a zigzag structure at ~90° direction with respect to the applied load.

Thus, the reinforcing effect in the composite films is actuated through the stress transfer between the matrix and the “regions” of nanotubes, which themselves move respect with each other during the polymer’s cold flow, setting themselves in a zigzag structure at 90° position with respect to the direction of the applied load. At the same time the polymer flow is hindered by the tortuous path around the nanotubes regions which might be the mode of dissipation of deformation energy of the composite film. This phenomena continues until one of more regions become a defect or a hole and thus a stress concentrator that induces the film failure (Figure 108).

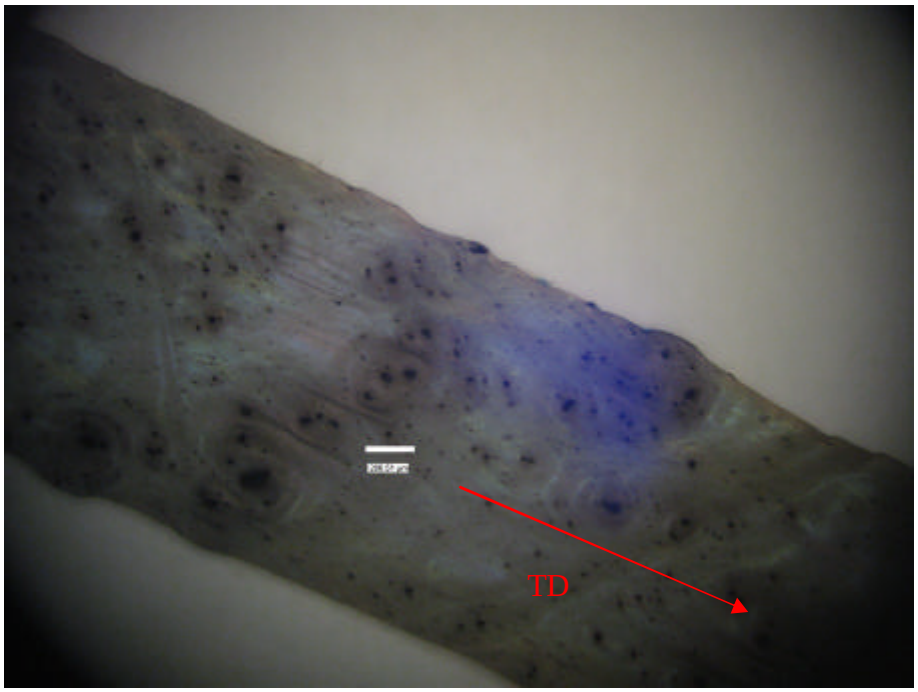

a)

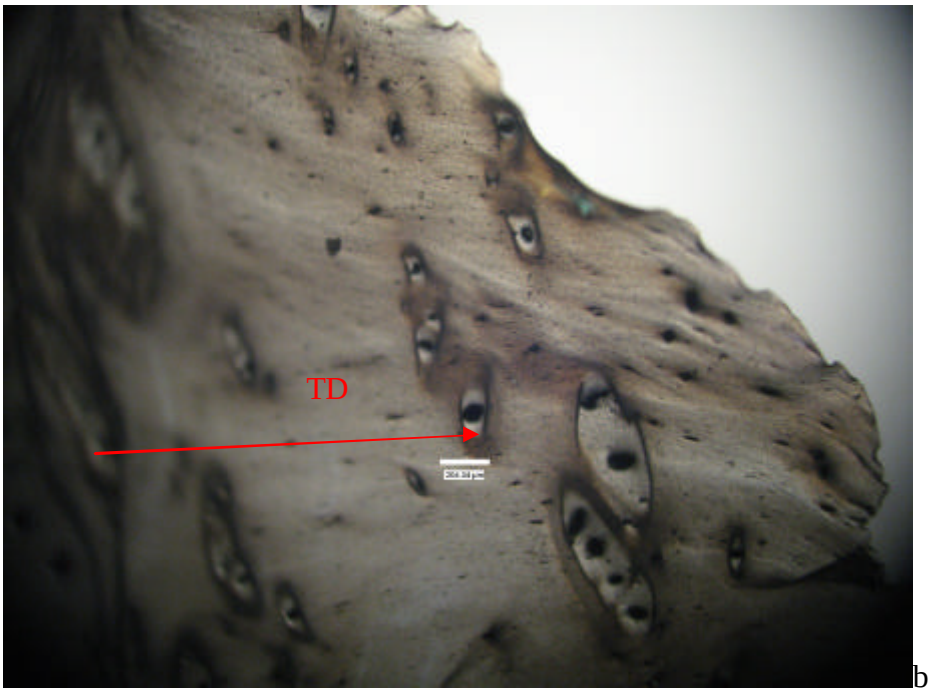

b)

Figure105: OM photograph of PP1L at a) necking zone and b) fracture zone

With further increasing CNT content, the films become more rigid and, at same time, less ductile (Figure 107), thus the length of the tortuous path during the "cold flow" shorter the higher the CNT concentration. In all cases, the crack seems to begin at the tip of a nanotube aggregate region from which it propagates through the polymer matrix. However, from the observation of the OM photographs, it seems that the higher the CNT concentration the earlier the failure of the film.

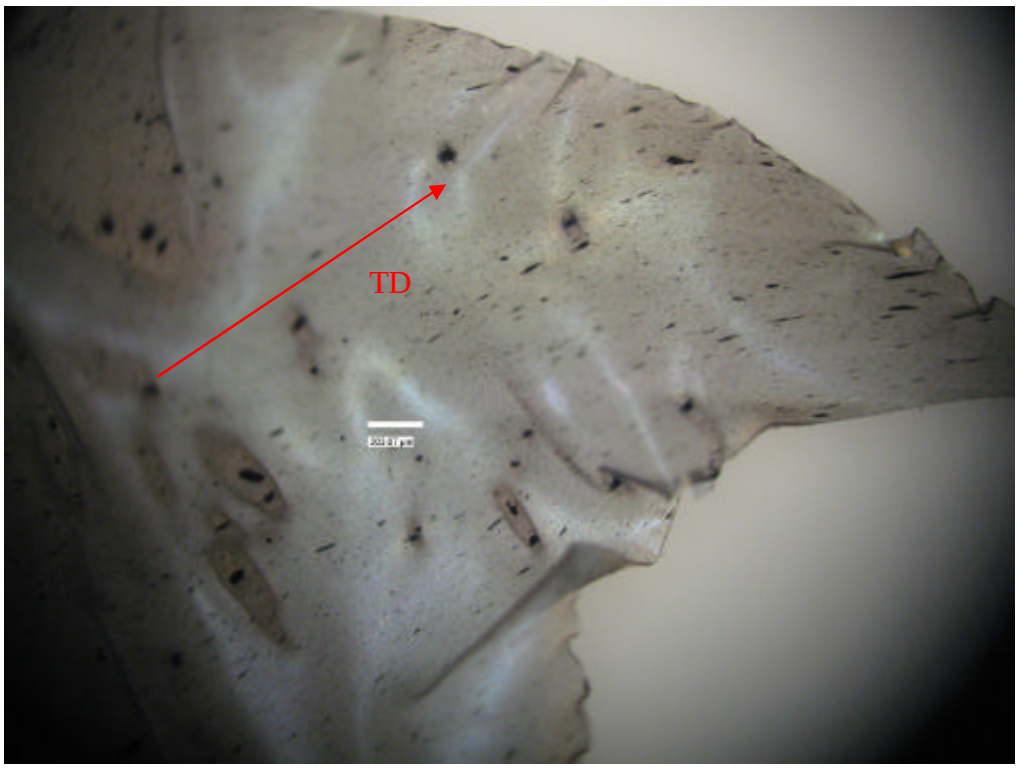

Figure 106: OM photograph of PP3L

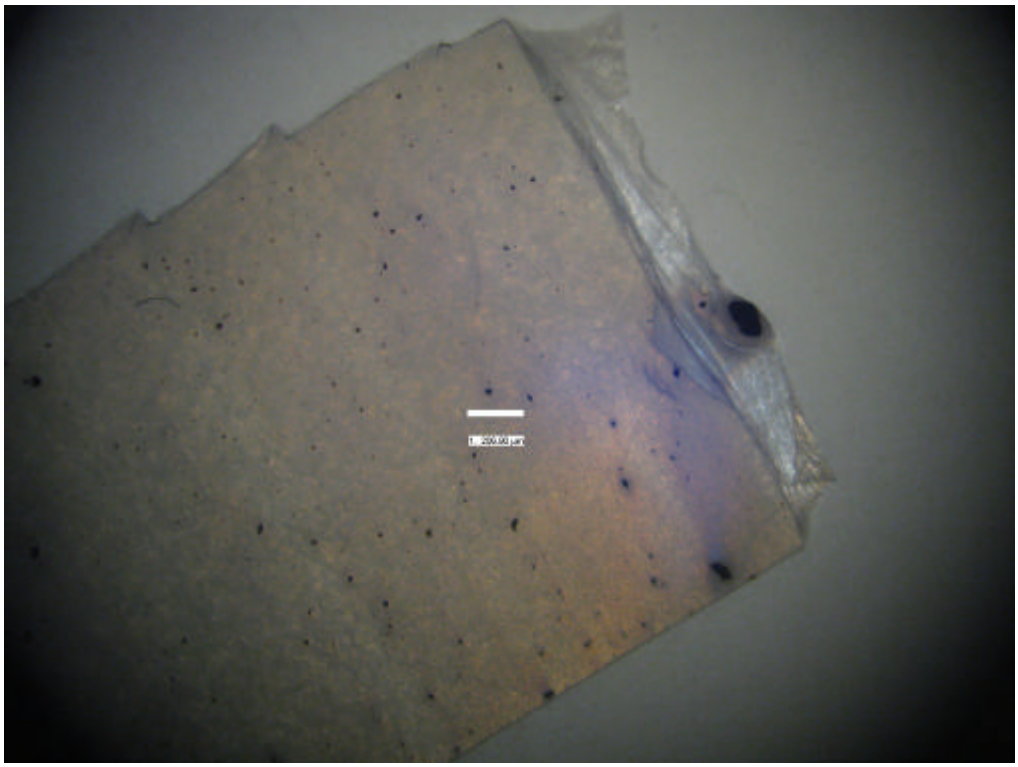

Figure 107: OM photograph of PP5L

Figure108: Crack propagation from the tip of a nanotube agglomeration

This type of behaviour represent a clear evidence of the type stress transfer which happens moreover between the polymer matrix and the regions of nanotubes than the single nanotube. Furthermore, it is likely that the mechanisms of reinforcement Finally, in Figure 109 an undeformed PP5L sample film is showed. It evident in the medium zone of the film the presence of a long zigzag “skeleton” in the take-up direction. This structure represents an evidence of the ability of CNTs of

forming well ordered arrangements even within a particular material system like polymer films. Their great potentiality in the field of mechanical properties was also here disclosed, regardless the numerous big challenges that have still to be pursued, like the possibility to control the main reinforcing effects, such as dispersion, waviness and agglomerate effects.

Figure 109: Undeformed PP5L sample film. It is visible the presence of a long zig-zag skeleton at the centre of the photograph

Conclusions

PP/CNTs composites were produced through traditional large scale polymer processing techniques. In particular PP/CNT composite plates were obtained through traditional extrusion technique by pressing the granulated melt-mixed composites while PP/CNT composite films were produced through the blown film extrusion technology.

The addition of CNTs affect the Tc that increases almost linearly with CNT wt content. Both the melting and crystallization peaks in PP/CNT composites are narrower than the pure PP and the full width at half maximum of crystallization peaks for PP is greater than that of PP/CNTs, which means a narrower crystallite size distribution in the CNT/PP composite as compared to pure PP. The sharper crystallization and melting peaks at least in part may be justified with the higher thermal conductivity of the carbon nanotubes with respect to that of the polymer, as heat distribution will be more uniform inside the samples containing the carbon nanotubes.

A significant effect of the addition of carbon nanotubes is visible also on the melting temperature (from ~150° to

155°C) and the glass transition temperature, which increases almost linearly from ~ -22°C to -12°C .

The film blowing process induced good level of nanotubes orientation in the PP/CNT composite films which positively affected the mechanical properties in terms of Young's modulus and strength.

Tensile test were performed either on suitable composite sample plates, To investigate on the effect of molecular and carbon nanotube orientation on the mechanical properties of PP, either on film samples. Furthermore, blown film samples were tested either in the blow-up direction (BD) either the take-up one (TD). Different behaviour were displayed by the blown films samples in the two directions of testing as a consequence of the biaxial orientation of molecules (and/or the carbon nanotubes) during the film blowing.

The incorporation of small weight fraction of CNTs in the PP matrix resulted in a significant increase in Young's modulus and strength in all composite system (plates and films).

Dynamic-mechanical properties were analyzed for PP/CNT composite plates in the solid state. The master curves obtained from the temperature-frequency scan have showed a significant

improvement in the elastic properties (E') for a certain weight content CNT (5 wt.%).

The rheological behaviour of c polypropylene/CNTs composite plates were investigated using oscillatory rheometry at constant temperature of 220°C. The nanotubes have a diameter of approximately 10nm while the length is at least 10 nm after the production with CVD. The viscosity increases significantly with increasing nanotube weight content. The viscosity of these was shown to be strongly dependent upon test frequency. Pure polypropylene and composites containing less or equal than 1 wt.% CNT show similar frequency dependence and reach a Newtonian plateau at low frequencies. Above 1 wt.% nanotubes, the viscosity curves exhibit non-Newtonian behaviour to much lower frequencies. Therefore, 1 wt.% may be regarded as a Rheological threshold composition. The viscosity increase is accompanied by an improvement in the elastic melt properties, represented by the storage modulus G', whose increase is much higher than that of the loss modulus G''.

The morphology of PP/CNTs composites and films was analyzed through SEM and OM technique. In the fracture surface of PP1%, containing 1 wt% CNT, carbon nanotubes

appear to be disperse in the form of 1 μm diameter cluster and they are observed as white spots dispersed independently through the matrix. With further increasing CNT content, a network of CNT particles is gradually formed within the matrix of the composites and films, leading to a sharp increase in the mechanical properties.

References

[1] Velasco JI, De Saja JA, Martinez AB. J Appl Polym Sci 1996;61:125.

[2] Liu X, Wu Q. Polymer 2001;42:10013.

[3] Qiu W, Mai K, Zeng H. J Appl Polym Sci 2000;77:2974.

[4] Chiang WY, Yang WD, Pukanszky B. Polym Engng Sci 1994;34:485.

[5] Kuhnert I, Fischer HD, Muras J. Kunstoff 1997;42:29.

[6] Wu C-M, Chen M, Karger-Kocsis J. Polymer Bull 1998;41:239.

[7] Assouline E, Pohl S, Fulchiron R, Gerard J-F, Lustiger A, Wagner HD, Marom G. Polymer 2000;41:7843.

[8] Hobbs SY. Nat phys Sci 1971;234:12.

[9] Campbell D, Qayyum MM. J. Polym Phys Ed 1980;18:83.

[14] Thostenson ET, Ren Z, Chou T-W. Composites Sci Technol 2001;61:1899

[15] Fornes TD, Yoon PJ, Keskkula H, Paul DR. Polymer 2001 ;42 :9929.

[16] Fu BX, Yang L, Somani RH, Zong SX, Hsiao BS, Phillips S, Blanski R Ruth P. J Polym Sci Part B: Polym Phys 2001;39:2727

[17] Lozano K, Barrera EV. J Appl Polym Sci 2001;79:125.

[18] Kumar S, Doshi H, Srinivasrao M, Park JO, Schiraldi DA. Polymer 2002;43:5133

[19] Ma J, Zhang S, Qi Z, Li G, Hu Y. J Appl Polym Sci 2002;831978

[20] Zhang M, Liu Y, Zhang X, Gao J, Huang F, Song Z, Wei G; Qiao J. Polymer 2002; 43:5133.

[21] Yakobson BI, Smalley RE, Am Sci 1997;85:324.

[22] Yu MF, Files BS, Arepalli S, Ruoff RS, Phys Rev Lett 2000;84(24):5552.

[23] Baughman RH, Zakhidov AA, de Heer WA, Science 2002;297:787.

[24]Andrews R, Jacques D, Rao AM, Rantell T, Derbyshire F, Chen Y, Chen J, Haddon RC, Appl Phys Lett 1999;75:1329.

[25] Haggenmueller R, Gommans HH, Rinzler AG, Fischer JE, Winey KI. Chem Phys Lett 2000;330:219.

[26] Kumar S, Dang TD, Arnold FE, Bhattacharyya AR, Min BG, Zhang X, Vaia RA, Park C, Adams WW, Hauge RH, Smalley RE, Ramesh S, Willis PA, Macromolecules 2002;35:9039.

[27] Smith BW, Benes Z, Luzzi DE, Fischer JE, Walters DA, Casavant MJ. Appl Phys Lett 2000;77:663-5

[28] Hone J, Llaguno MC, Nemes NM, Johnson AT, Fischer JE, Walters DA. Appl Phys Lett 2000;77:666-8

[29]Walter DA, Cassavant MJ, Qin XC, Huffman CB, Boul PJ, Ericson LM. Chem Phys Lett 2001;338:14-20

[30] Gommans HH,Allredge JW, Tashiro H, Park J, MagnusonJ, Rinzler AG. J Appl Phys 2000;88:2509-14

[31]Hwang J, Gommans H, Ugawa A, Tashiro Haggenmueller R, Winey KI. Phys Rev B 2000;62:R13310-3

[32] Vigolo B, Pénicaud A, Coulon C, Sauder C, Pailler R, Journet C Science 2000;290:1331-4

[33] Andrews R, Jacques D, Minot M, Rantel T, Macromol Mater Eng 2002 ;287 :395-403

[34] Battacharyya AR, Sreekumar TV, Liu T, Kumar S, Ericson LM, Hauge RH et al. , Polymer 2003;44:2373-7

[35] Barraza HJ, Pompeo F, O'Rear EA, Resasco DE. Nanoletterrs 2002;2(8):797-802

[36] Cooper CA, Ravich D, Lips D, Mayer J, Wagner HD. Compos Sci Technol 2002;62:1105-12

[37] Safadi B, Andrews R, Grulle EA. J Appl Poly Sci 2002;84:2660-9

[37] Sennett M, Welsh E, Wright JB, Li WZ, Wen JG, Ren ZF, Appl Phys A 2003;76:111-3

[38] Haggenmueller R, Gommans HH, Rinzler AG, Foscher JE, Chem Phys Lett 2000;330:219-25

[39] Wood JR, Zhao Q, Wagner HD. Compos Part A 2001;32:391-9

[40] Jin L, Bower C, Zhou O. Appl Phys Lett 1998;73:1197-9

[41] Hagerstrom JR, Green SL. Electrostatic dissipating compositescontaining Hyperion fiblril nanotubes. Commercialization of Nanostructured Materials, Miami, USA, 7 April 2000

[42] Subramoney S, Adv Mater 1998;10(15):1157-71

[43] Schadler LS, Giannaris SC, Ajayan PM, Appl Phys Lett 1998;74(26):3842-4

[44] Biercuk MJ, Llaguno MC, Radosavljevic M, Hyun JK, Jhonson AT, Fischer JE, Appl Phys Lett 2002;80:2767-9

[45] Pötschke P, Fornes TD, Paul DR, Polymer 2002;43:3247-55

[46] Roslaniec , Broza G, Schulte K, Compos Interf 2003;10(1):95-102

[47] Ferguson DW, Bryant EWS, Fowler HC. ANTEC '98 1998:1219-22

[48] Mitchell CA, Bahr JL, Arepalli S, Tour JM, Krishnamorti R, Macromolecules 2002;35(23):8825-30

[49] Smith BW, Benes Z, Luzzi DE, Fischer JE, Walters DA, Casavant MJ. Appl Phys Lett 2000;77:663-5.

[50] Hone J, Llaguno MC, Nemes NM, Johnson AT, Fischer JE, Walters DA. Appl Phys Lett 2000;77:666-8

[51] Walters DA, Casavant MJ, Qin XC, Huffman CB, Boul PJ, Ericson LM, Chem Phys 2001;338:14-20

[52] Gommans HH, Aldredge JW, Tashiro H, Park J, Magnuson J, Rinzler AG. J Appl Phys 2000;88:2509-14.

[53]Hwang J, Gommans H, Ugana A, Tashiro H, Haggenmueller R, Winey KI. Phys Rev B 2000;62:R13310-3

[54] Vigolo B, Pénicaud A, Coulon C, Sauder C, pailler R, Journet C: Science 2000;290:1331-4

[55] Iijima S. Helical microtubules of graphitic carbon.Nature 1991;354:56 –8.

[56] Kroto HW, Heath JR, O'Brien SC, Curl RF, Smalley RE.C60: Buckminsterfullerene.Nature 1985;318:162 –3.

[57] Chou T-W. Microstructural design of .ber composites.Cambridge,UK:Cambridge University press,1992.

[58] Collins PG, Avouris P. Nanotubes for electronics.Scienti .c American 2000;283(6):62 –9.

[59] Fan S, Chapline MG, Franklin NR, Tombler TW, Cassell AM, Dai H.Self-oriented regular arrays of carbon nanotubes and their.eld emission properties.Science 1999;283:512 –4.

[60] Wong SS, Joselevich E, Woolley AT, Cheung CL, Lieber CM. Covalently functionalized nanotubes as nanometre-sized probes in chemistry and biology.Nature 1998;394:52 –5.

[61] Rueckes T, Kim K, Joselevich E, Tseng GY, Cheung C-L, Lieber CM. Carbon nanotube-based nonvolatile random access memory for molecular computing.Science 2000;289:94 –7.

[62] Yao Z, Postma HWC, Balents L, Dekker C. Carbon Nanotube Intramolecular Junctions. Nature 1999;402:273 –6.

[63] Dresselhaus MS, Dresselhaus G, Eklund PC.Science of fullerenes and carbon nanotubes. San Diego:Academic Press,1996.

[64] Yakobson BI, Brabec CJ, Bernholc J. Nanomechanics of carbon tubes: instabilities beyond linear range. Physical Review Letters 1996;76(14):2511 –4.

[65] Yakobson BI, Samsonidze G. Atomistic theory of mechanica reaxation in fullerene nanotubes. Carbon 2000;38(11-12):1675 –80.

[66] Nardelli MB, Yakobson BI, Bernholc J. Brittle and ductile behaviour in carbon nanotubes. Physical Review Letters 1998; 81(21):4656 –9.

[67] Iijima S, Ichlhashi T. Single-shell carbon nanotubes of 1 nm diameter. Nature 1993;363:603 –5.

[68] Bethune DS, Kiang CH, Devries MS, Gorman G, Savoy R, Vazquez J et al. Cobalt-catalyzed growth of carbon nanotubes with single-atomic-layer walls. Nature 1993;363:605 –7.

[69] Journet C, Maser WK, Bernier P, Loiseau A, de la Chapelle ML, Lefrant S,et al. Large-scale production of single-walled carbon nanotubes by the electric-arc technique. Nature 1997;388:756–8.

[70] Rinzler AG, Liu J,Dai H, Nikolaev P, Human CB, Rodriguez-Macias FJ et al. Large-scale purification of single-wal carbon nanotubes:Process,product and characterization. Applied Physics A 1998;67(1):29 –37.

[71] Nikolaev P, Bronikowski MJ, Bradley RK, Fohmund F, Colbert DT, Smith KA et al. Gas-phase catalytic growth of single-walled carbon nanotubes from carbon monoxide. Chemical Physics Letters 1999;313(1-2):91 –7.

[72] Ren ZF,Huang ZP,Xu JW,Wang DZ,Wen JG, Wang JH et al. Growth of a single freestanding multiwall carbon nanotube on each nanonickel dot. Applied Physics Letters 1999;75(8):1086 –8.

[73] Ren ZF, Huang ZP, Xu JW, Wang JH, Bush P, Siegal MP et al. Synthesis of large arrays of well-aligned carbon nanotubes on glass. Science 1998;282:1105 –7.

[74] Huang ZP, Xu JW, Ren ZF, Wang JH, Siegal MP, Provencio PN.Growth of highly oriented carbon nanotubes by plasma-enhanced hot .lament chemical vapor deposition.Applied Physics Letters 1998;73(26):3845 –7.

[75] Shi Z, Lian Y, Liao FH, Zhou X,Gu Z, Zhang Y et al. Large scale synthesis of single-wal carbon nanotubes by arc discharge method.Journal of Physics and Chemistry of Solids 2000;61(7): 1031–6.

[76] Saito Y, Nishikubo K, Kawabata K, Matsumoto T. Carbon nanocapsules and single-layered nanotubes produced with plati-num-group metals (Ru,Rh,Pd,Os,Ir,Pt) by arc discharge. Journal of Applied Physics 1996;80(5):3062 –7.

[77] Thess A, Lee R, Nikolaev P, Dai HJ, Petit P, Robert J et al. Crystalline ropes of metallic carbon nanotubes. Science 1996;273:483 –7.

[78] Zhang Y, Iijima S. Formation of single-wal carbon nanotubes by laser ablation of fullerenes at low

temperatures. Applied Physics Letters 1999;75(20):3087 –9.

[79] Ge M, Sattler K. Bundles of carbon nanotubes generated by vapor-phase growth. Applied Physics Letters 1994;64(6):710 –1.

[80] Che G, Lakshmi BB, Martin CR, Fisher ER, Ruo RS. Chemical vapor deposition based synthesis of carbon nanotubes and nanofibers using a template method. Chemistry of Materials 1998;10(1):260 –7.

[81] Li WZ, Xie SS, Qian LX, Chang BH, Zou BS, Zho WY et al. Large-scale synthesis of aligned carbon nanotubes. Science 1996; 274:1701 –3.

[82] Zhang XX, Li ZQ, Wen GH, Fung KK, Chen J, Li Y. Microstructure and growth of bamboo-shaped carbon nanotubes. Chemical Physics Letters 2001;333(6):509 – 14.

[83] Bower C, Zhu W, Jin S, Zhou O. Plasma-induced alignment of carbon nanotubes. Applied Physics Letters 2000;77(6):830 –2.

[84] Bower C, Zhou O, Zhu W, Werder DJ, Jin S. Nucleation and growth of carbon nanotubes by microwave plasma enhanced chemical vapor deposition. Applied Physics Letters 2000;77(17): 2767–9.

[85] Cui H, Zhou O, Stoner BR. Deposition of aligned bamboo-like carbon nanotubes via microwave plasma enhanced chemical vapor deposition. Journal of Applied Physics 2000;88(10):6072 –4.

[86] Okai M, Muneyoshi T, Yaguchi T, Sasaki S. Structure of carbon nanotubes grown by microwave-plasma-enhanced chemical vapor deposition. Applied Physics Letters 2000;77(21):3468 –70.

[87] Choi YC, Shin YM, Lee YH, Lee BS, Park GS, Choi WB,et al. Controlling the diameter, growth rate, and density of vertically aligned carbon nanotubes synthesized by microwave plasma-enhanced chemical vapor deposition. Applied Physics Letters 2000;76(17):2367 –9.

[88] Treacy MMJ, Ebbesen TW, Gibson TM. Exceptionally high Young ’s modulus observed for individual carbon nanotubes. Nature 1996;381:680 –7.

[89] Wong EW, Sheehan PE, Lieber CM. Nanobeam mechanics: elasticity, strength, and toughness of nanorods and nanotubes. Science 1997;277:1971 –5.

[90] Salvetat JP, Briggs GAD, Bonard JM, Bacsa RR, Kulik AJ, Stockli T et al. Elastic and shear moduli of single-walled carbon nanotube ropes. Physical Review Letters 1999;82(5):944 –7.

[91] Walters DA, Ericson LM, Casavant MJ, Liu J, Colbert DT, Smith KA et al. Elastic strain of free suspended single-wal carbon nanotube ropes. Applied Physics Letters 1999;74(25):3803 –5.

[92] Yu MF, Lourie O, Dyer M, Moloni K, Kelly T. Strength and breaking mechanism of multi-walled carbon nanotubes under tensile load. Science 2000;287:637 –40.

[93] Yu MF, Files BS, Arepalli S, Ruo RS. Tensile loading of ropes of single wall carbon nanotubes and their mechanical properties. Physical Review Letters 2000;84(24):5552 –5.

[94] Xie S,Li W, Pan Z, Chang B, Sun L. Mechanical and physical properties on carbon nanotube. Journal of Physics and Chemistry of Solids 2000;61(7):1153 –8.

[95] Falvo MR, Clary GJ, Taylor RM, Chi V, Brooks FP, Washburn S et al. Bending and buckling of carbon nanotubes under large strain. Nature 1997;389:582 –4.

[96] Bower C, Rosen R, Jin L, Han J, Zhou O. Deforma tion of carbon nanotubes in nanotube-polymer composites. Applied Physics Letters 1999;74(22):3317 –9.

[97] Overney G, Zhong W, Tomanek D. Structural rigidity and low frequency vibrational modes of long carbon tubules. Zeitschrift Fur Physik D-Atoms Molecules and Clusters 1993;27(1):93 –6.

[98] Lu JP. Elastic properties of sing e and multi layered nanotubes. Journal of the Physics and Chemistry of Solids 1997;58(11):1649 –52.

[99] Yakobson BI, Campbell MP, Brabec CJ, Bernholc J.High strain rate fracture and C-chain unraveling in carbon nanotubes.Computational Materials Science 1997;8(4):341 –8.

[100] Bernholc J, Brabec CJ, Nardelli M, Maiti A, Roland C, Yakobson BI.Theory of growth and mechanica properties of nanotubes.Applied Physics A-Materials Science and Processing 1998; 67(1):39 –46.

[101] Iijima S, Brabec C, Maiti A, Bernholc J.Structural .exibility of carbon nanotubes.Journal of Chemical Physics 1996;104(5): 2089 –92.

[102] Ru CQ. Ective bending stiffness of carbon nanotubes. Physical Review B 2000;62(15):9973-6.

[103] Vaccarini L, Goze C, Henrard L, Hernandez E, Bernier P, Rubio A. Mechanical and electronic properties of carbon and boron-nitride nanotubes. Carbon 2000;38(11-12):1681 –90.

[104] Al-Jishi R, Dresselhaus G. Lattice dynamical model for graphite. Physical Review B 1982;26(8):4514 –22.

[105] Hernandez E, Goze C, Bernier P,Rubio A. Elastic properties of C and Bx Cy Nz composite nanotubes.Physical Review Letters 1998;80(20):4502 –5.

[106] Ru CQ. Elastic buckling of single-walled carbon nanotube ropes under high pressure.Physical Review B 2000;62(15):10405 –8.

[107] Popov VN, Van Doren VE, Balkanski M. Elastic properties of crystal of single-walled carbon nanotubes.Solid State Communications 2000;114(7):395 –9.

[108] Popov VN, Van Doren VE, Bakanski M.Lattice dynamics of sing e-walled carbon nanotubes.Physica Review B 1999;59(13):8355 –8.

[109] Ruo RS, Lorents DC. Mechanical and thermal-properties of carbon nanotubes. Carbon 1995;33(7):925 –30.

[110] Govindjee S, Sackman JL. On the use of continuum mechanics to estimate the properties of nanotubes. Solid State Communications 1999;110(4):227 –30.

[111] Ru CQ. Eect of van der Waals forces on axial buckling of a double-walled carbon nanotube. Journal of Applied Physics 2000;87(10):7227 –31.

[112] Ru CQ. Column buckling of multi-walled carbon nanotubes with interlayer radial displacements. Physical Review B 2000;62(24): 16962 –7.

[113] Ru CQ. Degraded axial buckling strain of multiwalled carbon nanotubes due to interlayer slips.Journal of Applied Physics 2001;89(6):3426 –33.

[114] Kolmogorov AN, Crespi VH. Smoothest bearings: interlayer sliding in multiwalled carbon nanotubes. Physical Review Letters 2000;85(22):4727 –30.

[115] Shaler MSP,Windle AH. Fabrication and characterization of carbon nanotube/poly (vinyl alcohol) Composites.Advanced Materials 1999;11(11):937 –41.

[116] Qian D,Dickey EC,Andrews R,Rantell T.Load transfer and deformation mechanisms in carbon nanotube-polystyrene composites.Applied Physics Letters 2000;76(20):2868 –70.

[117] Tibbetts GG, McHugh J. Mechanical properties of vapor-grown carbon fiber composites with thermoplastic matrices. Journal of Materials Research 1999;14:2871.

[118] Jia Z, Wang Z, Xu C, Liang J, Wei B, Wu Detal.Study on poly(methyl methacrylate)/carbon nanotube composites.Materials Science and Engineering A 1999;271(1 –2):395 –400.

[119]Gong X, Liu J, Baskaran S, Voise RD, Young JS. Surfactant assisted processing of carbon nanotube/polymer Composites. Chemistry of Materials 2000;12(4):1049 –52.

[120] Lordi V, Yao N. Molecular mechanics of binding in carbon nanotube-polymer composites. Journal of Materials Research 2000;15(12):2770 –9.

[121] Wagner HD, Lourie O, Feldman Y, Tenne R. Stress-induced fragmentation of multiwall carbon nanotubes in a polymer matrix. Applied Physics Letters 1998;72(2):188 –90.

[122] Jin L, Bower C, Zhou O. Alignment of carbon nanotubes in a polymer matrix by mechanical stretching. Appl Phys Lett 1998;73(9):1197–9.

[123] Haggenmueller R, Gommans HH, Rinzler AG, Fischer JE, Winey KI. Aligned single-wall carbon nanotubes in composites by melt processing methods. Chem Phys Lett 2000;330(3–4):219–25.

[124] Gommans HH, AldredgebJW, Tashiro H, Park J, Magnuson J, Rinzler AG. Fibers of aligned single-wall carbon nanotubes:polarized raman spctroscopy. Journal of Applied Physics 2000;88(5):2509-14

[125] Andrews R, Jacques D, Rao AM, Rantell T, Derbyshire F, Chen Yetal. Nanotube composite carbon fibers. Applied Physics Letters 1999;75(9):1329-31

[126] Vigolo B, Pénicaud A, Coulon C, Sauder C, Pailler R, Journet C et al. Macroscopic fibers and ribbons of oriented carbon nanotubes. Science 2000:290:1331-4

[127] J.F. Agassant, P. Avenas, J.Ph. Sergent, P.J. Carreau, Polymer Processing Principles and Modeling, Carl Hanser, Munich,1991.

[128] C.D. Han, Rheology in Polymer Processing, Academic Press, New York, 1976.
[129] J.M. Dealy, K.F. Wissbrun, Melt Rheology and its Role in Plastics Processing, Van Nostrand Reinhold, New York, 1990.
[130] M. Fleissner, Elongational flow of HDPE samples and bubble instability in film blowing, Int. Polym. Process. 2 (1988) 229.
[131] A. Ghaneh-Fard, P.J. Carreau, P.G. Lafleur, Study of kinematics and dynamics of film blowing, Polym. Eng. Sci. 37 (1997) 1148.
[132] T. Kanai, J.L. White, Dynamics, heat transfer and structure development in tubular film extrusion of polymer melts: a mathematical model and predictions, J. Polym. Eng. 5 (1985) 135.
[133] T. Kanai, J.L. White, Kinematics, dynamics and stability of tubular film extrusion for various polyethylenes, Polym Eng Sci 24 (1984) 1185.
[134] C.D. Han, J.Y. Park, Studies on blown film extrusion. 3. Bubble Instability, J. Appl. Polym. Sci. 19 (1975) 3291.138
[135] A. Ghaneh-Fard, P.J. Carreau, P.G. Lafleaur, Study of instabilities in film blowing, Am. Inst. Chem. Eng. J. 42 (1996) 1388–1396.
[136] P.A. Sweeney, G.A. Campbell, F.A. Feeney, Real time video techniques in the analysis of blown film instability, Int. Polym Process. 7 (1992) 229.
[137] J.R. Pearson, C.J.S. Petrie, The flow of a tubular film. Part 2. Interpretation of the model and discussion of solutions, J. Fluid Mech. 42 (1970) 60.
[138] J.R.A. Pearson, C.J.S. Petrie, The flow of a tubular film. Part 1. Formal mathematical representation, J. Fluid Mech. 40 (1970) 1.
[139] Mutel AT, Kamal MR, Rheological properties of fiber-reinforced polymer melts. In: Utracki LA, editor, Two phase polymer systems. Munich: Carl Hanser, 1991.p.305-31, Chapter 12.
[140] Kitano T, Kataoka T, Rheol Acta 1980;19:753-63
[141] Kitano T, Kataoka T, Nagatsuka Y. Rheol Acta 1984;23:20-30
[142] Utracki LA, Polym Compos 1986;7:274
[143] Utracki LA. Rheology and processing of multiphase systems. In:Ottenbrite RM, Utracki LA, Inoue S, editors. Current topics in polymer science, rheology and polymer

processing/multiphase systems, vol.II. Munich:Carl Hanser,1987.p.7-59.

[144] Dealy M, Wissbrun KF. Melt rheology and its role in plastic processing theory and application. Dordrecht:Kluwer Academic Publishers, 1999.

[145] Shaffer MSP, Windle AH. Fabrication and characterization of carbon/nanotube/poly(vinyl alcohol) composites. Adv Mater 1999;937-41.

[146] Feng X, Shi D, Huang Y, Hwang K, Micro and macro mechanics of carbon nanotubes composites. XXI International Congress of Theoretical and Applied Mechanics-Warsaw, Poland, August 15-21, 2004- CD proceeding.

[147] Herschel W H, Bulkley, Proc. Am. Test. Mater., 1926, 26, 621

Thanks to…

…first, Prof. Acierno, who has supported this work with high professionalism and kindness;

…second, all technicians and my co-workers, always ready to land me an help when needed;

…third, my love Aldo and my dear parents, who have had the patience to bear my difficult personality, and indeed was not at all easy for them…

…last, but not at all least, my beloved Alessandra, who, with her coming, has brought "life into my life".